Elastic and Inelastic Differential Scattering of Low Energy Electrons by Potassium

by

James A. Slevin

A dissertation submitted to the Graduate Faculty in Physics in partial fulfillment of the requirements for the degree of Doctor of Philosophy , The City University of New York .

1970

This manuscript has been read and accepted for the Graduate Faculty in Physics in satisfaction of the dissertation requirement for the degree of Doctor of Philosophy.

5/5/70
date

Chairman of Examining Committee

May 6, 1970
date

Executive Officer

Supervisory Committee

The City University of New York

ACKNOWLEDGEMENTS.

I wish to express my gratitude to my supervisor, Dr. Kenneth Rubin, for his continued and active interest in this work. His assistance with key computer programmes, his insight and the guidance he gave me throughout the entire course of this experiment were invaluable. Dr. Rubin was in addition responsible for the concept of the experiment.

I also wish to thank Mr. Paul Visconti for assistance in tne construction and assembly of the apparatus, and for supplying the total cross-section data.

I wish to acknowledge the assistance and cooperation of Dr. Benjamin Bederson, of New York University, who permitted us to use the electron gun designed in his laboratories, and supplied us with the detailed shop drawings.

I gratefully acknowledge many illuminating discussions with Dr. Richard Collins, of Amalgamated Wireless Australasia, who gave many valuable insights into the Atom Beam Recoil Method while performing an associated experiment at New York University.

Very capable technical assistance was provided by Messrs. J. Lane, P. Lynch, J. Giampetro, L. Oppegard, and M. Kolba. A special word of thanks is due to Mr. Jerry Cannella. His interest in and dedication to this project made possible the rapid construction and assembly of the experimental system.

I would also like to thank Mrs. Danziger and her secretarial staff for their assistance and cooperation during my stay at City College.

Finally, and most important of all, I wish to thank my wife, Frances, whose constant encouragement and support made it all possible.

TABLE OF CONTENTS

LIST OF FIGURES

I. Introduction

The excitation of atoms by collisions with electrons is a phenomenon of great interest in astrophysics, thermonuclear research, plasma physics and gaseous electronics. The number of papers and review articles relating to experiment and theory in inelastic collisions is legion. Among the more useful articles is a recent review by Moiseiwitsch and Smith[1] which covers both experimental and theoretical aspects of the problem, and outlines the present state of the art in both areas.

Although attempts were made in the 1930's and 40's to develop a theory for excitation by electron impact, significant progress was not made because of the great computational difficulties and the lack of experimental information about the different cross-sections. With the development of modulated beam techniques and the availability of fast electronic computers, this situation was greatly transformed in the 1950's.

Since the hydrogen atom offers the simplest many body problem in collision theory, much of the theoretical effort has been concentrated here though only with limited success. Calculations of inelastic cross-sections for excitation of the rare gases, oxygen and nitrogen atoms and the alkali metal atoms have also been made, but these are less extensive. In all cases, experimental data on excitation cross-sections are vital to the further development of the theory of inelastic collisions,

since they provide tests of the many assumptions and approximations necessarily made in these calculations.

Fite[2] has written an excellent review of the methods available for studying inelastic processes. The techniques employed to detect excitation fall into three main categories 1) radiation detectors 2) metastable atom detectors and 3) scattered electron detection.

Measurement of the radiation emitted from an excited atom is the most obvious way to monitor the excitation process. This method is restricted to the study of optically allowed transitions and is limited by the poor response of optical components in the far-and vacuum-ultraviolet regions of the spectrum. It is further complicated by cascade population of the excited state under study and difficulties in determining the absolute efficiency of the photon detector.

Metastable atoms can be detected by allowing them to impinge on a metal whose work function is less than the excitation energy of the metastable state. The efficiency of detection in this case can be as high as 30%, but the difficulty in obtaining an accurate estimate of this quantity limits the usefulness of this technique in obtaining absolute values.

Finally, the excitation process can be monitored by detecting those scattered electrons which have lost an amount of energy equal to the excitation energy. Since the basic measurement here is a current

measurement, this method is straightforward. The disadvantage of the method is that it requires sophisticated electron gun design, and the difficulty in measuring the number density in the atom beam again precludes an absolute determination of the cross-section.

The method used here to study inelastic scattering was outlined by Rubin[3] in 1966. It is a new and novel technique which utilizes in a crossed beam experiment certain of the kinematic properties of the recoiling atoms to distinguish between collisions involving elastic scattering and excitation to various atomic levels.

The recoil technique possesses certain advantages over the methods described above. In this method, one is not concerned with the trajectories of the scattered electrons, and consequently it is not necessary to use a highly collimated electron beam, or take extensive precautions in shielding the interaction region from stray electric or magnetic fields. This permits the use of simple electron gun design, large currents and an axial magnetic field to confine the electron beam. Further, since the measurement of the electron beam density is an easy matter, the determination of absolute cross-sections depends only on the ratio of the scattered atom current to the unscattered atom beam. Both quantities are measured with the same detector,and thus one does not have to know the detector efficiency. Finally, the recoil technique permits the measurement of inelastic cross-sections at 0^{o} and 180^{o}, a capability which is afforded by none of the above methods.

Since almost all the previous methods have had to resort to indirect and often unreliable methods to normalize the relative cross-sections to absolute values, the latter aspect of this technique and the ability to observe small and large angle scattering represent its real strength and is an important new development in the study of inelastic processes.

II. Theory

A. Introduction

Collisions of slow electrons with alkali metal atoms is in many ways similar to the electron-hydrogen atom scattering problem. The electron configuration of the ground state of alkali atom consists of a single valence electron, moving in the field of the relatively inert core and nucleus. This field is spherically symmetric since the filled shells always have an orbital angular momentum and total spin equal to zero.

Since the valence electron is weakly bound, it is easily polarized under the action of an external field. This leads to the large effective cross-sections which are typical of the alkalis. The cross-section for any alkali atom is usually an order of magnitude greater than the rare gas atom whose atomic number differs by only one, indicating the predominant role played by the valence electron in collisions.

Thus the problem of electron-alkali atom collisions can be reduced to a two electron problem, with the incident and valence electrons moving in the stationary field of the nucleus and inner electrons. The Hamiltonian of this two-electron system can be written in the form

$$H = -\frac{1}{2}\nabla_1^2 - \frac{1}{2}\nabla_2^2 + V(r_1) + V(r_2) + \frac{1}{r_{12}} \qquad (1)$$

where V(r) is the effective potential of the nucleus and filled shells,

r_1 and r_2 are the coordinates of the atomic and incident electrons and H is expressed in atomic units. Magnetic and relativistic interactions are not included in (1) and can easily be shown to be less than 1% of H.

B. General Formulation

The general formulation of the scattering problem has been outlined in great detail in many papers and review articles, most notably by Burke and Smith[4] in 1962. Only a brief summary will be included here.

The Schrodinger equation describing the two electron system takes the form in atomic units

$$\left(-\frac{1}{2}\nabla_1^2 - \frac{1}{2}\nabla_2^2 + V(r_1) + V(r_2) + \frac{1}{r_{12}} - E \right) \Psi(\vec{r}_1, \vec{r}_2) = 0 \qquad (2)$$

The standard method for solving (2) is to expand the total wave function $\Psi(\vec{r}_1, \vec{r}_2)$ in the eigenstates of the target Hamiltonian. Thus

$$\Psi(\vec{r}_1, \vec{r}_2) = \left(\sum_{\nu} + \int \right) \psi_\nu(\vec{r}_1) F_\nu(\vec{r}_2) \qquad (3)$$

where

$$\left(-\frac{1}{2}\nabla^2 + V(r) - \epsilon_n \right) \psi_\nu(\vec{r}) = 0 \qquad (4)$$

The expansion in (3) includes a sum over discrete and integral over continuum states. The symbol ν represents the quantum numbers of the

atom. Substitution of (3) into (2) leads to an infinite set of coupled equations for $F_\nu(\vec{r}_2)$ which describe the relative motion of the incident electron. These equations may be written

$$\left(\nabla_2^2 + k_n^2\right) F_\nu(\vec{r}_2) = \left[\sum_{\nu'} + \int d\nu'\right] U_{\nu\nu'} F_{\nu'}(\vec{r}_2) \tag{5}$$

where

$$U_{\nu\nu'}(\vec{r}_2) = 2 \int d^3\vec{r}_1 \, \psi_\nu^*(\vec{r}_1)\left[\frac{1}{r_{12}} - V(r_2)\right] \psi_\nu(\vec{r}_1) \tag{6}$$

and

$$k_n^2 = (E - \epsilon_n)$$

The set of equations (5) must now be solved subject to the following boundary conditions

$$F_{\nu'}(\vec{r}_2) \xrightarrow{r_2 \to \infty} e^{i\vec{k}_n \cdot \vec{r}_2} \delta_{\nu\nu'} + e^{ik_{n'} r_2} f_{\nu\nu'}(\hat{r}_2)/r_2 \tag{7}$$

where $f_{\nu\nu'}(\hat{r}_2)$ is the scattering amplitude for excitation from state ν to ν'.

Since the centrifugal barrier will exclude the higher angular momentum states from the scattering at low energies, a partial wave expansion can be expected to converge rapidly. Thus we can write

$$F_\nu(\vec{r}_2) = \sum_{\ell=0}^{\infty} \sum_{m_2=-\ell_2}^{+\ell_2} f_{\nu \ell_2 m_2}(r_2) Y_{\ell_2 m_2}(\hat{r}_2)/r_2 \tag{8}$$

When (8) is substituted into (5) we obtain an infinite set of coupled equations for the radial functions $f_{\nu \ell_2 m_2}(r_2)$. Since both the total orbital angular momentum L and the total spin S are separately conserved during the collision, it is often more convenient to describe the collision in a representation which is diagonal in these quantum numbers. This is easily effected using the appropriate vector addition coefficients, and the expression for the total wave function can now be written in terms of the expanded basis

$$\Psi_{\nu LM_L SM_S}(\vec{r}_1, \vec{r}_2) = \sum_{m_1^{\ell}, m_2^{\ell}} C^{\ell_1 \ell_2 L}_{m_1^{\ell} m_2^{\ell} M} \Psi_{\nu}(\vec{r}_1) Y_{\ell_2 m_2}(\hat{r}_2) \times F_{\nu}(r_2)/r_2 \qquad (9)$$

where the C's are Clebsch-Gordon coefficients and it should be remembered that $F_{\nu}(r_2)$ is now a <u>radial</u> function. In order to take account of the inherent indistinguishability of the free and bound electrons, the total wave function must be antisymmetrized with respect to interchange of both the space and spin coordinates of the two electrons. This is achieved by multiplying (9) by $1/\sqrt{2}(1 - P_{12})$ where P_{12} is the exchange operator. When this final form for the total wave function is substituted into the Schrodinger equation, an infinite set of coupled integrodifferential equations for the radial

functions $F_\nu(r_2)$ results:

$$\left[-\frac{d^2}{dr^2} - \frac{\ell_2(\ell_2+1)}{r^2} + k_n^2\right] F_\nu(r) = \sum_{\nu'} \left[V^L_{\nu\nu'} - W^{LS}_{\nu\nu'}\right] F_{\nu'}(r) \qquad (10)$$

where the $V_{\nu\nu'}$ are potential interaction terms and $W_{\nu\nu'}$ are exchange interaction terms which arise from the antisymmetrization of the wave function. The detailed forms of these potentials are given by Percival and Seaton.[5]

An alternative and perhaps more intuitive method for deriving the system of equations (10) is to assume that the total wave function Ψ satisfies Hartree-Fock equations. The solutions of these equations can then be shown to satisfy the Kohn variational principle and the values obtained for the elements of the K matrix will be correct to second order in the errors of the wave functions. Furthermore, the variational nature of these calculations permits bounds on the cross-section to be deduced, when detailed information is available on the bound states of the system. Although the recent discovery of large numbers of resonance states have complicated this aspect of the theory, useful extremum properties of the K matrix can still be deduced in some cases.

The set of equations (10) must now be solved with the appropriate boundary conditions. The asymptotic form of the radial

function $F_\nu(r)$ may be chosen to have the form

$$F_\nu(r) \xrightarrow{r \to \infty} \frac{1}{\sqrt{k_n}} \{ \sin(k_n r - \ell_2 \pi/2)\, \delta_{\nu\nu'} + \cos(k_n r - \ell_2 \pi/2)\, K_{\nu\nu'} \} \tag{11}$$

where $K_{\nu\nu'}$ are the elements of the reaction matrix. The K-elements are related to the T matrix by the formula

$$T = -[2iK/(1-iK)] \tag{12}$$

The particular form (11) is chosen because the K-matrix is real, and is often more convenient to use than T. Further, the K-matrix formulation is a very convenient way to introduce approximations which will automatically preserve the unitary property of the S-matrix, and hence satisfy conservation theorems.

In practical calculations it is impossible to solve the set of equations (10) exactly, since there are an infinite number of them. Various techniques have been used to obtain approximate solutions. Two of the more prominent of these will now be discussed.

C. Born Approximation

The simplest way to introduce the Born approximation is to rewrite (5) in the following form:

$$\left(\nabla_2^2 + k_n^2\right) F_n(\vec{r}_2) = 2 \int \psi_n^*(\vec{r}_1) \left\{ \frac{1}{r_{12}} - V(r_2) \right\} \Psi(\vec{r}_1, \vec{r}_2)\, d^3\vec{r}_1 \tag{13}$$

The Born approximation consists in replacing the total wave function with the wave-function of the non-interacting system i.e.

$$\Psi(\vec{r}_1, \vec{r}_2) = e^{i\vec{k}_o \cdot \vec{r}_2} \psi_o(\vec{r}_1)$$

where $\psi_o(\vec{r}_1)$ is the atomic ground state wave function. A solution for the scattering amplitude is now easily obtained.

The Born approximation has not proved to be a very successful technique for calculating excitation cross-sections for the resonance transitions in the alkalis in the energy range close to threshold. Because of the strong coupling between initial and final states, the cross-sections are much too large. In many cases, the partial cross-sections exceed the theoretical limit imposed by conservation theorems.

Various modifications of the Born approximation have been employed. A Born approximation to the K-matrix is sometimes used, thus ensuring the unitary property of the S-matrix is satisfied. Since the problems usually arise with the lowest order partial waves, another technique involves replacing these partial cross-sections by half the theoretical maximum.

A very detailed account of the Born approximations in all its forms is contained in reference 1. As far as the alkalis are concerned, most of the effort has been made on excitation of sodium though total cross-sections for the 4s-4p transition in potassium

have been calculated.[6] Differential cross-sections have not been published. It is, however, widely assumed that the Born cross-sections in the energy range of interest to this experiment are excessive and probably not reliable.

D. Close Coupling Approximation

Since the system of equations (10) is infinite, and any practical calculation can include only a finite number, a standard approach has been to truncate the eigenfunction expansion of the wave function after the first few terms. This method for calculating the cross-section is called the close coupling approximation. There is no rigorous mathematical justification for this procedure, nor even a plausibility argument to show that the series converges. Comparison with available experimental data and other approximations which are expected to be much more accurate for a given scattering problem have provided the only checks thus far on this approximation technique.

A very extensive series of calculations using the close coupling approximation have been carried out by the theoretical group at the Latvian Academy of Science, Riga, for low energy electron-alkali scattering. Phase shifts for elastic scattering and K-matrix elements for scattering above threshold have been tabulated in reference 6.

A two state 4s-4p approximation is used and leads to 3 coupled integro-differential equation for $L > 0$ and 2 for $L=0$.

The third equation arises from the fact that for a given total angular momentum L, the free electron can be scattered with momentum L + 1 or L - 1. The state for which the electron is scattered with momentum L has different parity from the others and does not contribute to the scattering.

Although only two states have been included in the wave function expansion, Burke[4] has emphasized the importance of the antisymmetrization imposed by the exchange operator P_{12} acting on (9). It gives rise to the exchange term in (10) and can be regarded as representing part of the continuum explicitly omitted from the summation. It can thus take up part of the distortion induced by the electron-electron interaction as well as satisfying the Pauli Principle.

It is important now to consider what range of validity can be expected from these calculations in the light of available experimental evidence and comparison with other calculations. Burke and his co-workers have investigated this problem thoroughly in relation to electron-hydrogen atom scattering, and there is a vast literature of critical analysis of the close coupling approximation.

It is now generally recognized that this approximation gives very accurate results for the phase shifts of elastic scattering in hydrogen and the alkalis when the p-level closest to the ground

state is included in the expansion. Physically this is so because the inclusion of the p-state accounts for the long range $1/r^4$ interaction which is predominant in low energy scattering. This approximation is especially good for the alkalis where the p-state comprises almost 99% of the atoms' polarizability which gives rise to the long range interaction. Furthermore, from a computational point of view, the $1/r^4$ dependence ensures a fairly rapid convergence of the partial wave expansion.

The situation for inelastic scattering is not nearly so promising. The earliest calculations included only the initial and final states in the eigenfunction expansion. In order to find out how the excluded states might affect results, very lengthy calculations on the behavior of the 1s-2s and 1s-2p cross-sections employing a 6-state approximation have been carried out by Burke.[7] He concludes that "provided the total energy is below the spectrum of the channels omitted from the expansion", this approximation technique can be expected to yield reliable results. This very severely restricts the domain of validity of the close coupling approximation. In the case of potassium, the two state approximation would thus only be reliable up to energies of 2.6e Volts, the excitation energy for the 3d state, since this state is excluded in the expansion.

The computational difficulties involved in calculating the excitation cross-sections are further complicated by the fact that for optically allowed transitions the long range interaction falls off only as $1/r^2$. (For an excellent quantum mechanical derivation of the $1/r^2$ and $1/r^4$ long range interactions see reference 8). Thus many more partial waves have to be included, and the calculations become increasingly cumbersome at energies beyond two or three times threshold.

Finally, the choice of atomic wavefunctions for the eigenfunction expansion must be considered. Since the choice of atomic wave functions dictates the magnitude of the long range potential, which is the predominant interaction at these energies, the final results will depend greatly on the particular functions used. This problem does not arise for hydrogen where exact wave functions are known. For Li and Na, Hartree-Fock functions are available, but Sternheimer[9] has shown that these are slightly too external and predict polarizabilities much larger than the experimentally observed values. Wave functions which reproduce the observed ionization potentials were constructed by Sternheimer to calculate the polarizabilities; the agreement between theory and experiment is good for Li and Na, but the theoretical predictions of the polarizabilities for the heavier alkalis lie well above the experimental values.

Karule and Peterkop[6] have used semiempirical wave functions based on a potential determined by Gaspar.[10] In order to determine the effect of wave functions on the results, they repeated the calculations on Cs, using wave functions corresponding to Stone's potential. These wave functions were chosen to give agreement between experimental and calculated oscillator strengths. The resulting cross-sections were increased by 15%.

Thus the effectiveness of the close coupling approximation in determining excitation cross-sections for the alkalis is limited not only by the exclusion of important states from the expansion for computational reasons, but also by the sensitivity of the final results to the particular choice of wave functions. It seems that only experimental data can resolve these difficulties.

III. Experiment

A. General Description

A block diagram of the apparatus used is shown in Figure 1. The oven produces a beam of potassium atoms which is velocity selected by a Stern-Gerlach magnet. The beam is cross-fired by a modulated electron beam causing scattered atoms to recoil from their initial trajectories. The atom beam is then incident upon a conventional hot wire detector and the resulting ion current amplified by a Bendix electron multiplier. The entire detector assembly rotates about a gimbel placed close to the interaction chamber and at any given angle detects the number of atoms scattered into a small angular range about that angle.

The apparatus consists of four chambers containing the oven source, electron gun, detector and a differentially pumped section. One side of the Stern-Gerlach magnet is connected to the differentially-pumped chamber, and the other side to the interaction chamber through a bellows and a bakeable valve.

The entire experimental apparatus is mounted on two long parallel I-beams which are isolated from the floor by four Korfund shock absorbers. These isolate the system from floor or building movements, and thus eliminate a potential source of noise in the experiment.

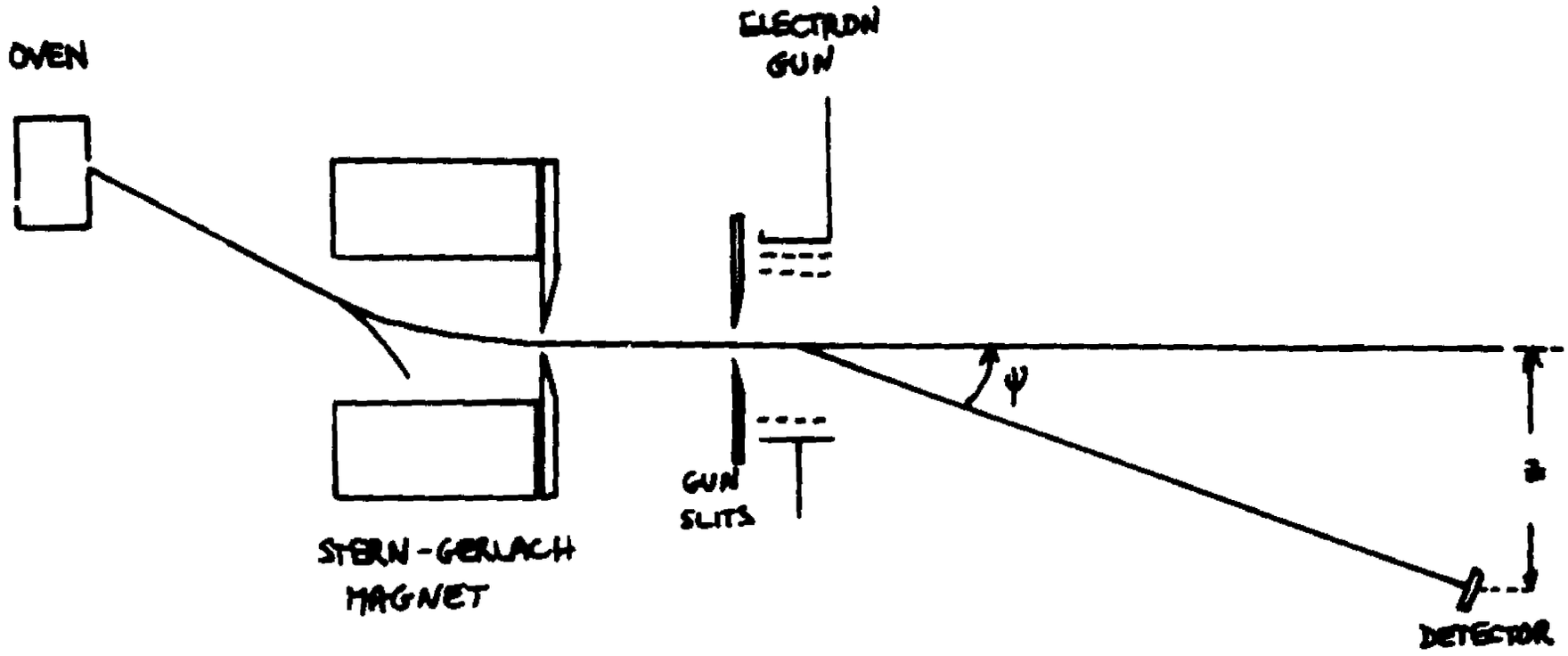
OVEN
ELECTRON GUN
STERN-GERLACH MAGNET
GUN SLITS
ψ
a
DETECTOR

FIGURE 1

B. Detailed description of experimental system

1) Source and differentially pumped chambers:

A 24" long by 11" diameter stainless steel cylinder with a bulkhead welded in the center provides two chambers, one of which is used to house the alkali oven source and the other to provide a stage of differential pumping. The source chamber is pumped by a 2400 liter/sec NRC diffusion pump, freon cooled baffle and liquid nitrogen trap, and a stainless steel gate valve permits the isolation of the chamber from the pump stack. The differentially pumped chamber is evacuated by a 1000 liter/sec Dresser diffusion pump with freon cooled baffle and a gate valve again allows this section to be isolated from the pumps. The chambers are connected by a 1/4" hole in the bulkhead. The foreline connection of both NRC and Dresser pumps are joined in series to a two stage Model ED-500 Edwards forepump which reduces the pressure to about 10 microns. The forepump is also connected through appropriate valves to both source and differential chambers thus allowing them to be opened up and evacuated to foreline pressure without letting the pump stacks up to air. This provides fact recycling time when modifications are made or alkali ovens reloaded. Two Ultek zeolite traps, installed in the foreline between forepump and diffusion pumps prevent migration of forepump oil to the diffusion

pumps which use DC 705.

The foreline pressure is monitored by an Edwards Model B5 vacuum gauge. When the pressure exceeds a preset value (say 40 microns), a pneumatically operated valve in the foreline is closed, power to the diffusion pumps is shut off, and the source and differential chambers isolated from the pump stacks by means of the gate valves (also pneumatically operated). This prevents"disaster" in case of an electrical power failure or sudden leak in the vacuum system.

Both chambers are mounted on Thompson ball bushings which permit them to be moved perpendicularly to the I beams. The bushings are in turn mounted on steel plates which can slide along the I beams on bearing surfaces constructed by mounting rows of 1/4" steel balls on plates rigidly bolted to the beams. Both motions, parallel and perpendicular, facilitate the alignment and hook-up of this section with the rest of the experimental system.

The alkali oven is identical to one used at New York University and is constructed from monel. It basically consists of a well to contain the potassium and a long narrow (0.040" in diameter) channel which allows the potassium vapor to emerge. Two knife edge slits at the end of the channel are used to form the atom beam. The slit

spacing is typically 0.004". The oven is brought up to operating temperature by two Vulcan heaters mounted close to the slits and its temperature monitored by chromel-alumel thermocouples mounted at the rear. Further details of the oven can be found in reference 5.

In order to maintain an atom beam for as long as possible without opening up the system to atmosphere, two identical ovens are used in the source chamber. They are supported on two plates attached to a 5/8" Edwards feedthrough, and rest on steel pins which provide thermal isolation. The feedthrough is attached to a 10" brass flange which is mounted on a 12" diameter port at the top of the chamber. It can be moved vertically to bring either oven into position, and can also be rotated to move the ovens on or off the apparatus axis. Leads for the heating elements and thermocouples are brought to two 8 pin feedthroughs brazed into this flange. In addition this flange supports a copper cylinder, wrapped with coils and freon cooled. This trap is used to condense the unwanted potassium vapor which emerges from the oven.

With the oven at operating temperature, the pressure in the source chamber is typically $4x10^{-7}$ Torr, while that in the differential chamber is on the order of $8x10^{-8}$ Torr.

2) Stern-Gerlach magnet:

The Stern-Gerlach magnet is conventional with pole faces machined to follow the equipotential of a two wire inhomogeneous magnet field[11]. Figure 2 shows a cross section of the magnet used. This geometry gives a calculated field to gradient ratio of 10/cm. The pole pieces are 4" long and are mounted inside a rectangular stainless steel tube on supports which permit independent horizontal and vertical adjustment of both ends. Accurately machined stainless steel spacers fix the magnet gap at 0.032". Slits at the exit end of the magnet were set at 0.010" in the center of the gap.

3) Interaction chamber:

This chamber is constructed from Type 304 stainless steel and is evacuated by a General Electric 120 liter/sec ion pump appended to a 6" port at the bottom. The Stern-Gerlach magnet is connected to a $1\frac{1}{2}$" O.D. inlet port by suitable adapters through a stainless steel bellows and 3/4" I.D. straight through valve supplied by California Physics Products. This valve which is capable of being baked to 300° C closed enables the interaction chamber to be isolated from the source chamber when an experiment isn't being run, and reduces the possibility of contamination in the electron gun due to migration of oil vapor from the diffusion pump in the differential chamber.

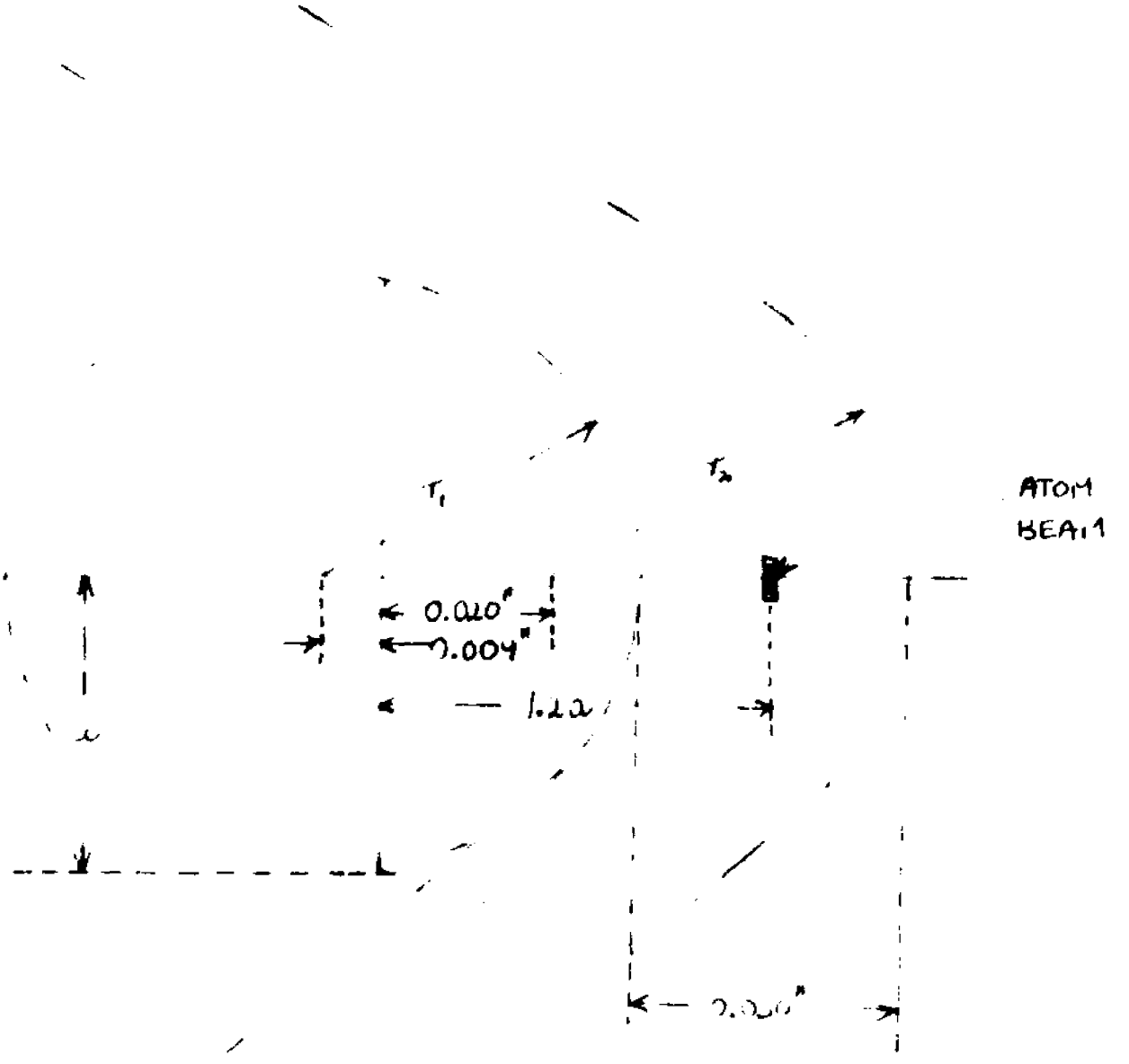

$a = 0.040"$
$r_1 = 0.041"$
$r_2 = 0.045"$

FIGURE 2 DETAIL OF POLE PIECES

The bellows allows the interaction and differentially pumped chambers to be moved independently. An 8" flange mounted on a port at the top of the chamber is used for the electron gun support and electrical feed throughs. The gun support consists of a hollow stainless steel tube attached to a 2-3/4" Varian flange. The mate for this flange is welded to one side of a Metal Bellows Corporation bellows which permits 1" of vertical movement. The other side of the bellows is welded to a 1-1/2" aperture located in the center of the 8" flange. A micrometer head with 1" travel is attached to the 2-3/4" flange and supported on a rigid structure which is bolted to the face of the large flange. The micrometer thus drives the small flange to which the gun support tube is attached, and the gun can be moved vertically over a range of 1".

A liquid nitrogen dewar is also supported from the 8" flange and can be filled through a tube connecting the flange and dewar. When the gun has been assembled and is in position, a stainless steel cylinder, with entry and exit apertures for the atom beam, can be attached to this dewar enabling the area around the gun to be cooled to liquid nitrogen temperatures.

The chamber is bolted to an aluminum table which is mounted on two Thompson ball bushings, and can be moved perpendicular to

the I-beams with a micrometer drive. Additionally, it can be rotated relative to this table with the use of two lead screws. Thus the gun itself can be moved vertically, horizontally or rotated. All of these motions are used in the line up of the apparatus.

Under operating conditions, the pressure in this chamber is typically on the order of 7×10^{-9} Torr.

4) Detector chamber and two dimensional motion:

This chamber and the connecting pieces to the interaction chamber are also fabricated from Type 304 stainless steel, and all parts are bakeable to 450° C. It is evacuated by a General Electric 8 liter/sec ion pump appended to a 1-1/2" port at the side. The chamber itself is almost identical to the one just described. The tube used to support the atom beam detector is identical to that used to support the gun and can be moved vertically over the same range. A liquid nitrogen dewar is again appended to the top flange. The atom beam enters through a 1-1/2" port, and visual sighting along the entire apparatus is provided by a 1-1/2" window opposite the entry port.

The detector chamber is connected to the interaction chamber by a 13" long by 1-1/2" O.D. steel tube and 4-1/2" I.D. Metal

Bellows Corporation bellows. A liquid nitrogen dewar is constructed around the connecting tube. The bellows flange nearest to the detector chamber is connected to a gimbel through two steel pieces with bronze bushings. The gimbel itself is mounted on a 1" thick aluminum table which is bolted rigidly to the I-beams, and permits the detector chamber to rotate in two planes about the gimbel axes.

The chamber is counterbalanced by a suitable weight suspended from a structure bolted to the frame of the apparatus. The pulley from which the counterbalancing weight is suspended is attached to the support structure in such a way that it can move in two dimensions in the horizontal plane, thus allowing the weight to follow the chamber as it moves, and ensuring that it is properly balanced wherever it moves. The two dimensional motion of the counterbalancing support structure is provided by Thompson ball bushings.

The experiment being reported here requires the detector to be moved out of the plane of scattering, which in this case means vertically, as well as in a horizontal direction so that all points in the differential region can be scanned. This is accomplished by the use of two lead screws, driven by Slosyn stepping motors. The lead screw for the vertical motion pushes against the smooth surface of the flange at the bottom of the chamber, while that for the horizontal motion

pushes against a right angled plate lapped to a 5 micron finish and bolted to the side of the chamber. The nuts for these screws, 4" long to prevent any transverse movement, are bolted rigidly to the support frame of the apparatus, and the stepping motors are free to move on tracks provided by ball bushings. Backlash problems are eliminated almost completely by counterbalancing the chamber so that it is always forced against the lead screws. In the case of the vertical lead screw, this is achieved by offsetting the counterbalancing already in effect; for the horizontal a suitable weight is allowed to hang vertically and is attached to the chamber by means of a pulley. Care is taken to ensure that the size of the counterbalancing weights is sufficient to eliminate the backlash and yet small enough to prevent scratching of the contact surfaces by the ball bearings mounted at the end of the screws.

Two linear potentiometers, fed by a constant voltage power supply, are mounted on the lead screw support structure and enable the detector coordinates to be monitored electronically. The potentiometers are calibrated by dial gauges mounted alongside, and with the voltage measuring system described later have a resolution of better than 0.0001".

The motion just described has performed exceedingly well

throughout the course of this experiment. The Slosyn stepping motors used in conjunction with a two-axis Slosyn indexer permit very precise movements of the lead screws; each step of either motor corresponds to a lateral movement of about 0.0001". With the elimination of lead screw backlash, and the spatial resolution which the stepping motor system permits, detector coordinates are reproducible to better than 0.0005", an accuracy which is more than adequate for the experiment being reported here.

5) Hot wire detector:

The atom beam detector is a conventional heated hot wire made from 0.010" x 0.0005" platinum strip. To ensure the largest work function possible, the highest purity grade obtainable for platinum was procured. The wire is mounted on a ceramic block, with one end rigidly fixed and the other free to move along its length and suitably counterbalanced to ensure that the wire remains taut at all temperatures. The wire is fed by a constant current power supply.

Potassium atoms striking the hot wire surface are adsorbed and then evaporate as ions. They emerge at right angles to the surface, and are accelerated to a plate. A slot is cut in the plate to permit the incident atom beam to pass through and the ion current to be collected. It is then amplified using a Bendix M-3 10B electron multiplier.

The width of the detector is fixed by the width of the wire, in this case 0.010", and the height depends on the angle of the wire in relation to the direction of the incident beam, the width of the slot in the accelerating plate and its distance from the hot wire itself. This is illustrated in Figure 3 . The slotted plate has a focusing effect on the ions emerging from the hot wire surface, and this can be used additionally to vary the effective height of the detector. An atom beam is formed by placing an 0.004" x 0.004" slit in front of the electron gun in the interaction chamber, and Figure 4 shows vertical profiles of this beam for various accelerating plate voltages. It is clear that the shape of one side of the profile is unaffected by the choice of bias voltage, while the other side depends critically on the bias. Figure 3 shows that in fact one side of the ion profile should not be affected by the plate, whereas the other side will be determined to a great extent by any curvature in the ion paths from wire to accelerating plate. At higher bias voltages, the shape of the curve remains unchanged indicating that the ions are following straight line paths. The effective detector height calculated on this basis and shown in Figure 3 agrees well with that found experimentally from the shape of the profiles and the known dimensions of the beam. During an experiment the plate is held at a very high voltage (about - 450 Volts) to ensure that all

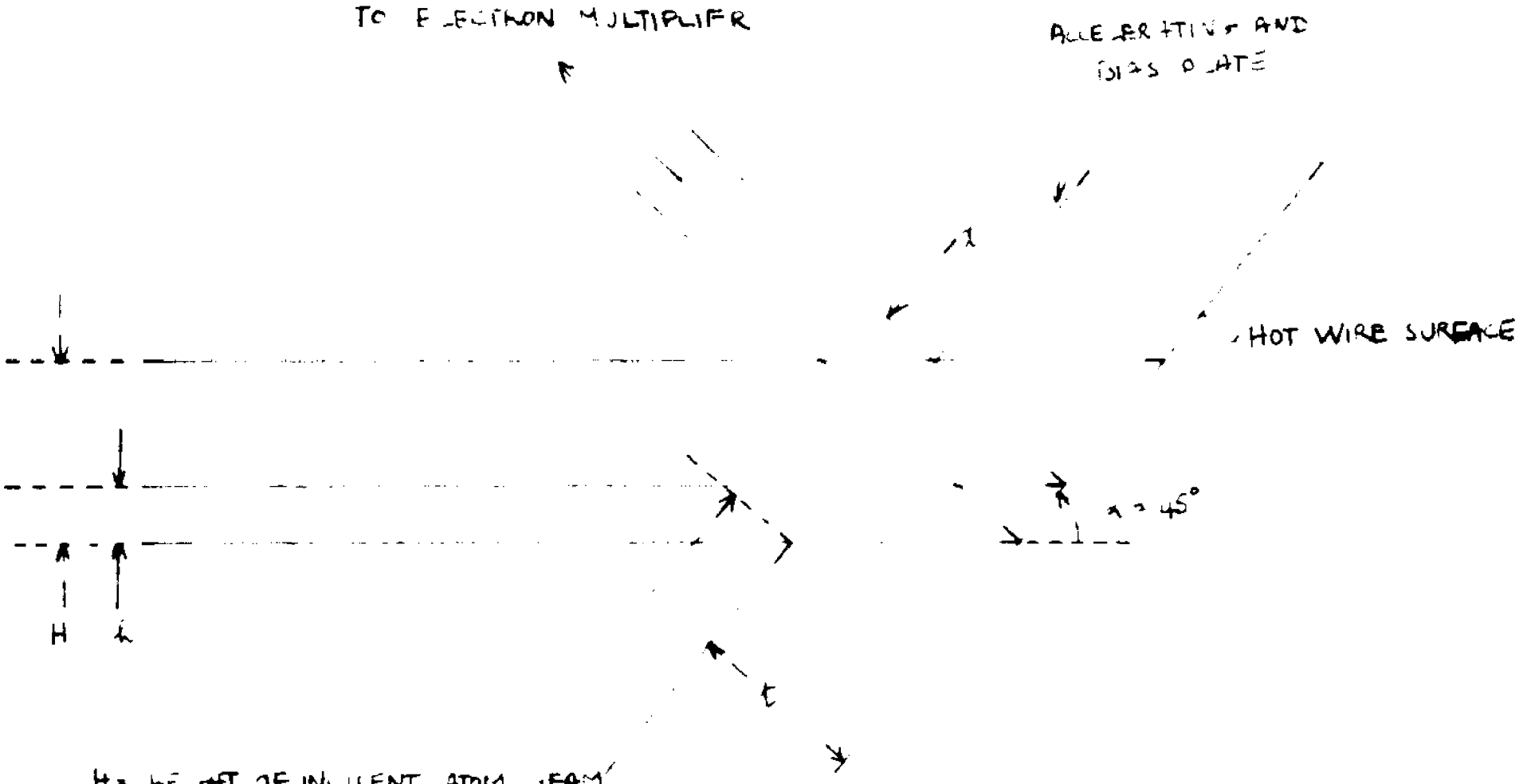

H = HEIGHT OF INCIDENT ATOM BEAM

L = EFFECTIVE HEIGHT OF DETECTOR = $\frac{d}{\sin\alpha} - \frac{d}{\tan\alpha}$

FIGURE 3 ION AND ATOM TRAJECTORIES IN LETELTOR

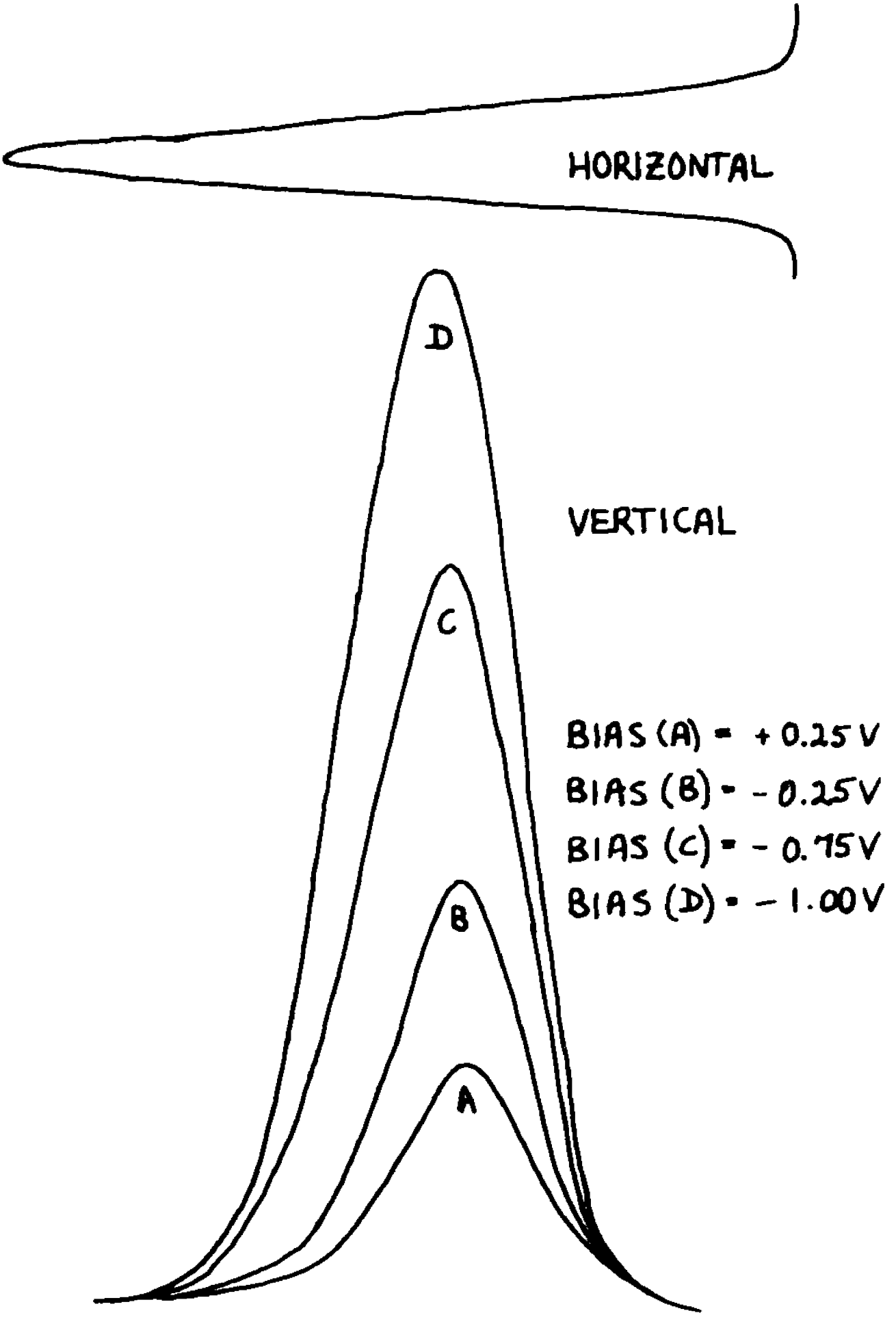

FIGURE 4 ATOM BEAM PROFILES

the ions are collected, (although there is less than a 10% change in ion current from -5 Volts up to -500 Volts).

The efficiency of the detector just described is not known accurately, but experiments have been done elsewhere to measure this quantity, and it is generally recognized to be greater than 90%.

6) Stern-Gerlach patterns and velocity selector:

In order to produce a velocity selected beam on the axis of the apparatus, the oven was displaced about 0.040" off axis. This was acoomplished by simply rotating the Edwards feedthrough to which the oven support plate is attached. Trajectories of atoms in the required spin state are bent towards the axis, the slower atoms being deflected more. The exit slit of the magnet acts as a virtual source of atoms; trajectories of spin selected atoms diverge from this slit, and the entire spectrum of velocities is distributed spatially across the emerging beam. The magnet gap is sufficiently great that only the very fast and very slow atoms are removed from the state selected beam due to collision with magnet pole faces.

Figure 5 shows a plot of atom beam intensity at the detector as a function of the horizontal position of the hot wire. This profile represents a modified Maxwellian distribution.

$$f(V) \sim V^3 \quad -mv^2/2kT$$

plotted as a function of $1/v^2$. It is evident that conditions are such that both spin states leave the magnet, but that the two are spatially separated. Figure 5 also shows the atom beam profile after the electron gun with its 0.004" x 0.004" slits has been lowered into position.

A detailed analysis on the use of a Stern-Gerlach magnet as a velocity selector has been given by Rubin and Bederson[12]. They calculate the atom beam velocity distribution to be w/s where w is the oven slit width, and s the distance the oven is moved off axis. The figure obtained by this method agrees well with the value calculated by simply comparing the full beam intensity with the oven on axis to the maximum beam transmitted with the magnet on and the oven off axis.

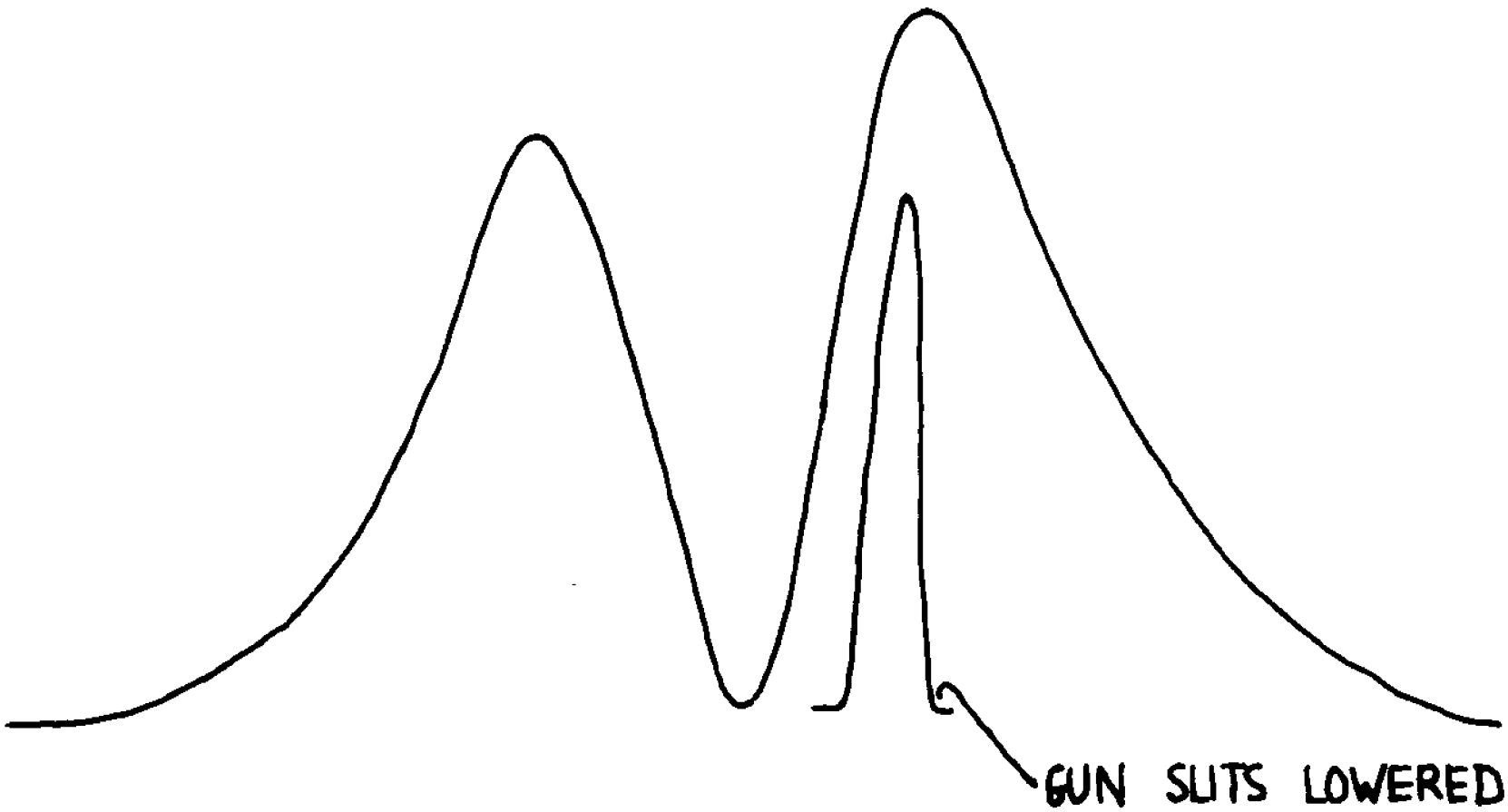

FIGURE 5 STERN GERLACH PATTERN

C. Electron Gun

1) Design:

The electron gun employed in the present experiment is identical to one designed and now in extensive use at the Atomic Beams Laboratory of New York University. It has been described in great detail in references (13) and (14), and only a brief description will be given here. Figures 6 through 12 show details of the gun elements and assembly.

Four 0.060" diameter ceramic rods, mounted in accurately located holes in a molybdenum "channel" block, form the basis for the gun. All gun elements have four matching holes, 0.061" in diameter, and are stacked sequentially on the rods. The grids, supplied by Buckbee Mears Company, are made by photoetching 0.002" molybdenum sheet, a process which permits the locating holes to be drilled to a very precise tolerance with respect to the grid mesh. When stacked on the ceramic rods, spatial alignment of the grid meshes is thus assured, and the number of secondary electrons produced by collisions with the grid structure is greatly reduced.

The electron source for the gun is an indirectly heated oxide coated cathode taken from a Raytheon 4D32 tube. The mica insulators

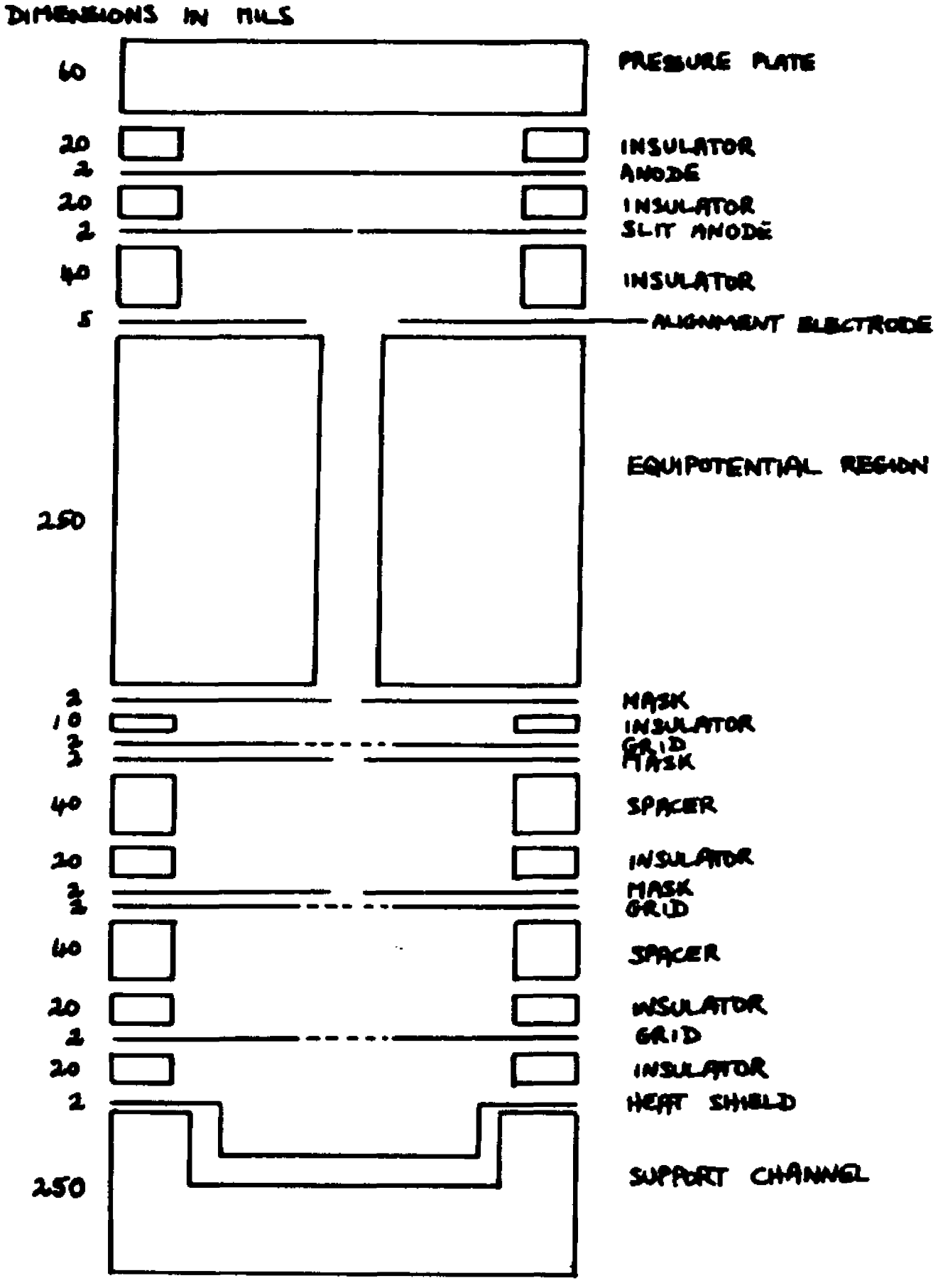

FIGURE 6 GUN ASSEMBLY

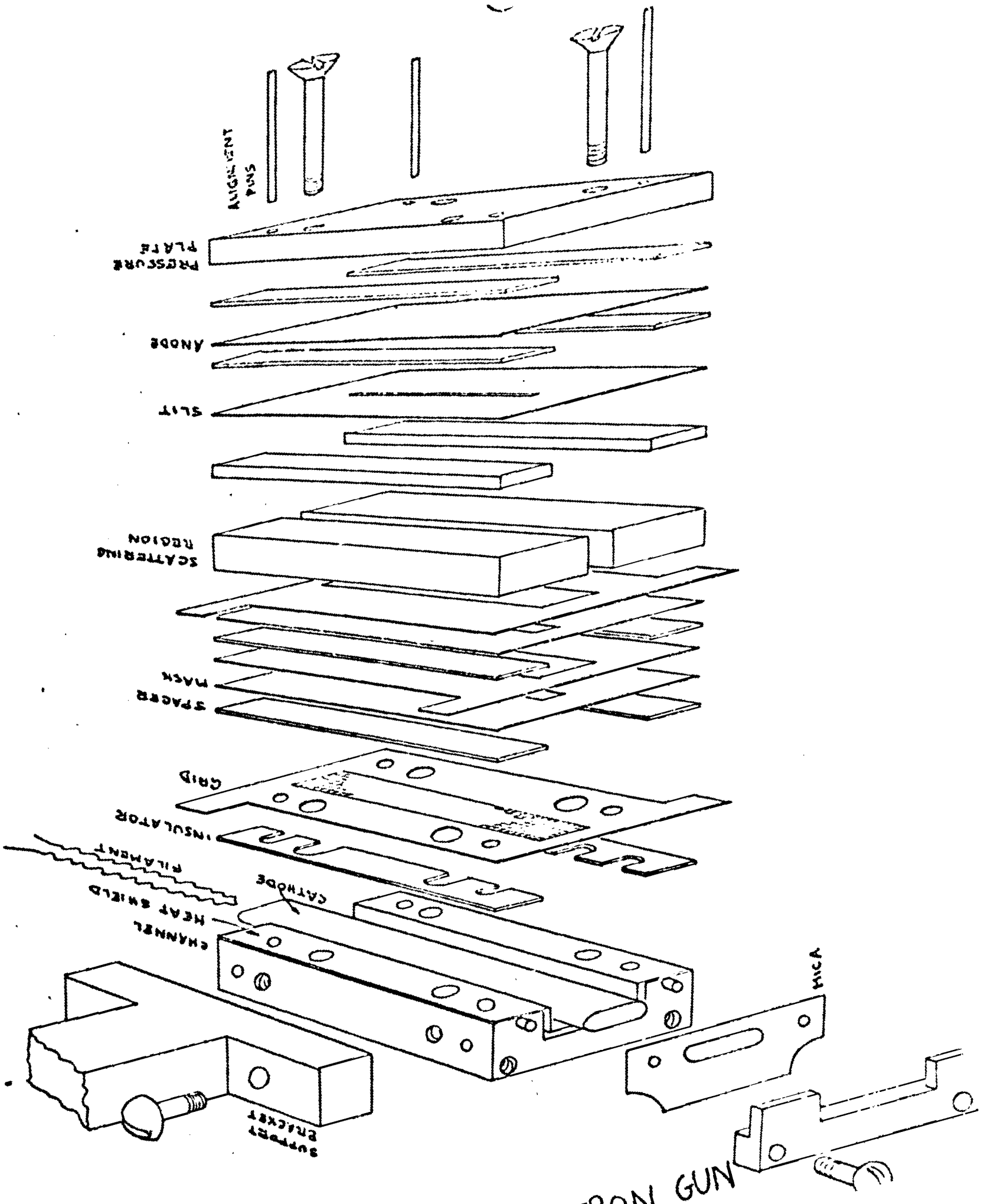

FIGURE 7 ELECTRON GUN

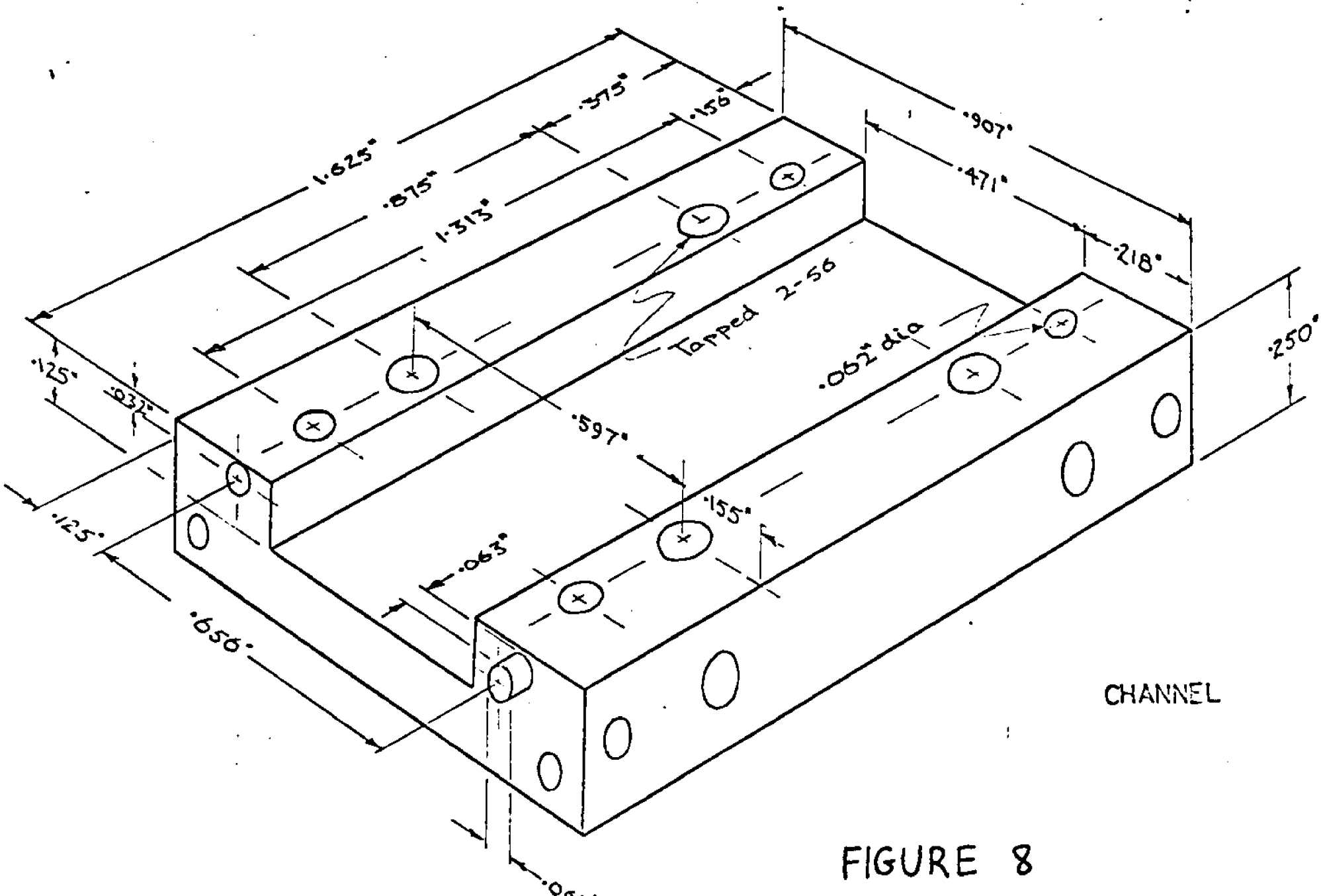
1.625"
.875"
1.313"
.375"
.156"
.907"
.471"
.218"
.250"
.125"
.032"
.597"
.155"
.062" dia
Tapped 2-56
.063"
.125"
.650"
CHANNEL

FIGURE 8

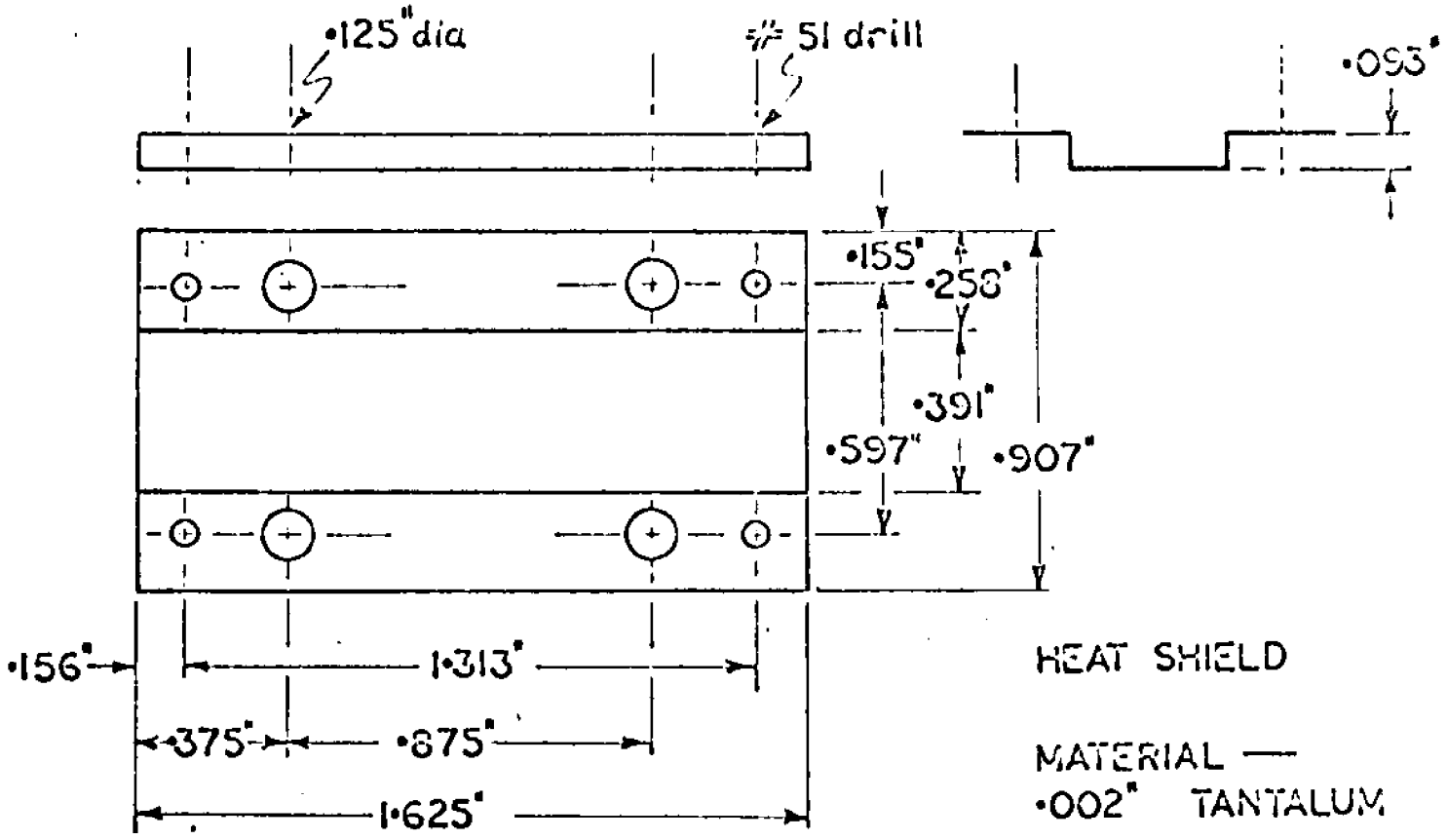

HEAT SHIELD

MATERIAL —
.002" TANTALUM

ALL DIMENSIONS ± .005"

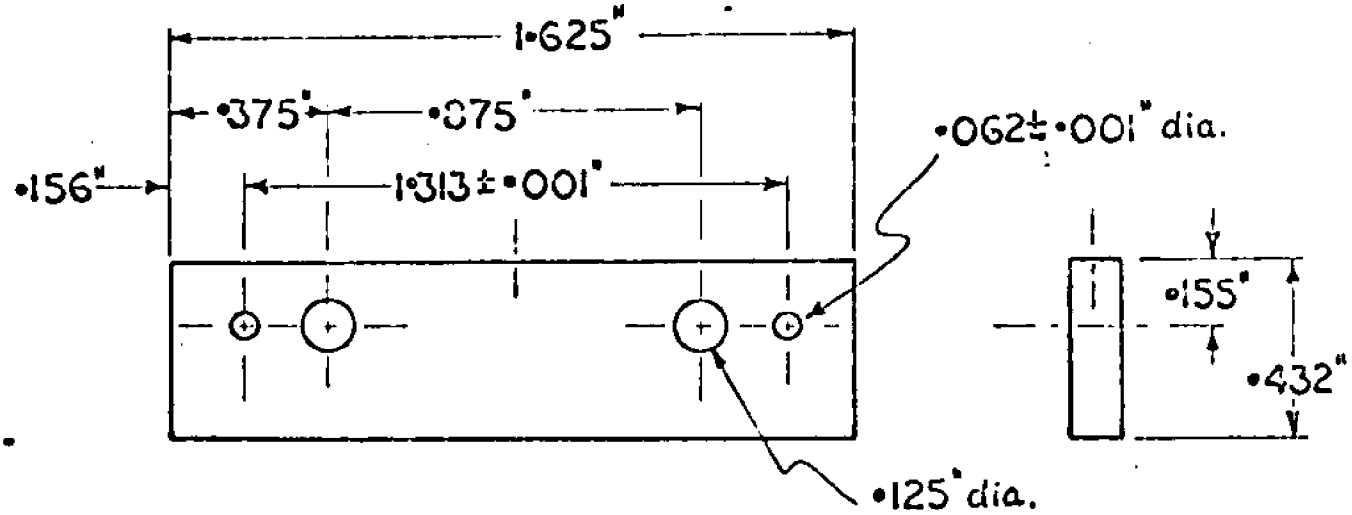

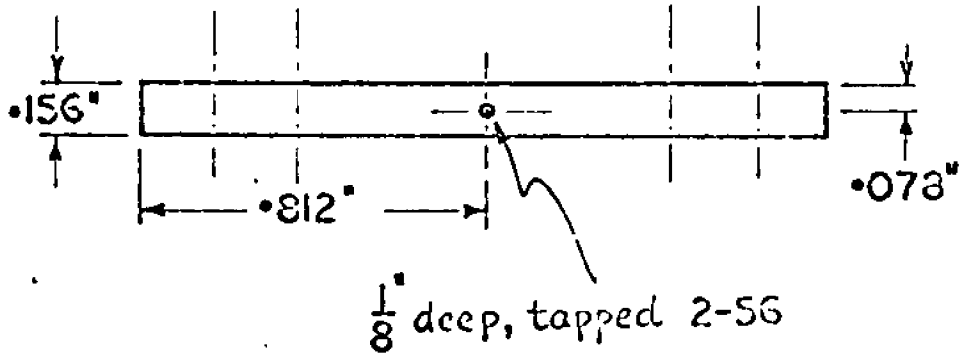

SCATTERING REGION
(TWO REQUIRED)

MATERIAL —
MOLYBDENUM

ALL DIMENSIONS ± .005"
EXCEPT AS NOTED

FIGURE 9

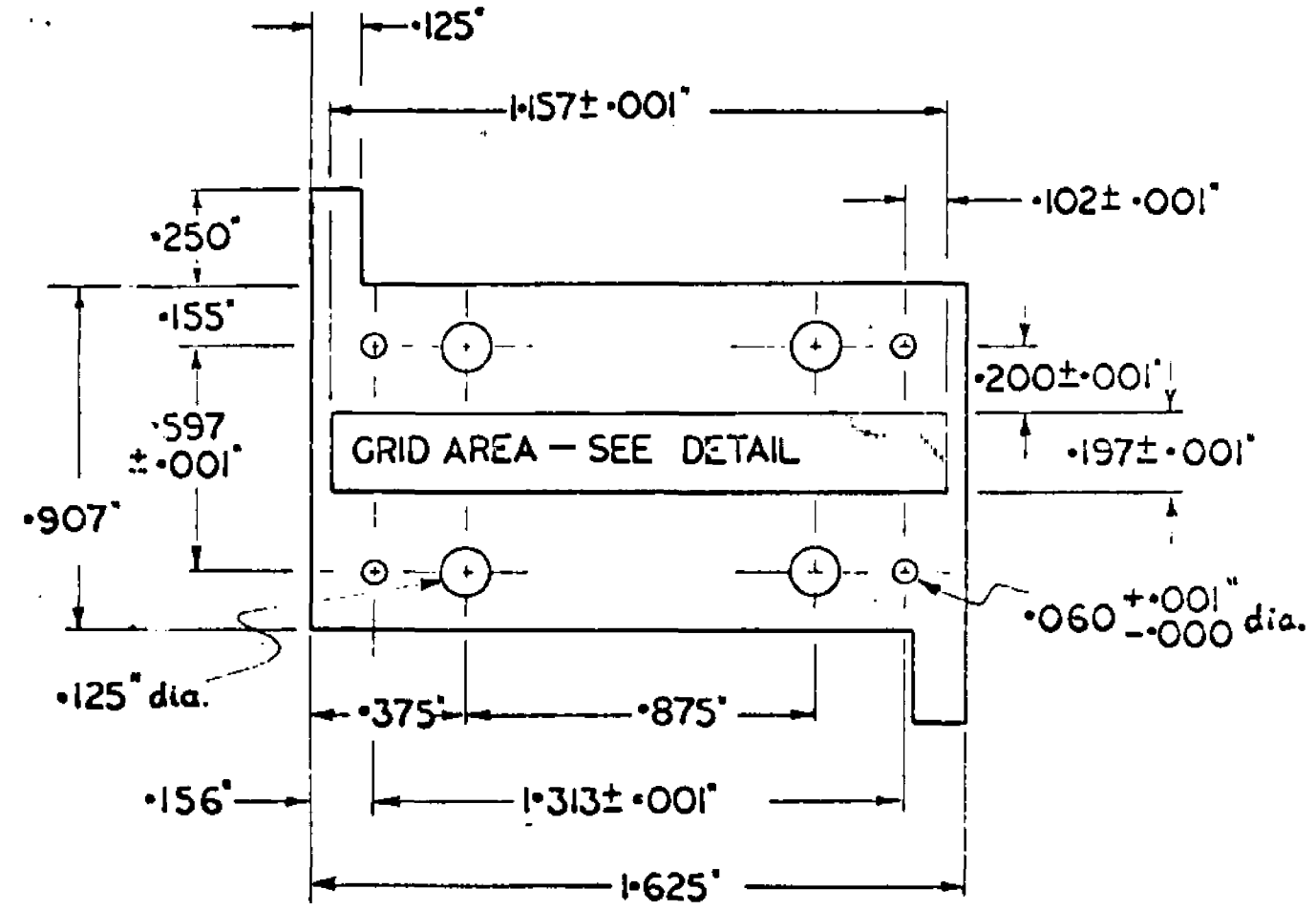

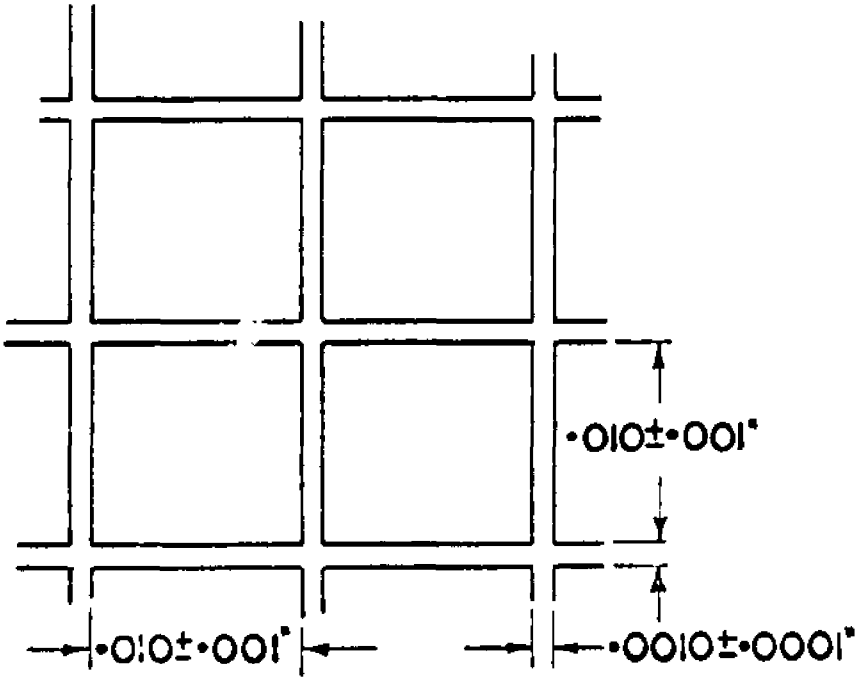

GRID DETAIL

GRID

MATERIAL —
.002" MOLYBDENUM

ALL DIMENSIONS ±.005
EXCEPT AS NOTED

FIGURE 10

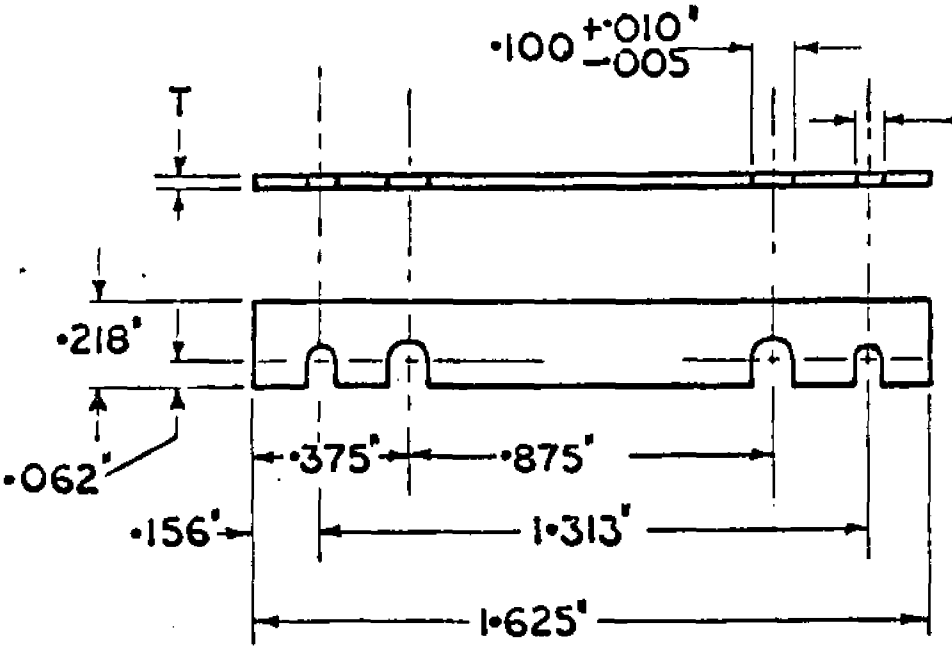

T = .010±.002" / .020±.002"

INSULATOR

MATERIAL — ALUMINUM OXIDE

ALL DIMENSIONS ±.010" EXCEPT AS NOTED

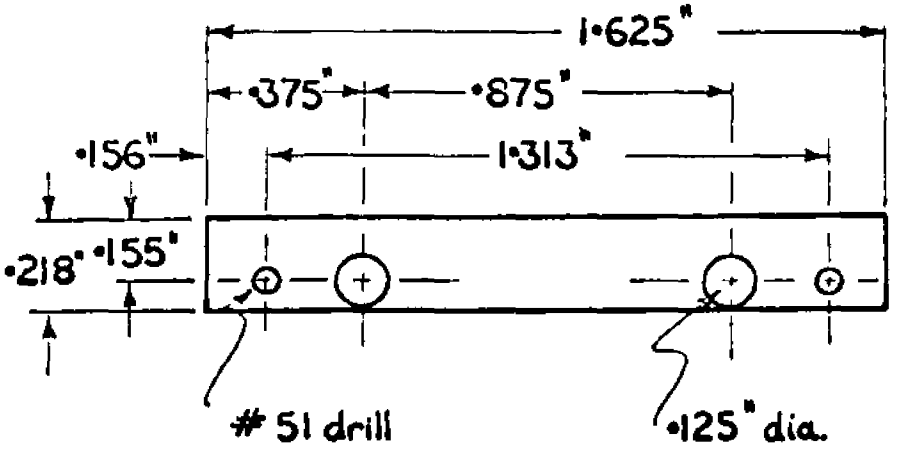

SPACER

MATERIAL —
.005"
.010"
.020"
} MOLYSDENUM

ALL DIMENSIONS ±.005

FIGURE 11

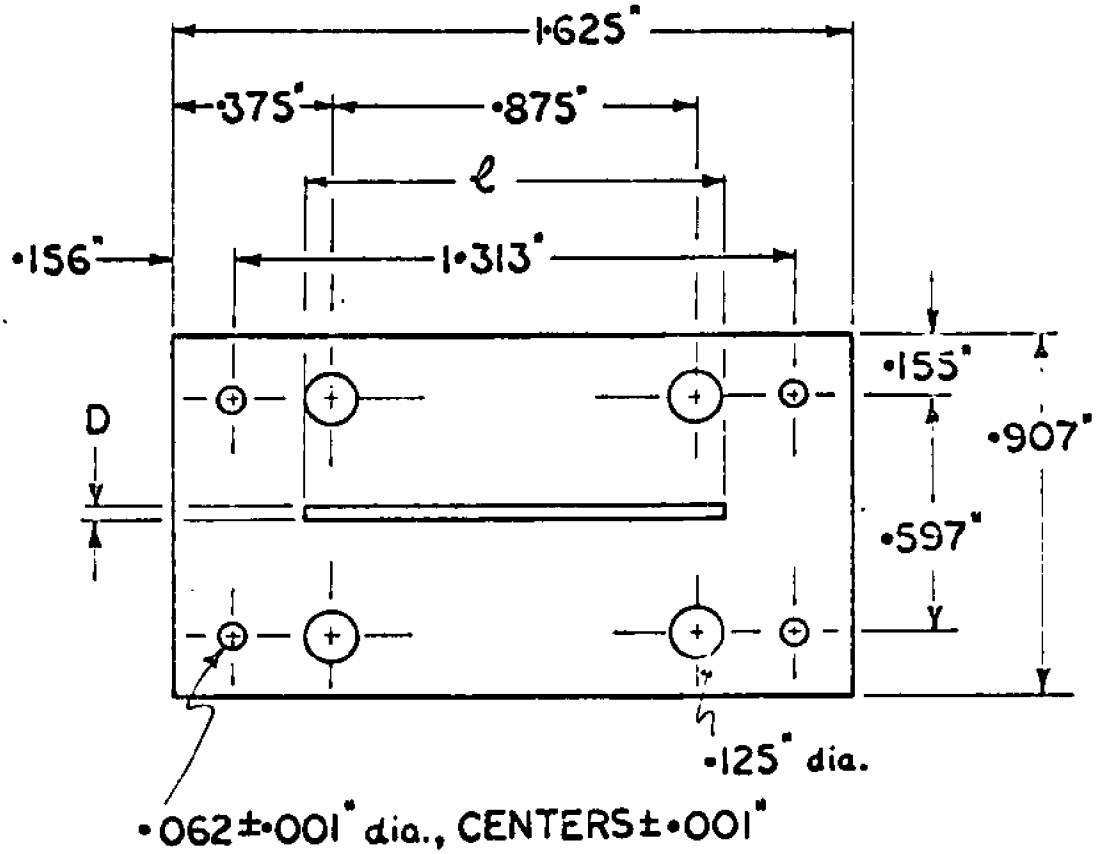

	D	ℓ
MASK	·032±·001"	1·000"
SLIT ANODE	·004±·001"	1·000"
ANODE	—	—

MATERIAL —
·005" MOLYBDENUM

ALL DIMENSIONS ± ·005"
EXCEPT AS NOTED

FIGURE 12

from this tube are mounted on the "channel" block and are used to support the cathode. A tantalum heat shield reduces heat loss from the cathode by radiation. The cathode is operated at a temperature of 700° K, somewhat less than its operating temperature in the 4D32.

The insulators were made from 99.99% Aluminum Oxide and supplied by Sheffield Precision Ceramics, New Jersey in two thicknesses, 0.010" and 0.020". The use of an open structure ensures that they are well removed from the path of the electron beam to prevent charge accumulating on them and thus causing unwanted transverse fields. Two molybdenum blocks, with locating holes machined to a very high tolerance, form the equipotential region which is 0.250" long and 0.062" high. The atom beam is collimated to 0.004" x 0.004" at the entrance to the channel by a set of slits mounted on the gun. The slits are adjusted so that the beam passes through the center of both the 0.250" and 0.062" dimensions. The height 0.062" was chosen so that all atoms scattered by electrons with less than 6 eV energy can escape from the equipotential region without making collisions with the walls. The beam was located in the center of the 0.250" dimension, since a calculation by Celotta[15] has shown that the spatial variation of the space charge depression here is a minimum. Celotta has further shown that field penetration

from the ends of the long narrow equipotential region can be neglected at the center, so that the electron energy at the atom beam is controlled by the potential applied to the walls.

The electron beam is formed by 0.032" x 1.000" masks. Grid separation is fixed at 0.060" which is six times the mask size in order to reduce interelectrode field penetration. This is important if the grids are to be used to shape or alter the electron energy distribution.

At the exit end of the equipotential region a 0.010" mask, which protrudes 0.250" beyond the gun structure itself, is used to position the electron gun so that the electrons intersect the atom beam at right angles. This is accomplished by raising the gun until the atom beam passes just below it, and then moving the gun horizontally (by moving the interaction chamber itself) until it strikes the alignment mask. The gun is then rotated (again by rotating the chamber) to a position where the beam intensity is reduced by the same amount when the chamber is rotated through the same angle in either direction. At this point the atom beam is parallel to the electrode, and hence perpendicular to the electron beam.

Two electrodes, separated by an 0.020" insulator, are used to collect the electron current. The first electrode has an 0.006" x 1.000"

slot cut in the center so that the second collects less than 20% of the total current. Space charge effects on retarding potential difference measurements taken at the second electrode are this reduced.

The gun elements are clamped together by an 0.060" pressure plate screwed onto the main channel support block with four long screws. Four oversized holes were drilled in all the gun elements to allow these screws to pass through.

A magnetic field of about 1000 gauss is used to collimate the electron beam. The field is provided by a C-shaped magnet which was encapsulated in a stainless steel housing, evacuated and then sealed. The magnet is bakeable to 450° C. It is clamped to a plate and mounted on the gun support inside the vacuum system in such a way that the B-field is parallel to the direction of the electron current.

Finally, all gun parts, with the exception of insulators and the pressure plate, were fabricated from molybdenum because of its superior properties at elevated temperatures.

2) Operation of the gun:

Collins[13] and others[14,15] have given great detail on the operation and characteristics of the electron gun, and the gun used in the present experiment conforms by and large to their description. A brief summary follows below.

The first grid, G_1, is used to control the amount of current, and is typically set at 2.5 volts. The second grid, G_2, is used to cut off the low energy tail of the electron energy distribution and is typically operated at around 3.2 volts. The third grid G_3, is operated at the same potential as the equipotential channel, and is insulated from the channel so that the current collected by it can be monitored. The current collected by G_3 is less than 5% of the total collected current and is an indication of how effective the spatial alignment of the grids is. The current collected by the channel is usually about 1% of the total current, and illustrates the effectiveness of the beam masks and magnetic field in collimating the electron beam.

For the measurement of gun current, the slit anode and anode are connected and run at 25 volts positive with respect to the equipotential region. The high voltage prevents secondary electrons emitted from the slit anode surface from returning into the scattering region, and as Celotta's calculation has shown, penetration of this electrode's field at the location of the atom beam (which is in the center) is almost completely negligible.

All voltages for the gun elements are supplied by Kepco modular power supplies operated in the constant voltage mode. The power supply for the heating filament for the cathode is operated in constant current mode to assure the constancy of the cathode temperature.

The gun just described is rugged, mechanically robust and versatile. It's overall reliability is borne out by the fact that is has delivered large currents, constant to within 1%, over long periods, with predictable and reproducible operating characteristics. The basic design, with it's emphasis on spatial alignment of the grid meshes, has been very successful in eliminating almost completely the problem of secondary electrons, a factor which has hitherto affected the usefulness of this type of gun.

3) Retarding potential measurements and absolute energy determination:

The retarding potential difference (RPD) technique has been used to determine the absolute energy and energy spread of the electron beam. Since the energy at the point of intersection between the electron and atom beams is required, it is necessary to correct the RPD measurements for space charge depression of the potential in this region. These corrections involve a solution of Poisson's Equation in the equipotential region and are discussed in detail later.

The recoil technique itself affords the opportunity of making an absolute determination of the energy, and has been exploited with some success in the present experiment. Because of the novelty of this approach and the fact that it enables absolute energies to be

measured directly, it will be dealt with in some detail after the RPD technique is outlined.

Retarding potential difference measurements are performed at the anode, which samples only 20% of the total electron beam and reduces space charge distortion of the electron energy distribution. Figure 13 shows the control circuit used for the measurement. The retransmitting potentiometer of Varian X-Y recorder is fed by a constant voltage power supply, and the output is applied between cathode and anode. A step down transformer is used to introduce a small modulation voltage. The primary of the transformer is connected to the reference output of Princeton Applied Research lock-in amplifier operated at 400 cps. As the voltage applied to the anode is increased, current begins to flow and a voltage with a small AC component appears across the 100 ohm resistor. This AC signal is connected to the input of the lock-in and the output is applied to the Y-input of the recorder.

Curve A of Figure 14 is a typical example of the resulting curve which, in the AC technique, is a plot of $\frac{dI}{dV}$ vs V, where I is the anode current and V the anode voltage. Absolute energies are obtained by reducing the channel potential to a point where the current obtained is so low (usually about 10 μamperes) that space charge

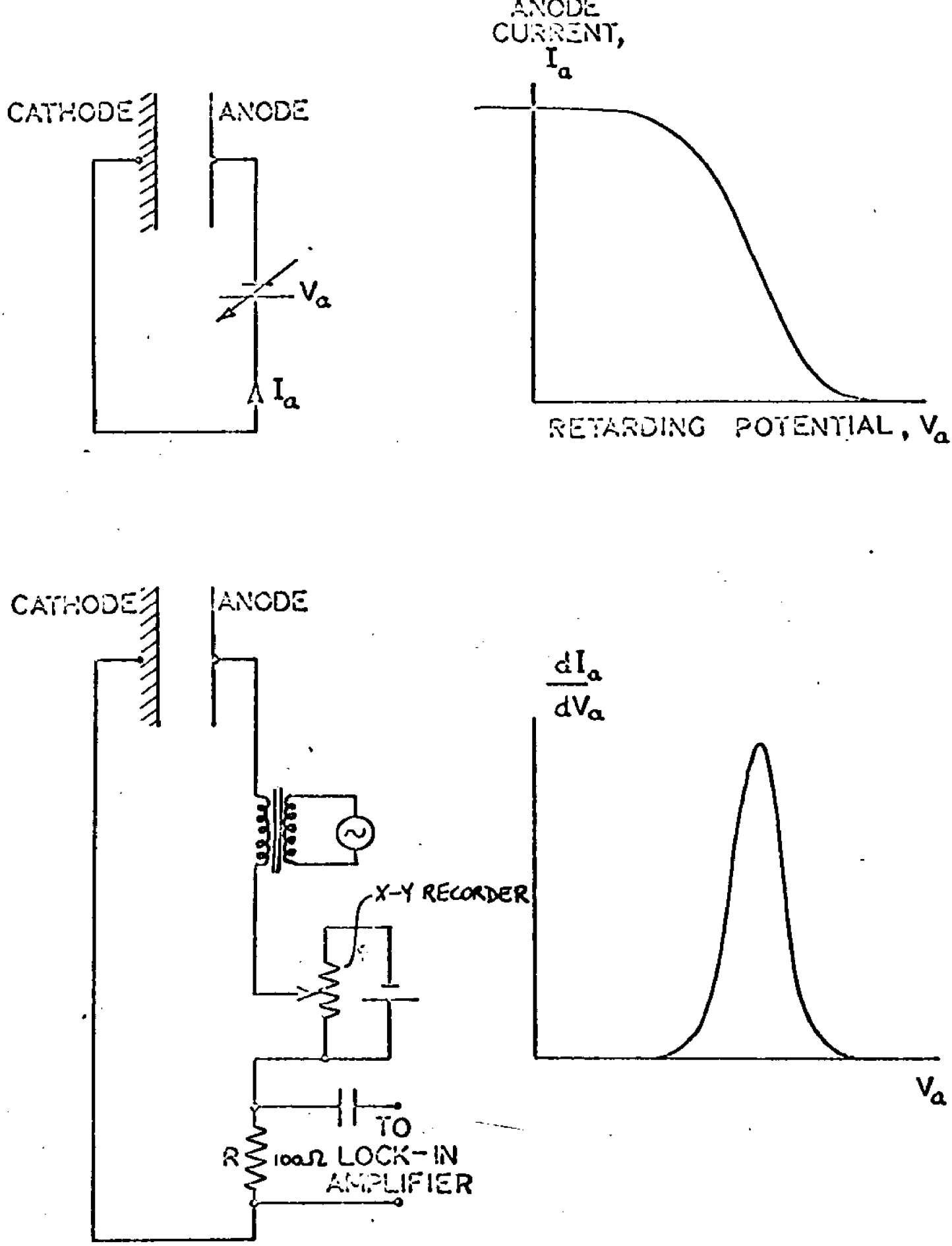
CATHODE
ANODE
V_a
I_a
ANODE CURRENT, I_a
RETARDING POTENTIAL, V_a
CATHODE
ANODE
X-Y RECORDER
TO
R 100Ω LOCK-IN AMPLIFIER
$\frac{dI_a}{dV_a}$
V_a

FIGURE 13

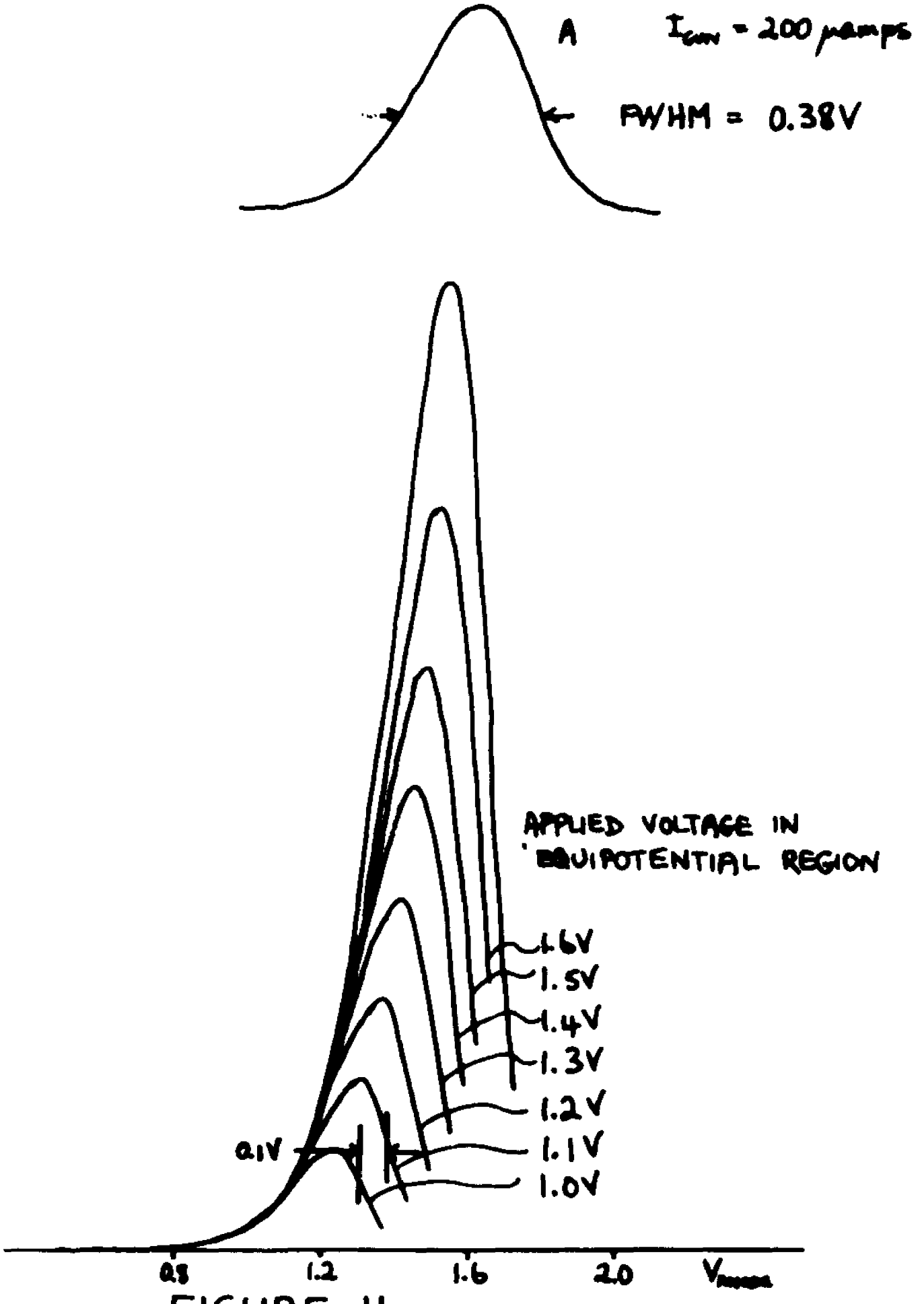
A
I_{emi} = 200 μamps
FWHM = 0.38V
APPLIED VOLTAGE IN EQUIPOTENTIAL REGION
1.6V
1.5V
1.4V
1.3V
1.2V
1.1V
1.0V
0.1V
0.8
1.2
1.6
2.0
V_{accel}

FIGURE 14

considerations don't play a significant role. The difference between the anode potential and applied channel voltage is the contact potential and this plus a determination of the voltage at the peak of the RPD $\left(\frac{dI}{dV}\right)_x$ curve (which allows for the space charge depression in front of the cathode) yields absolute energies to within 0.15 eV. A series of curves of $\frac{dI}{dV}$ versus dialled voltage is shown in Figure 14. The point at which the low energy tail of the curves moves at the same rate as the applied scattering voltage is the point where space charge no longer plays a role.

The electron energy spread measured by the above technique is typically 0.35 volts FWHM in this experiment. However, there is considerable space charge distortion of the RPD curve at the relatively large currents used (about 200 μamperes). It has already been pointed out that because of the slowly varying nature of the space charge depression and the size of the atom beam cross section, there is little variation in potential across the atom beam due to space charge. It is thus felt that the above estimate of the energy spread is considerably greater than the true value.

The method for determination of absolute energies just outlined has to be corrected for space charge modification of the potential.

Since the potential of the atom beam is determined by that applied to the walls, a one-dimensional solution of Poisson's equation yields the necessary correction. Details of this calculation are given in Appendix A.

As an alternative and check on the above technique, a procedure to find the true potential was used which makes use of the properties of the recoil method itself. The method, in essence, consists in the location of a peak in the scattering signal as the detector is swept horizontally into the differential region. The peak occurs for two reasons: 1) the detector collects all potassium atoms excited from the 4S to the 4P state by electrons scattered through zero degrees (polar), 2) the inelastic cross section is peaked in the forward direction. This will be treated in much greater detail in the section on momentum transfer analysis. Equation 18 shows that the angle of recoil of atoms excited by an electron scattered through zero degrees is given by

$$\psi = \frac{mv}{MV_A} \left\{ 1 - \frac{v'}{v} \right\} \tag{14}$$

where V_A is the atomic velocity

v is the electron velocity before collision

v' is the electron velocity after collision

m is the mass of the electron

M is the mass of the atom.

This equation is easily rearranged to yield

$$Z_{peak} = L \frac{m}{M} K \frac{E^{\frac{1}{2}}}{V_A} \left\{ 1 - \left(1 - \frac{Ex}{E} \right)^{\frac{1}{2}} \right\} \qquad (15)$$

where Z is now displacement in the plane of the detector, L the distance between the detector and the electron gun, E the energy of the electrons in volts, Ex the excitation energy (in this case 1.61 eV), and K a constant (= 7.5×10^7).

In order to check the validity of the above equation, an experiment was performed to locate the position of the excitation peaks as the energy E of the electrons is changed. Figure 15 shows some of these curves as well as a profile of the unscattered beam. The peaks at high energy reproduce the beam shape fairly well. The broadening which occurs at the low energies arises primarily from the distributions in atom and electron velocities.

Since the contact potential is only a small correction at the highest energy used, a reasonable estimate of it yields E to high accuracy. A variation of ± 0.2 volts in the contact potential results in an error of less than 1% at 30 volts. With the value of Z obtained from the measurement of peak displacement at this energy, the atom velocity is found. Equation 15 is now reduced to

$$Z = (\text{const})\ E^{\frac{1}{2}} \left\{ 1 - \left(1 - \frac{Ex}{E} \right)^{\frac{1}{2}} \right\} \qquad (16)$$

where the value of the constant is now known.

A simple computer program was written to calculate Z as a function of E. The circles in Figure 16 show the peak displacements

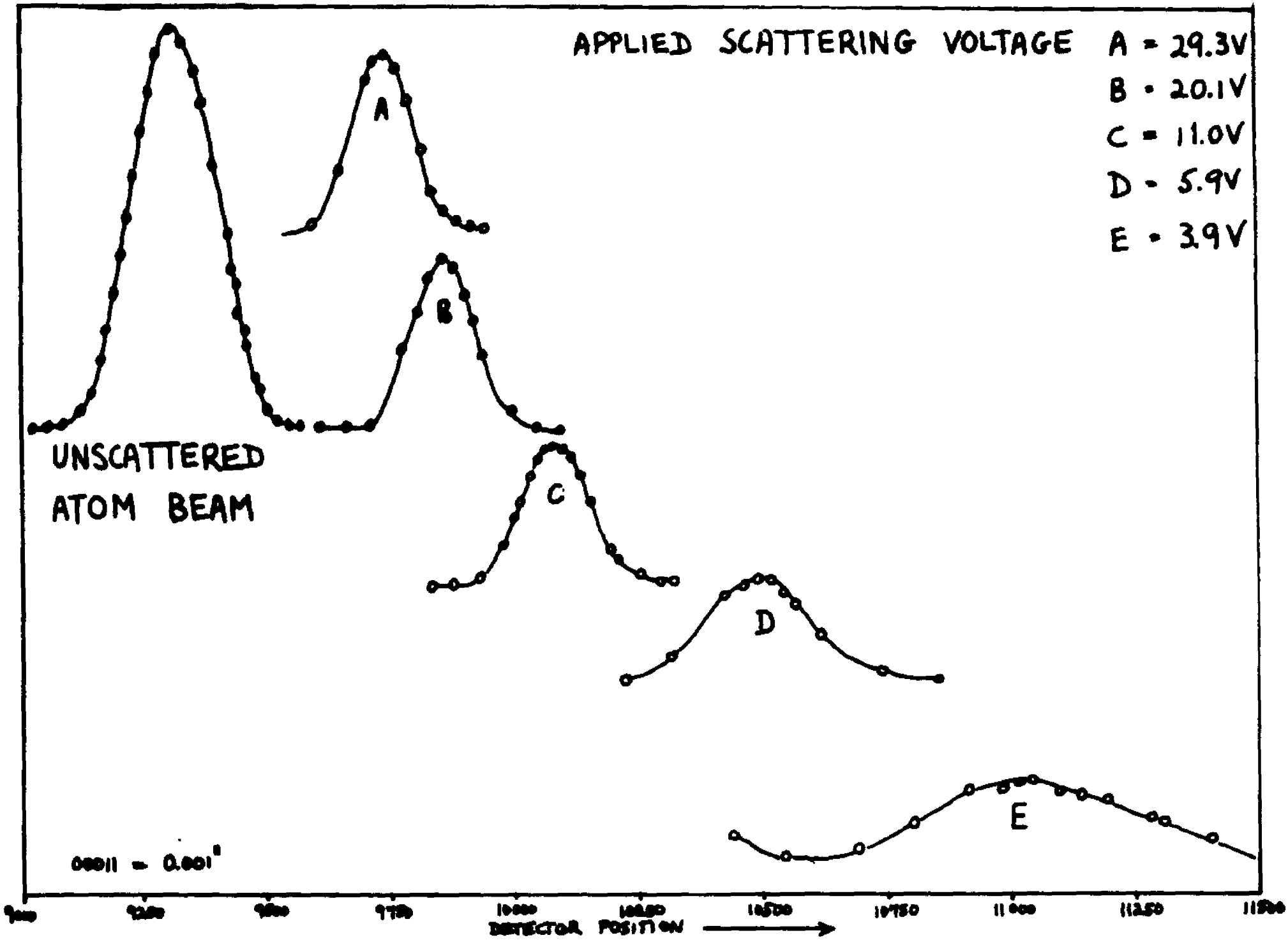

FIGURE 15 DISPLACEMENT OF EXCITATION PEAK

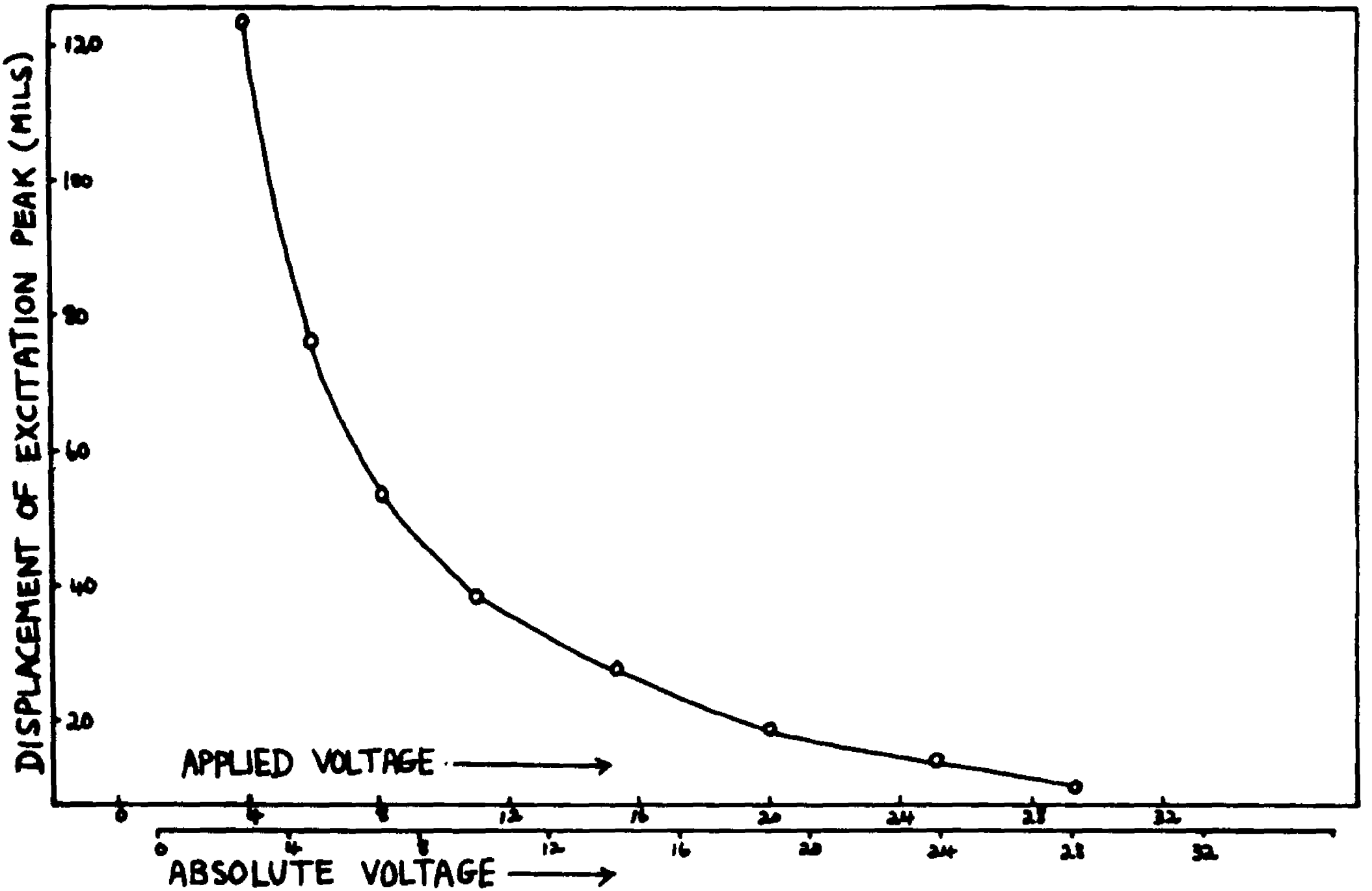
DISPLACEMENT OF EXCITATION PEAK (MILS)
120
80
40
20
APPLIED VOLTAGE
0
4
8
12
16
20
24
28
32
ABSOLUTE VOLTAGE
0
4
8
12
16
20
24
28
32

FIGURE 16

plotted as a function of the applied scattering voltage. The theoretical curve is fitted to the data by sliding it along the voltage axis until a best fit is found. The contact potential can then be read off by comparing experimental and theoretical voltage scales. The excellent fit between theory and experiment in addition confirms the accuracy with which the above equations predict the kinematics of the recoiling atoms.

In practice to find the electron energy for a particular experiment only two determinations are made: the location of the excitation peak at a scattering voltage of 31.6 volts (which is taken as 30 volts absolute) and at the voltage to be used for the experiment. It is easily shown that the energy is given by

$$E = \frac{K^2}{C^2}\left\{\frac{2K}{C} - Ex\right\} - 1 \qquad (17)$$

Where $K = E_o\left\{1 - \left(1 - \frac{Ex}{E_o}\right)^{\frac{1}{2}}\right\}$

E_o = 30 volts

C = X_o/X the ratio of the peak displacements

X_o = peak displacement for E_o

X = peak displacement for E.

The experimental error involved in the location of the peaks is about ± 0.001". This leads to an uncertainty of ± 0.15 eV in the determination of absolute energies.

Since the above method is direct in contrast to RPD measurements which require two measurements, and a <u>theoretical</u> correction for the space charge depression of potential, it provides an interesting

and novel technique for the determination of absolute energies especially when large currents resulting in significant space charge corrections are employed. In order to see how the potential changes with current, a series of measurements of peak displacements against electron gun current with the scattering voltage fixed was performed. These are shown in Figure 17. Two features are immediately obvious: 1) the peak displacement increases with gun current indicating that the potential at the location of the atom beam is decreasing as predicted by the solution of Poisson's Equation outlined in Appendix A, 2) the shape of the curves and in particular the width FWHM is by and large unaffected by the change of current. This is in agreement with the earlier stated supposition that space charge broadening of the electric energy distribution is unimportant because of the atom beam cross section.

The curves of Figure 17 also agree well with the theoretical predictions of Poisson's Equation. The energy shift from curve A to E, calculated by taking ratios of the peak displacements is 0.40 ± 0.15 eV, while the calculations of Appendix A show the space charge minimum moving from 4.16 eV to 3.74 eV. The experiment will be repeated again at much lower energies where peak displacements are much larger and consequently can be more accurately determined, and where the space charge corrections themselves are significantly greater.

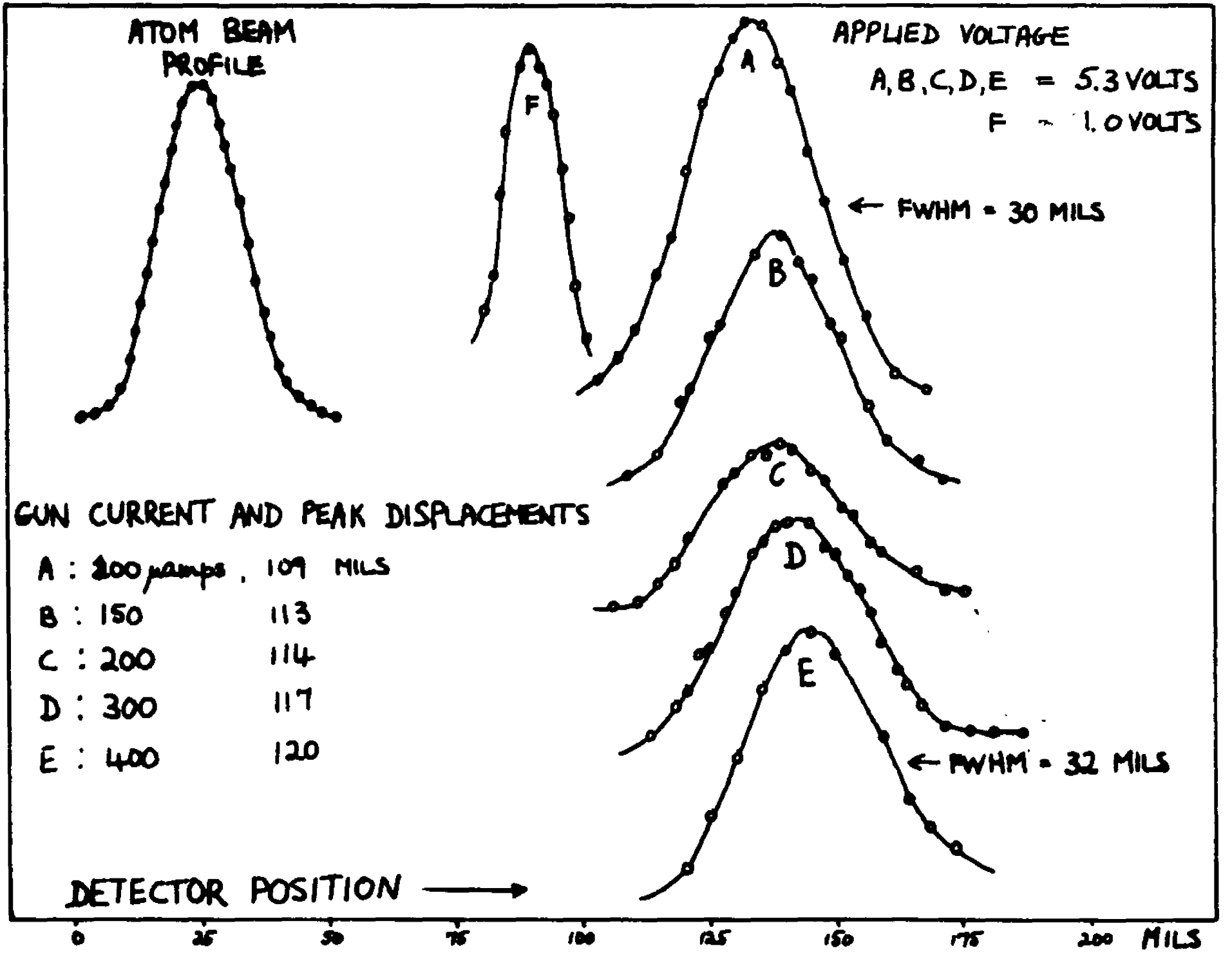

FIGURE 17 PEAK DISPLACEMENT VS GUN CURRENT

In summary, the above technique can be used to determine absolute energies to within ±0.15 eV. It is simple, direct and requires knowledge only of the kinematics of the recoiling atoms. Quantitative comparisons with the predictions of Poisson's equations in situations where space charge is an important factor are possible. It should also be recognized that although the technique is useful only above excitation energies the excellent agreement with the RPD method modified by appropriate space charge corrections assures the validity of the latter approach at energies below threshold.

Finally, the location and shape of the excitation peak can be used to study the use of the Stern-Gerlach magnet as a velocity selector. Figure 18 shows how the peak position and width changes with the displacement of the oven off axis. It is clear that the greater the oven displacement the smaller the spread in atom velocities and the smaller the mean velocity of the transmitted atom beam are. This is in agreement with the predictions of Rubin and Bederson[12].

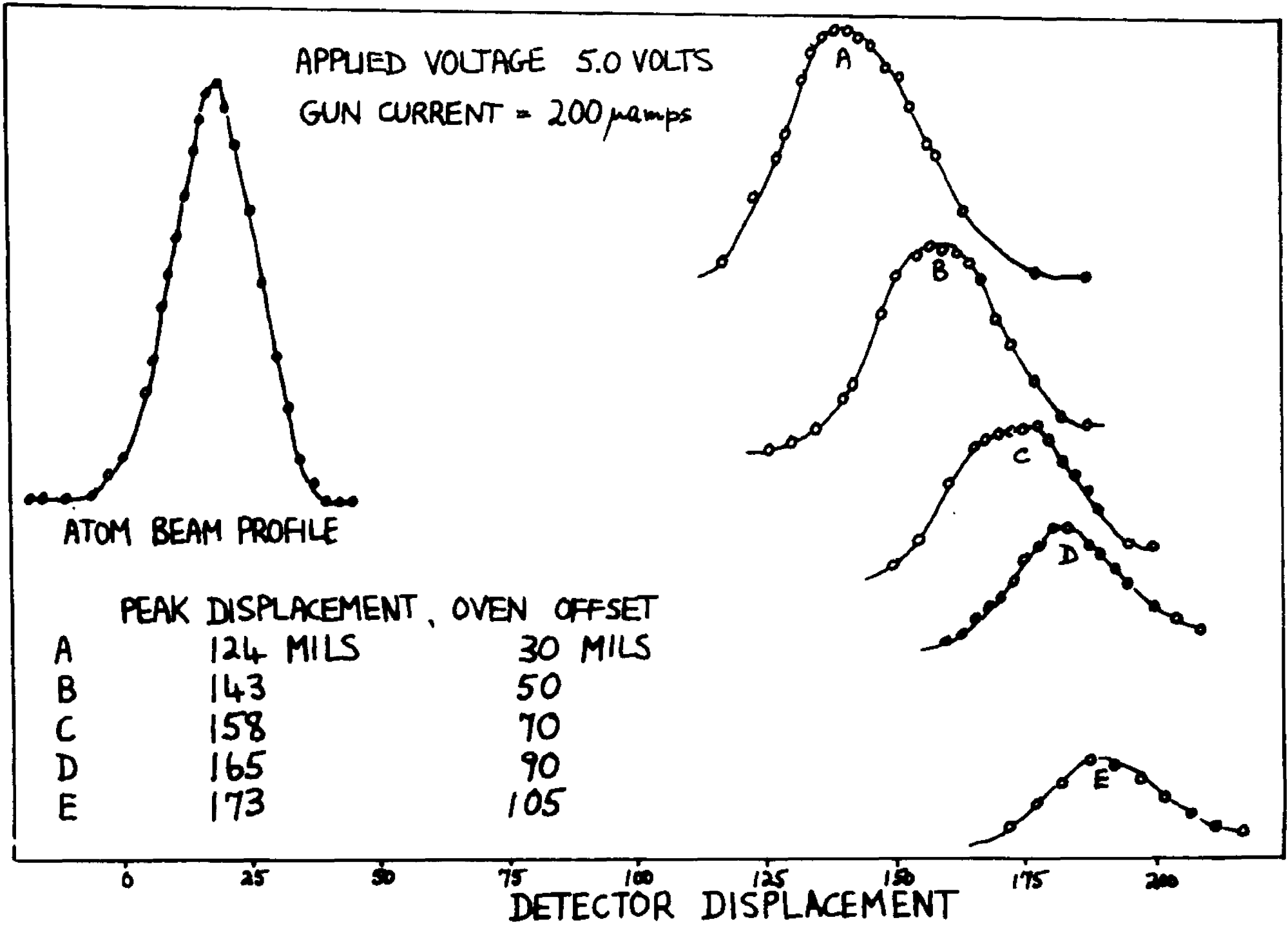

FIGURE 18 PEAK DISPLACEMENT VS OVEN OFFSET

IV. Momentum transfer analysis*

Consider the momentum transfer problem for an atomic beam which is cross fired at right angles by an electron beam. The electron beam travels in the +z direction while the atoms travel within a small cone of angles about the y axis (see Fig. 19). The coordinates of an unscattered atom in the interaction region are (x_o, y_o, x_o) and in the plane of the detector are (x', y', z'), while the coordinates of a scattered atom in the detector plane are (x, y, z). The direction of the velocity of an unscattered atom is specified by the angles (ϕ, χ). Here ϕ is the angle between the projection of the atomic velocity in the y-z plane and the y axis, and χ is the angle between the atomic velocity and its projection in the y-z plane. (When $\phi_o, \chi_o << \phi, \chi$, then ϕ, χ are simply the scattering angles in the plane of scattering and perpendicular to the plane of scattering respectively).

The detector motion has two degrees of freedom so that the atom scattering signal can be measured as a function of ϕ and χ. The relationship between the atom and electron scattering angles are given by

$$\phi_i' = a - \beta_1 \cos\theta \tag{18}$$

$$\chi_i' = \beta_1 \sin\theta \sin\varphi \tag{19}$$

* This analysis was first presented in reference 16.

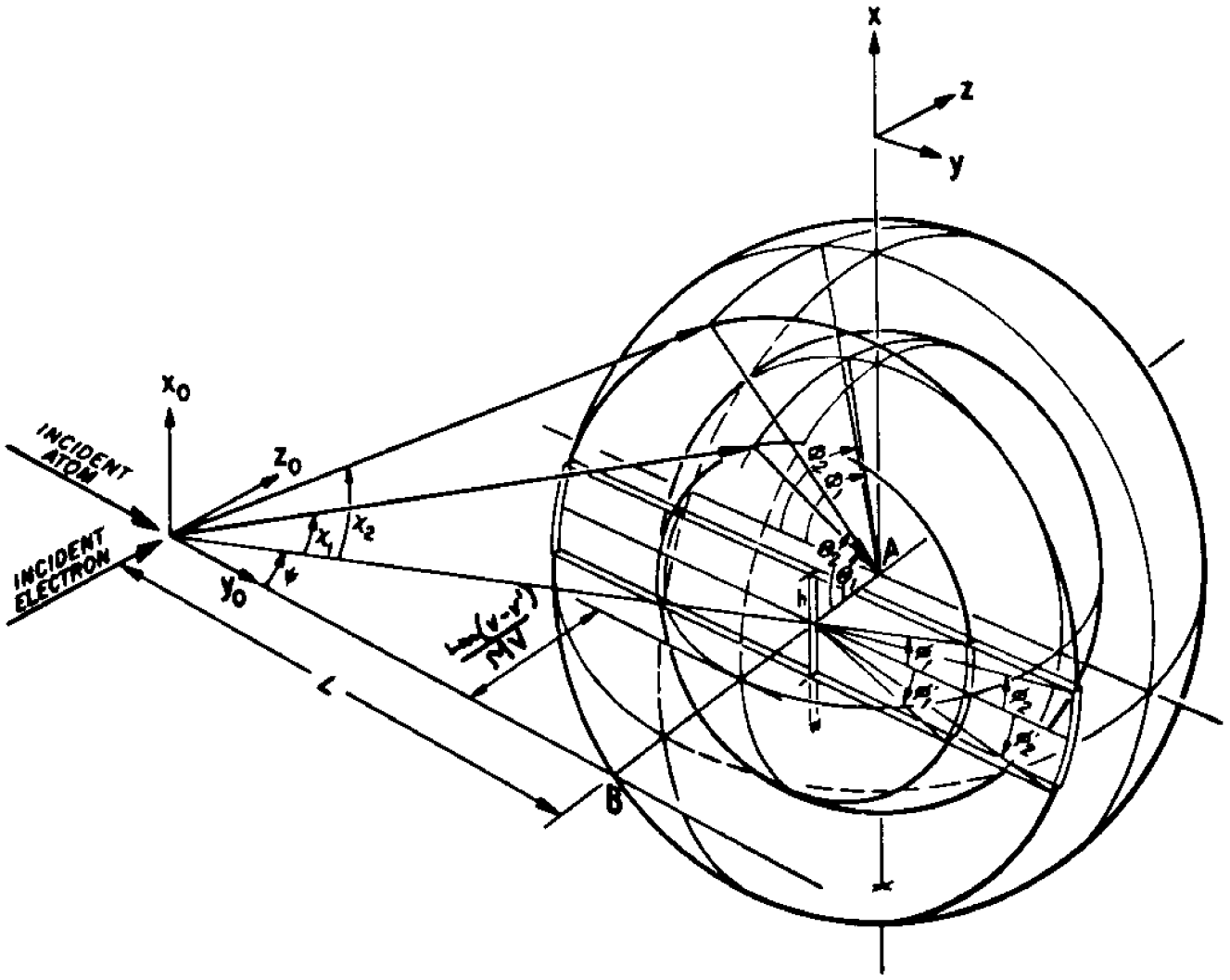
X
Z
y
x_0
z_0
INCIDENT ATOM
INCIDENT ELECTRON
y_0
x_1
x_2
$\frac{L(v-v')}{Mv}$
L
A
B
h

FIGURE 19

where $\phi' = \phi - \phi_o$

$\chi' = \chi - \chi_o$

$\alpha = \frac{mv}{MV}$ $\beta_i = \frac{mv_i'}{MV}$

m = Mass of the electron

v = velocity of the incoming electron

v_i' = volocity of the scattered electron after excitation of the i^{th} channel

M = mass of the atom

V = velocity of the incoming atom

It has been assumed that ϕ_i' and χ_i' are small and that the magnitude of the atoms' velocity is not changed in the collision. Under this assumption there is a one-to-one relationship between the atom scattering angle ϕ_i' and the electron scattering angle θ. Thus by measuring the number of atoms scattered as a function of ϕ_i' and using equation (18) one obtains the number of electrons scattered as a function of θ.

The dependence of the atom scattering signal on the angle χ_i' plays the major role in distinguishing between elastic and inelastic events. The maximum value of χ_i' for a given value of θ is given by

$$\chi_i'_{max} = \beta_i \sin \theta \qquad (20)$$

Notice that $\chi_i'_{max}$ is proportional to v_i' the velocity of the scattered electron. $\chi_i'_{max}$ will therefore be greater for an elastic than inelastic event. Thus there will be a range of values of χ_i' for which only

elastic events will be observed. There will be another range of χ_i' 's in which the scattering signal will represent a combination of two events, elastic and excitation to the 1^{st} excited state, and so on. This is demonstrated in Fig. 20. Here we have plotted equation 20 for the scattering of a 3 volt electron from a potassium atom. The three curves represent an elastic event in which the atom is excited to the 1^{st} excited state, and an event is which the atom is excited to the 2^{nd} excited state. The ranges of χ_i' discussed above can be obtained from the figure as a function of ψ_i'.

Consider now the interaction of the elctron and atom beams within an element of volume $dx_o dy_o dz_o$. The electron-number current density within this region for electrons whose energies are in the range dE is $J_e(x_o, y_o, z_o; E)dE$, while the number of density of atoms in this region with velocities lying within the angular range $d\psi_o$, $d\chi_o$ and possessing speeds in the range of dV is

$$M_a(x_o, y_o, z_o; \psi_o, \chi_o, V)\, d\psi_o\, d\chi_o\, dV$$

The number of atoms scattered from the element dx_o, dy_o, dz_o into the angular range $d\psi$, $d\chi$ possessing speeds in the range dV is

$$dN_s = \sum_i J_e(x_o, y_o, z_o; E)dE\, dx_o dy_o M_a(x_o, y_o, z_o; \psi_o, \chi_o, V)d\psi_o d\chi_o dV$$
$$\times\, \sigma_i'(\psi-\psi_o, \chi-\chi_o; E, V)\, d\psi d\chi dz_o \qquad (21)$$

where $\sigma_i'\, d\psi d\chi$ is the probability of scattering an atom of velocity

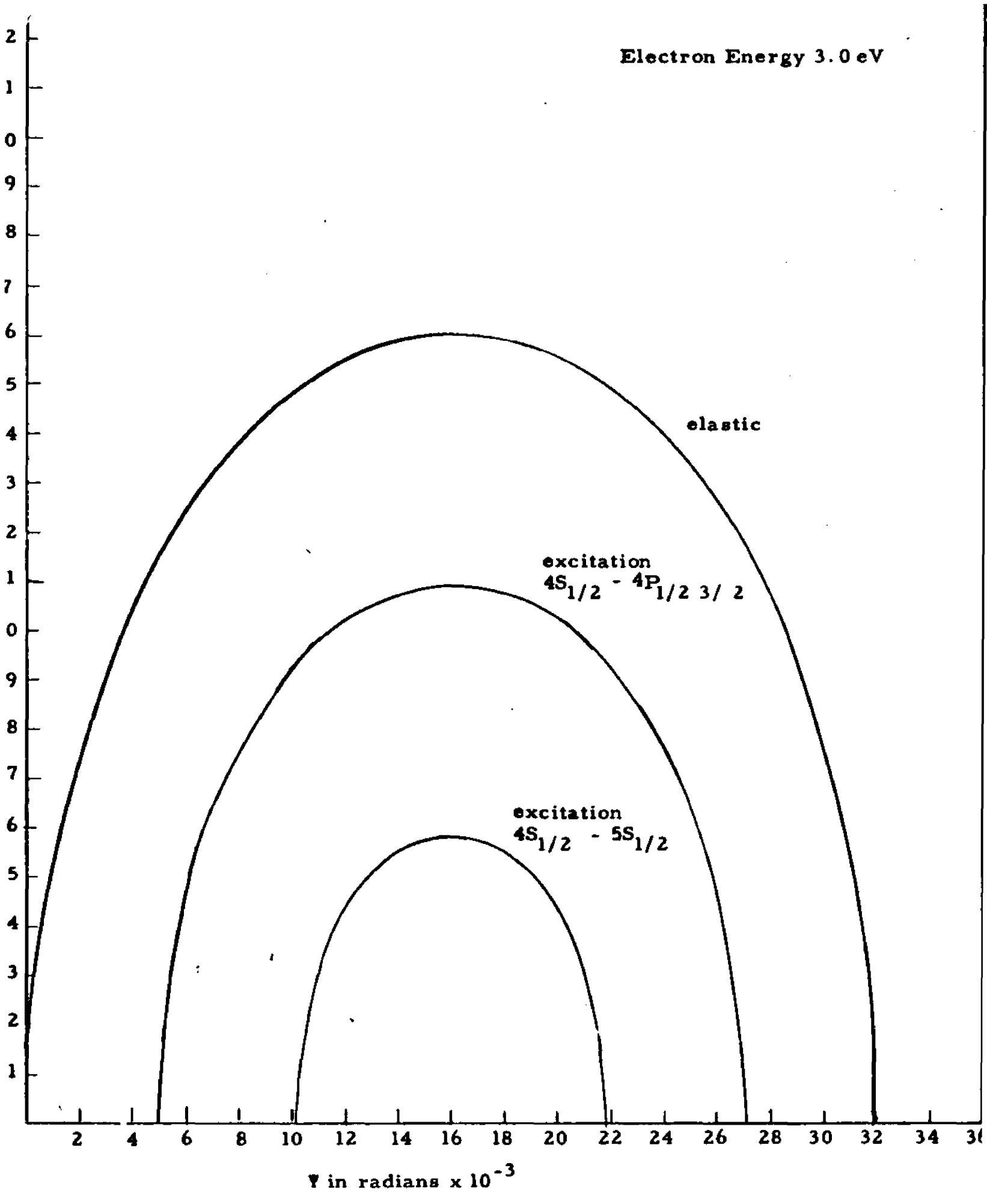
Electron Energy 3.0 eV
elastic
excitation
$4S_{1/2} - {}^4P_{1/2\ 3/\ 2}$
excitation
$4S_{1/2} - 5S_{1/2}$
2 4 6 8 10 12 14 16 18 20 22 24 26 28 30 32 34
ϑ in radians x 10^{-3}

FIGURE 20

V by an electron of energy E into the angular range $d\psi$, $d\chi$ from the angles ψ_o, χ_o with excitation of the $i^{\underline{th}}$ channel. All recoil angles are assumed to be small and we therefore write

$$d\psi_o = dz_o'/(L+y_o), \qquad d\chi_o = dx_o'/(L+y_o)$$

$$\psi-\psi_o = (z-z_o')/(L+y_o), \qquad \chi-\chi_o = (x-x_o')/(L+y_o)$$

where L is the distance from the detector plane to the center of the interaction region. The total number of atoms ΔN_s scattered into dxdz at x, z is

$$\Delta N_s = dxdz \sum_I \int M_A[x_o, y_o, z_o; (z_o'-z_o)/(L+y_o), (x_o'-x_o)/(L+y_o), V],$$
$$xJ_e(x_o, y_o, z_o; E))dE dx_o dy_o dz_o' dx_o' (L+y_o)^{-2} dV$$
$$x\ \sigma_i'[(z-z_o')/(L+y_o), (x-x_o')/(L+y_o); E, V] dz_o/(L+y_o)^2 \qquad (22)$$

Now the number of unscattered atoms reaching $dx_o'dz_o'$ per second with speeds in dV is

$$J_a(x_o', z_o'; V)dx_o'dz_o' = \left\{\int M_a(x_o, y_o, z_o; \frac{z_o'-z_o}{L+y_o}, \frac{x_o'-x_o}{L+y_o}, V\frac{dx_o dz_o}{(L+y_o)^2}, VdV)\right\}$$
$$x\ dx_o'dz_o' \qquad (23)$$

If J_e is not a function of x_o, z_o, Equation 22 can be integrated over x_o, z_o to obtain

$$\Delta N_s = dxdz \int \sum_I J_e(y_o, E)dy_o dE J_a(x_o', z_o', V)dx_o'dz_o'(L+y_o)^{-2}\sigma_i' dV/V \qquad (24)$$

The total electron current intersecting the atom beam in the energy range dE is

$$I_e(E)dE = \int J_e(x_o, y_o; E)dx_o dy_o dE \qquad (25)$$

and if J_e is not a function of x_o'

$$I_e(E)dE = H\int J_e(y_o; E)dy_o dE \qquad (26)$$

where H is the height of the scattering region. If, finally, $y_o << L$ and since J_a is not a function of y_o, we perform the y_o integration to obtain

$$\Delta N_s = \frac{1}{HL^2} dxdz \sum_I I_e(E)dE J_a(x_o', z_o', V)dx_o' dz_o' \sigma_i' dV/V \qquad (27)$$

A detector of width D and height H will therefore receive a signal

$$\Delta N_s = \frac{1}{HL^2} \sum_I \int_{z-D/2}^{z+D/2} dz' \int_{x-H/2}^{x+H/2} dx' \int I_e(E)dE J_a(x_o', z_o', V)dx_o' dz_o' \sigma_i' dV/V \qquad (28)$$

The cross section as a function of the atom scattering angles $\sigma(\Psi_i', \chi')$ is related to the cross section as a function of the electron polar and azimuthal scattering angles θ, φ by

$$\sigma(\theta) \sin\theta d\theta d\varphi = \sigma'(\Psi', \chi') d\Psi' d\chi' \qquad (29)$$

This gives

$$\sigma_i'(\Psi'\chi') = \sigma_i(\theta)/\beta_i^2 \sin\cos\varphi$$

If the integration over dx in 28 with $z-z_o'$ and hence θ fixed is performed first, we obtain

$$\Delta N_s = \frac{1}{HL} \sum\int J_e(E)dE J_a(x_o', z_o', V)\frac{dV}{V} dx_o' dz_o' \int_{z-D/2}^{z+D/2} dz' \frac{\sigma(\theta)}{\beta_i} \int_{\varphi_1}^{\varphi_2} d\varphi \qquad (30)$$

where

$$\varphi_2 = \sin^{-1}\left\{\frac{x-x_o'+H/2}{L\beta_i \sin\theta}\right\} \quad (x-x_o'+H/2) < L\beta_i \sin\theta$$

$$\varphi_1 = \sin^{-1}\left\{\frac{x-x_o'-H/2}{L\beta_i \sin\theta}\right\} \quad (x-x_o'-H/2) < L\beta_i \sin\theta$$

$$\varphi_2 = \pi/2 \qquad (x-x_o'+H/2) \geq L\beta_i \sin\theta$$

$$\varphi_1 = \pi/2 \qquad (x-x_o'-H/2) \geq L\beta_i \sin\theta$$

Finally, integration over dz gives

$$\Delta N_s = \frac{1}{H} \sum\sum I_e(E)dE J_a(x_o' z_o 1, V)dx_o' dz_o' \frac{dV}{V} \int_{\theta_1}^{\theta_2} \sigma(\theta) \sin\theta(\varphi_2 - \varphi_1)d\theta \tag{31}$$

where

$$\theta_1 = \cos^{-1}\left\{\frac{a-(z-z_o'-D/2)/L}{\beta_i}\right\}$$

$$\theta_2 = \cos^{-1}\left\{\frac{a-(z-z_o'+D/2)/L}{\beta_i}\right\}$$

The fraction of the total scattered atom collected by the detector of height H for a given polar angle θ is called the "azimuthal form factor" (AFF) and is defined

$$\gamma_i(\theta, V, E) = (\varphi_2 - \varphi_1)/\pi$$

Equation 31 is the general equation relating recoil-scattering signal at a detector of height H and width D at a displacement z from the beam axis to the beam currents, shapes, and velocity distributions. It should be noted that the relation between electron and atom

scattering angles depend upon electron energy loss and there is thus a separate $\theta - \psi$ relation for each scattering channel. Thus 31 includes a summation over all energetically allowed inelastic (as well as elastic) collision channels.

The AFF is a sharply peaked function of θ with maxima at 0° and 180°, and as a result it is expected that ΔN_s will be sharply peaked at z corresponding to 0° scattering. There should also be a second peak in ΔN_s corresponding to 180° scattering. However, this will be much smaller than the 0° peak, first, because $\sigma(180^{\circ})$ is usually much smaller than $\sigma(0^{\circ})$, and second because the velocity distribution in both atom and electron beams produces a larger dispersion in ΔN_s at 180° than at 0°. Figure 21 illustrates these points, referring to calculated AFF's for the elastic scattering in potassium at 3.0 eV.

The horizontal displacement of the peak corresponding to excitation of the $i^{\underline{th}}$ channel is given by

$$z_i - z_o' = L(\alpha - \beta_i)$$

This particular property of the atom beam recoil method is used to determine absolute energies. A detailed description of this application is given in the section dealing with determination of absolute energies.

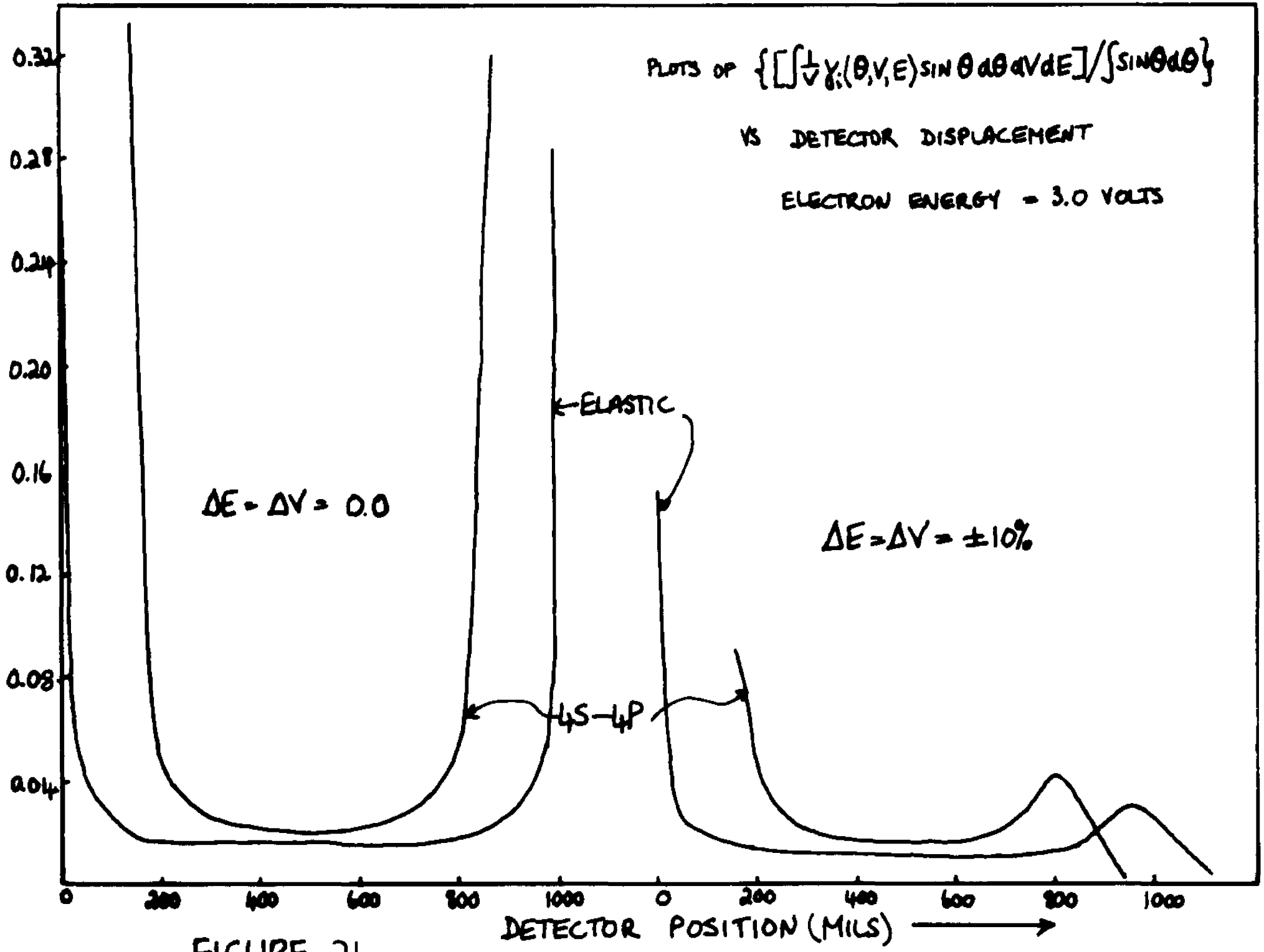
PLOTS OF $\{[\int\int \gamma_i(\theta,V,E)\sin\theta\, d\theta\, dV\, dE]/\int\sin\theta\, d\theta\}$
VS DETECTOR DISPLACEMENT
ELECTRON ENERGY = 3.0 VOLTS
0.32
0.28
0.24
0.20
0.16
0.12
0.08
0.04
ELASTIC
$\Delta E = \Delta V = 0.0$
$\Delta E = \Delta V = \pm 10\%$
4S-4P
0
200
400
600
800
1000
0
200
400
600
800
1000
DETECTOR POSITION (MILS)

FIGURE 21

V. Description of experimental and data taking procedures

1) Atom Beam

A Thermo-Electric temperature controller is used to bring the oven up to operating temperature for the duration of the experiment which is often as long as 7 or 8 days. The operating temperature is usually fixed at around 310°C.

The oven is then offset 0.040", which is ten times the slit width, and the B-field on the Stern-Gerlach magnet adjusted so that the transmitted atom current is a maximum. The atom beam current is amplified by a Bendix electron multiplier and read on a Model 600A Keithley electrometer.

It usually takes 2 hours for the oven temperature to reach equilibrium. At operating temperature the atom beam current which passes through the interaction region is typically on the order of 2×10^7 atoms/sec. During the course of an experiment, the detector is periodically scanned onto the beam axis to check the magnitude of the beam current and the temperature of the oven is monitored before a measurement is made in the differential region. The temperature is held constant to within $\pm 1^\circ$ C. by the controller and variations in atom beam current are rarely found to be greater than 3 or 4%.

2) Method of detection of scattering signal:

A block diagram of the circuit used to detect the scattering signal is shown in Figure 22. An AC technique is used to detect and amplify the scattering signal. An electronic switch, driven by the reference output of a Model HR-8 lock-in amplifier, is used to turn the voltage on G_2 of the electron gun on and off at a frequency of 40 cps. The scattering signal now appears at the detector at the modulation frequency and is fed to the input of the lock-in through the Keithley electrometer which acts as a cathode follower. The output of the lock-in is then fed into a data acquisition system where the scattering signal is recorded.

Total cross section measurements are obtained by moving the detector onto the beam axis, and measuring the 'scattering-out' signal, which is a measure of the number of atoms scattered out of the detector when the atom beam is crossfired by the electron beam. When the detector is in the differential region, the number of atoms scattered into the detector is recorded and the phase of this signal is opposite to that of the scattering in signal. Scattering signals vary typically from 1×10^2 to 2×10^4 atoms/sec in the differential region. Care is taken to ensure that the input impedence of the Keithley is such that scattering signal is not lost through cable and other stray capacitance.

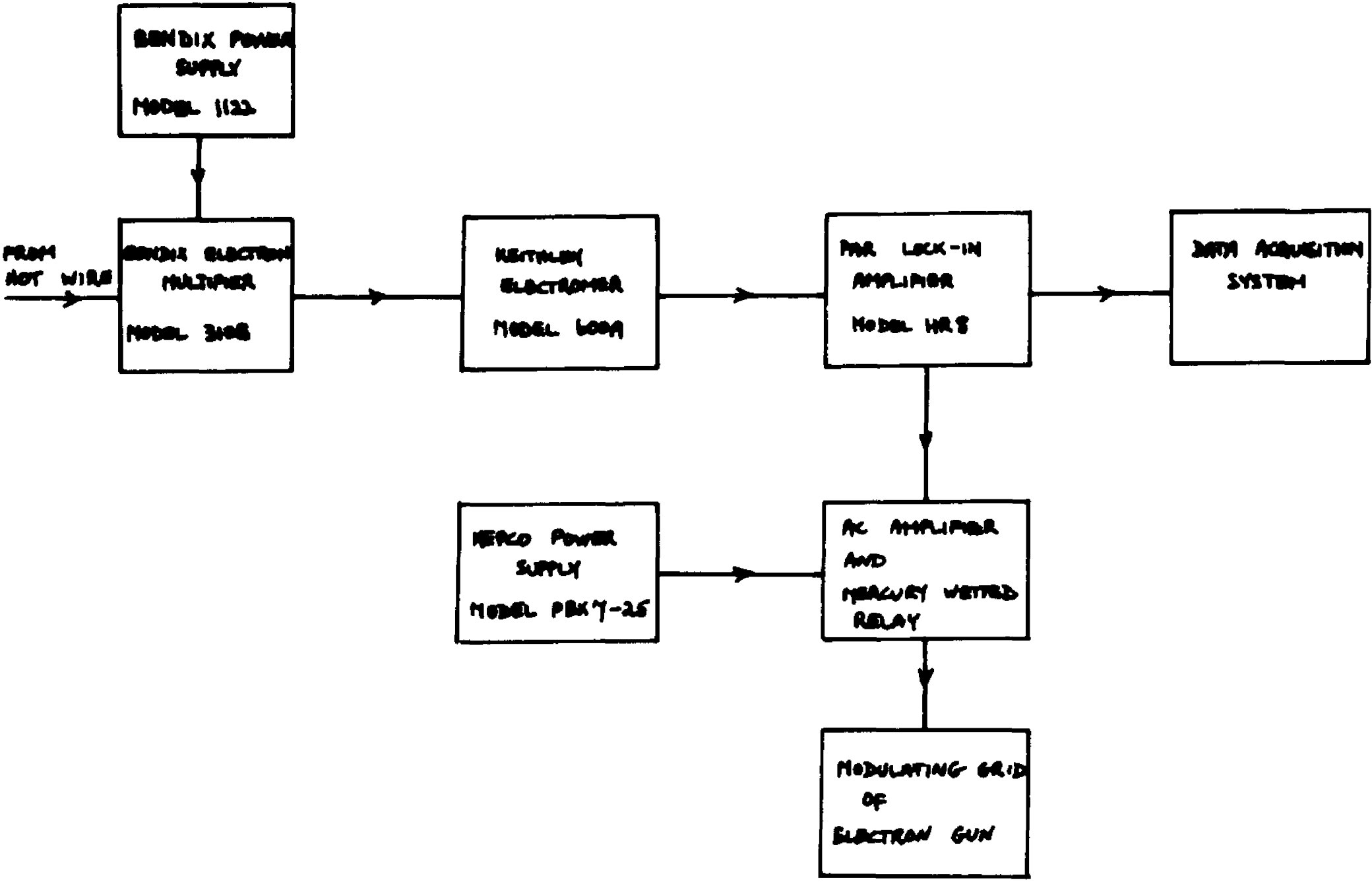

FIGURE 22 SCATTERING SIGNAL CIRCUITRY

Typical settings of the instruments are as follows:

Keithley:	Multiplier	0.1 volts
	Range	10^{-6} amperes
Lock-in:	Sensititvity	200 μ volts or 500 μ volts
	Frequency	40 HZ
	Time constant	10 secs, 12db/octave
	Q	10

Electron Multiplier Dynode Voltage 1500 volts.

A full scale reading on the 200 μ volt range corresponds to 1×10^{3} atoms/second. Little useful information can be obtained when signals are less than 20 μ volts which corresponds to 100 atoms/sec. A review of the sources of noise in the experiment will be included later. Suffice to say at this stage that care was taken in the choice of the above list of instrment settings to ensure that amplifier noise did not play any role.

3) Data acquisition system:

Because it is necessary in this experiment to accumulate data at a large number of points in the differential region and integrate over long periods of time, a data acquisition system was designed and assembled to permit automatic recording of the data and allow the experiment to be run on a 24 hour basis.

Figure 23 illustrates the main features and logic of the system. All

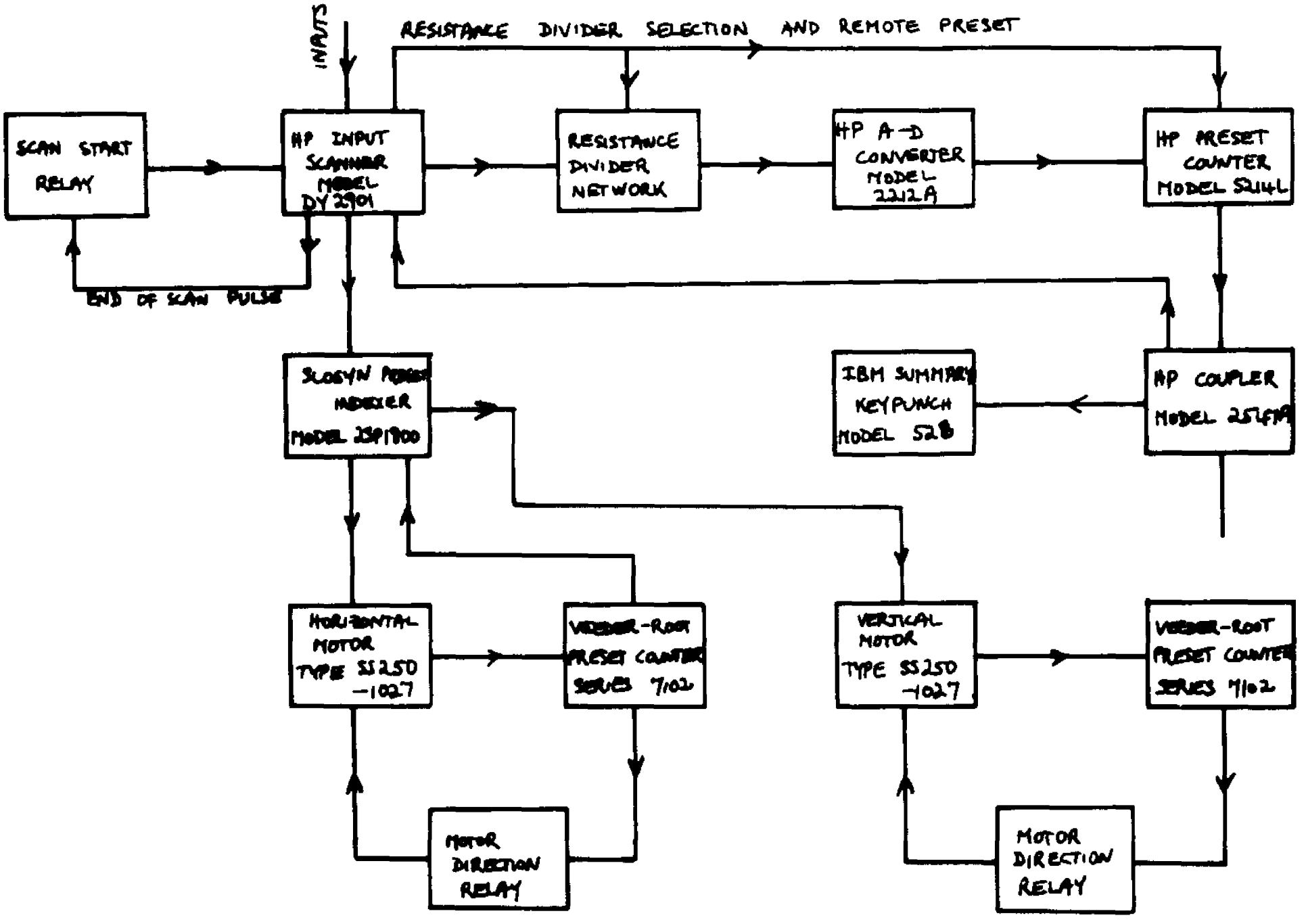

FIGURE 23 DATA ACQUISITION SYSTEM

the parameters of interest in the experiment are connected to the input of a 25 channel Hewlett-Packard (HP) DY 2901 input scanner. An HP Model 2212A analog digital (AD) converter and an HP Model 521 4L preset counter are used to digitize the output from the scanner which is then recorded as a five digit numer on an IBM card using an HP Model 2547A coupler and an IBM 526 Summary Keypunch. Contact closures are available at each channel setting to permit automatic ranging, which is accomplished in this case by means of voltage dividers at the input of the AD converter and by changing the number of preset counts.

The stepping motors which drive the vertical and horizontal lead screws move the detector, on signal, a distance determined by the settings on the Slosyn two axis control panel. When either motor has scanned the predetermined number of steps, a Veeder-Root preset counter is advanced. When a counter reaches the preset number, it is automatically reset to zero. A contact closure is used to drive a ratchet relay which then reverses the direction of that moter.

A scan of all the important variables in the experiment is initiated by placing the scanner in the continuous mode. The scanner then steps off home to the first channel and records the signal on an IBM card. When the information is passed to the keypunch for printing, a signal from the coupler is used to advance the scanner to the next channel and

the process is repeated until the last channel has been recorded. The scanner then advances to home and a programming card on the summary keypunch causes a new card to be fed into position. All the information from one complete scan is thus contained on one card. The last channel of the scan does not contain any information and is used only to provide a contact closure which advances the horizontal stepping motor a predetermined distance. When the scanner reaches home an end of scan signal drives a time delayed relay. This time is adjusted to permit the motors to move the detector to a new position and allow approximately 6 time constants before the scattering signal is recorded. The contacts of this relay are used to initiate a new scan again, and the entire process is repeated. When the horizontal motor has scanned a predetermined number of steps, the preset counter is reset, and contact closures used to reverse its direction and advance the vertical motor. The direction of the vertical motor itself is reversed when it has advanced a preset number of times.

Thus the detector scans back and forth horizontally, each time moving to a new vertical position and covering a rectangular (or square) mesh of points. The overall size of the mesh structure is determined by the motor preset counters, and the mesh separation, which determines the spatial resolution of the recorded data, is fixed by the Slosyn control indexer.

Thus when the first scan is started by pressing the continuous button, the experiment continues to run automatically, recording on IBM cards relevant parameters at a mesh of points over and over again unitl the STOP button is pressed on the scanner. Theaccuracy of the Slosyn indexer and the absense of backlash from the lead screws assures that the coordinates of any point within the mesh are reproduced to within ±0.0005" each time the detector moves to that position.

Eight parameters are usually recorded at each detector position. The voltage applied to G_1, the equipotential region and the collector plate of the electron gun, are fed into the first three channels. Although variations in these are seldom observed, it is useful to have them recorded. Channel 4 is used to monitor the electron gun current, which is obtained by amplifying the voltage drop across a resistor in the collector circuit. A DC amplifier with a gain of 100 is used to amplify the output from a chromel-alumel thermocouple attached to the potassium oven, and the output from the amplifier is fed into channel 5. The scattering signal, which is the output of the lock-in amplifier, is connected to channel 6, while the output from the vertical and horizontal linear potentiometers are fed into channels 7 and 8.

At the start of each experiment, a standard cell is connected to each channel, thus enabling the counts on each channel to be converted to volts. A computer program firstly prints all the raw data and then

converts the numbers to the relevant units. A formula given in the Handbook of Physics is used to convert the voltage in channel 5 to degrees Kelvin.

Since the detector passes through each spatial point several times, it is necessary to reorder and group together all the data collected at a given pair of coordinates. This is achieved by first grouping together all the data accumulated at one coordinate (say the horizontal) and then ordering the data at each value of the other coordinate. The process is then repeated for the next value of the coordinate selected initially. The end result of this two channel sorting routine is that the data corresponding to each pair of coordinates, i.e. to each detector position is assmebled and then printed. The program then calculates and prints out the average values, the RMS values and RMS deviation of the data accumulated at each detector position. If any number deviates from the RMS value by a factor of 3 or greater, that number is rejected and the averages recalculated.

The scattering signal is integrated for 100 seconds during each scan, and a complete run typically scans through each point 6 times. Thus the scattering signal is integrated for a total of 10 minutes at each detector position. The RMS deviation for the larger signals is typically 5%-10%, while that for the smaller signals varies form 10% to 20%. Since the smaller signals correspond to about 100 atoms/sec, it is clear that the

system noise is much larger than the shot noise. Most of the noise (80%) is the result of stray potassium in the detector chamber arising from ineffective trapping of the potassium beam. The remainder is due primarily to spurious emission from the hot wire itself.

The data acquisition system outlined above thus permits data to be collected in the optimum way. There is little delay, human error in recording is eliminated and the experiment can be operated on a 24 hour basis. In addition, the fact that the data is punched on IBM permits easy reduction by computer, and obviates the need for lengthy calculations. The data for each electron energy presented in the next section is typically accumulated over a period of 100 hours. Without the use of an automatic system the collection and reduction of data for this experiment is clearly a task of Herculean proportions.

VI Experimental results

Measurements taken at three different energies, 3.0, 4.4 and 5.2 volts are reported here. Figures 24 thru 27 illustrate the raw data at 3.0 volts, Figures 28 thru 30, the raw data at 4.4 volts, and Figures 31 thru 34 correspond to 5.2 volts. Each curve shown represents a vertical profile of the scattering signal at a givaen horizontal detector position. In an ideal experiment, where electron and atom beams are truly monoenergetic and beam and detector widths are negligible, these profiles would represent scattering at a given electron polar angle θ as a function of the azimuthal angle φ^*. The deviation of the present experimental system from this ideal is treated in some detail in the next section.

Figures 24 thru 37 illustrate the entire vertical profile, and clearly show that the curves are symmetrical about the plane of scattering. This is a direct consequence of the lack of azimuthal dependence of the scattering, and the fact that the geometric properties of the detector are symmetrical about the plane of scattering. Having demonstrated this predictable feature, data at the other energies were taken only at detector positions above (or below) this plane, and computed areas multiplied by a factor of 2.

In the section dealing with momentum transfer, it was

* This is true only to first order in the ratio of electron to atom momentum. See section on momentum transfer.

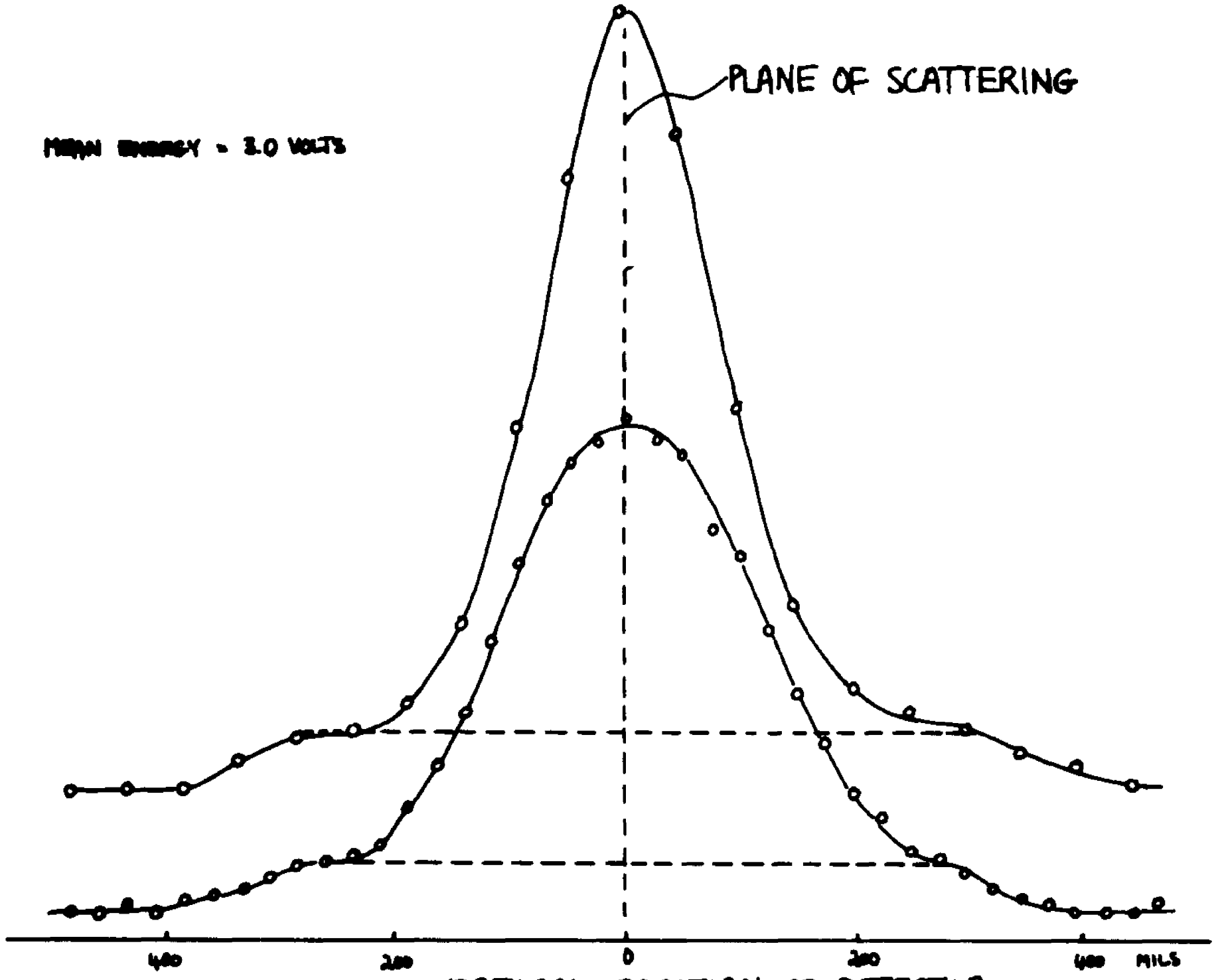
PLANE OF SCATTERING
MEAN ENERGY = 3.0 VOLTS
400
200
0
200
400
MILS
← VERTICAL POSITION OF DETECTOR →

FIGURE 24

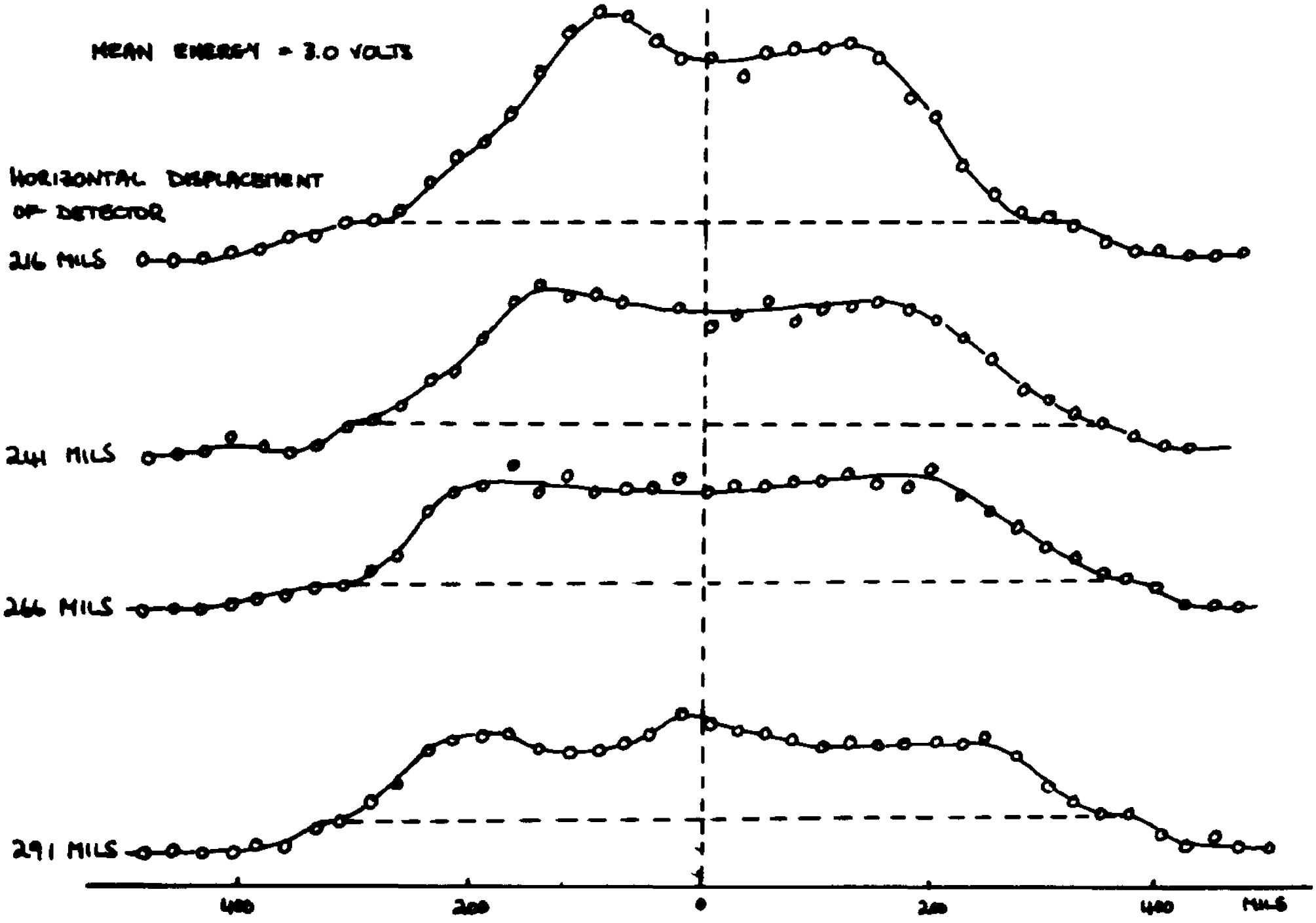
MEAN ENERGY = 3.0 VOLTS
HORIZONTAL DISPLACEMENT OF DETECTOR
216 MILS
241 MILS
266 MILS
291 MILS
400
200
200
400
MILS

FIGURE 25

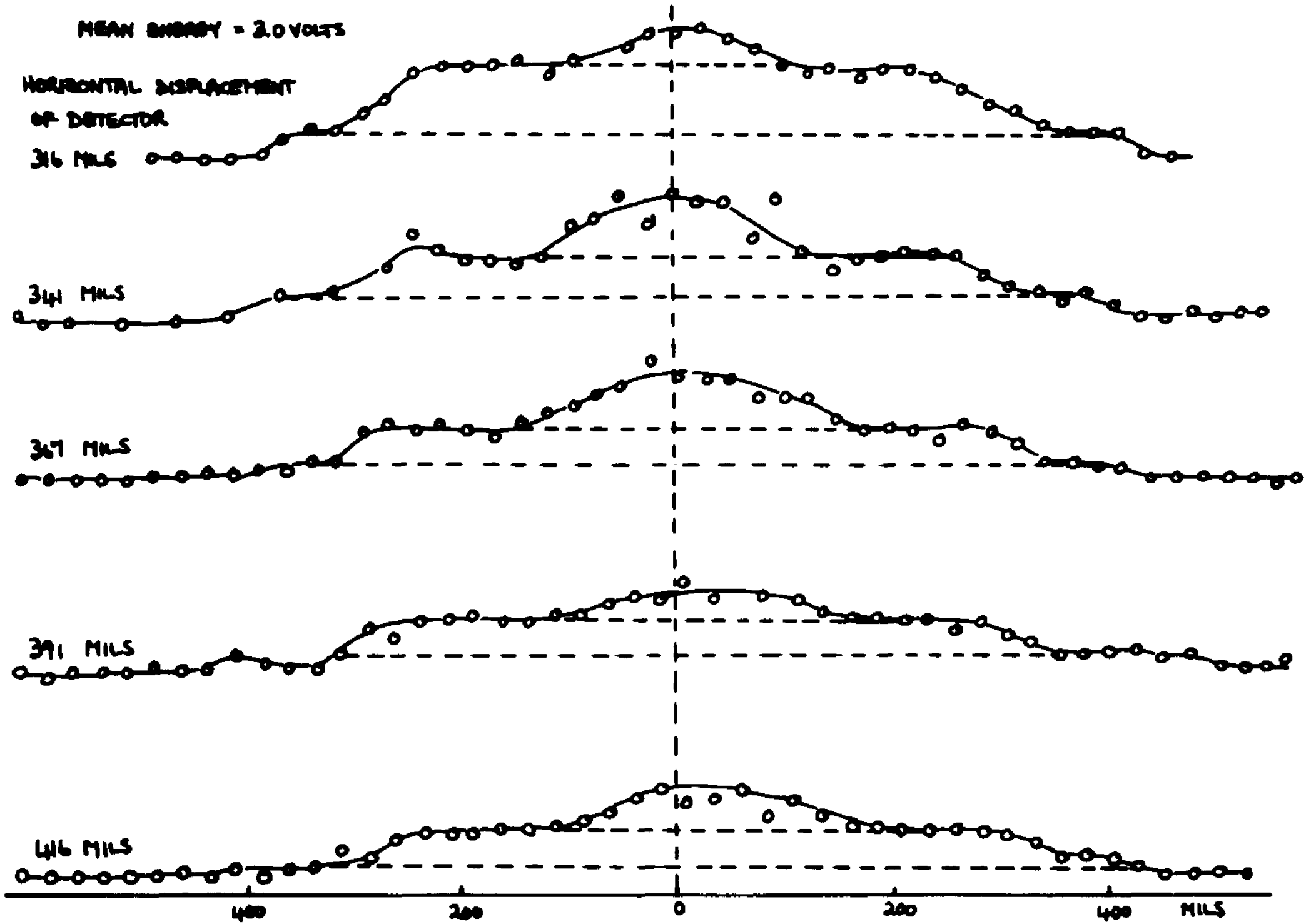
MEAN BUBBLY = 2.0 VOLTS
HORIZONTAL DISPLACEMENT OF DETECTOR
316 MILS
341 MILS
367 MILS
391 MILS
416 MILS
400
200
0
200
400
MILS

FIGURE 26

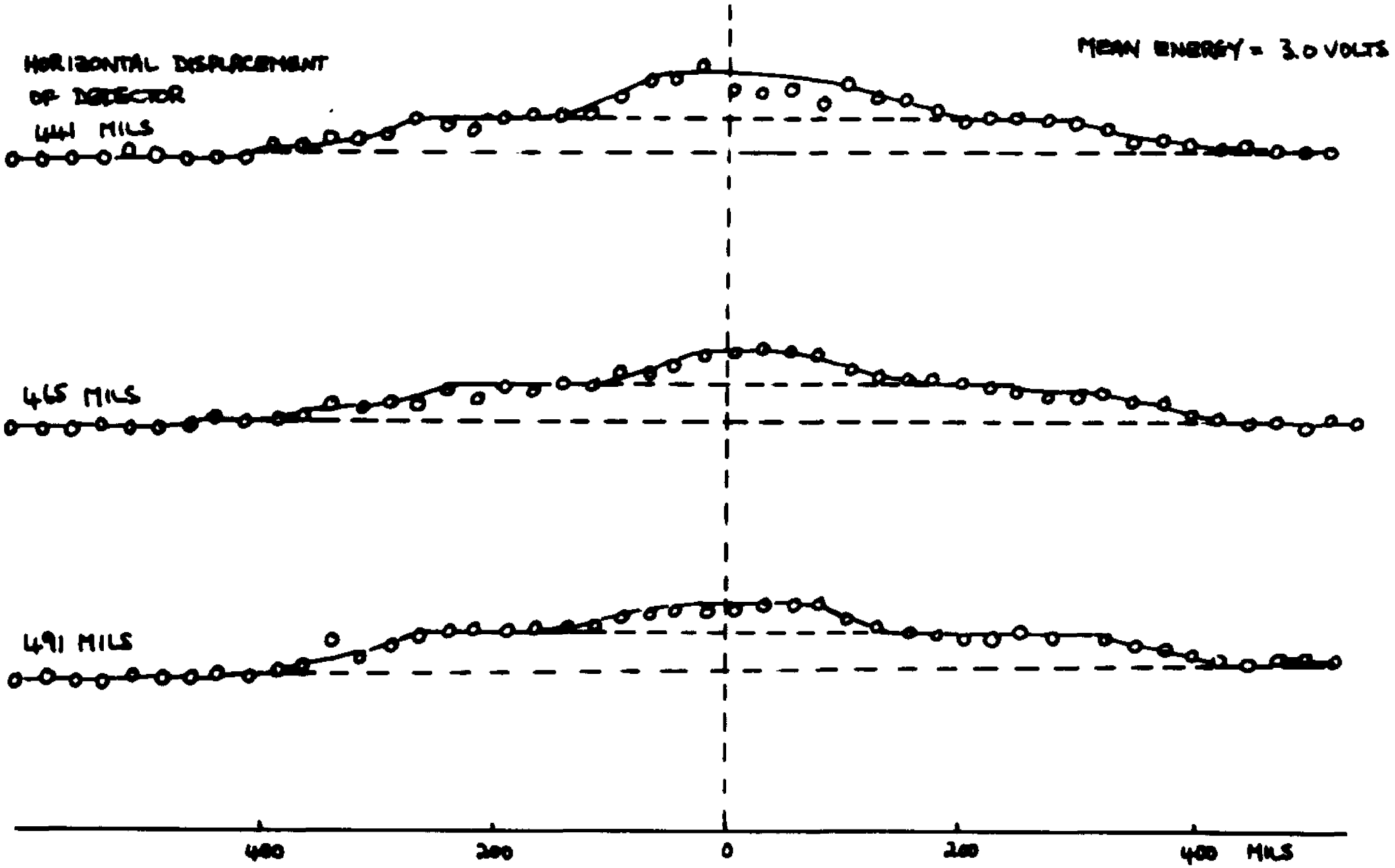
HORIZONTAL DISPLACEMENT
OF DETECTOR
441 MILS
MEAN ENERGY = 3.0 VOLTS
465 MILS
491 MILS
400
200
0
200
400 MILS

FIGURE 27

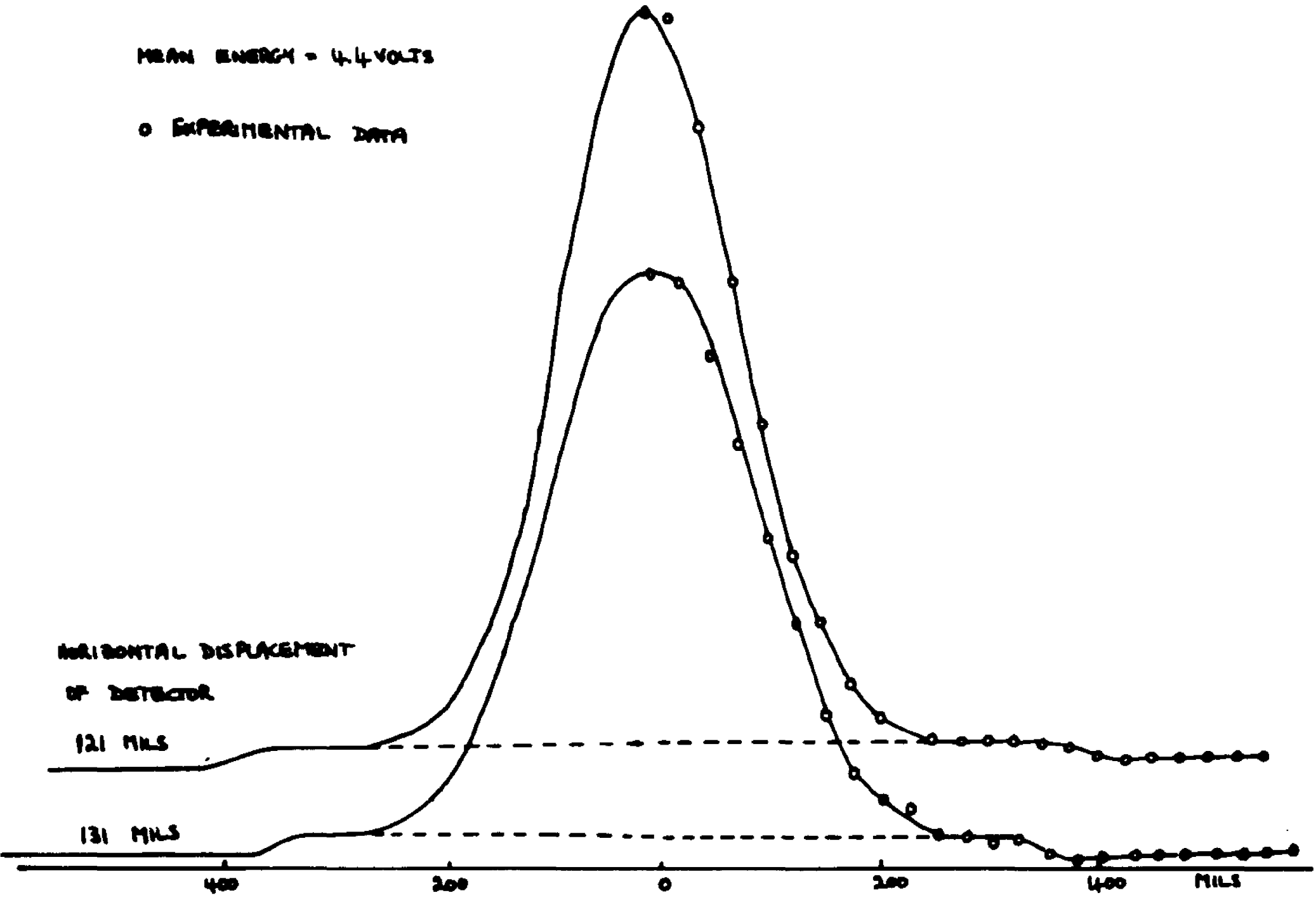
MEAN ENERGY = 4.4 VOLTS
o EXPERIMENTAL DATA
HORIZONTAL DISPLACEMENT
OF DETECTOR
121 MILS
131 MILS
400
200
0
200
400
MILS

FIGURE 28

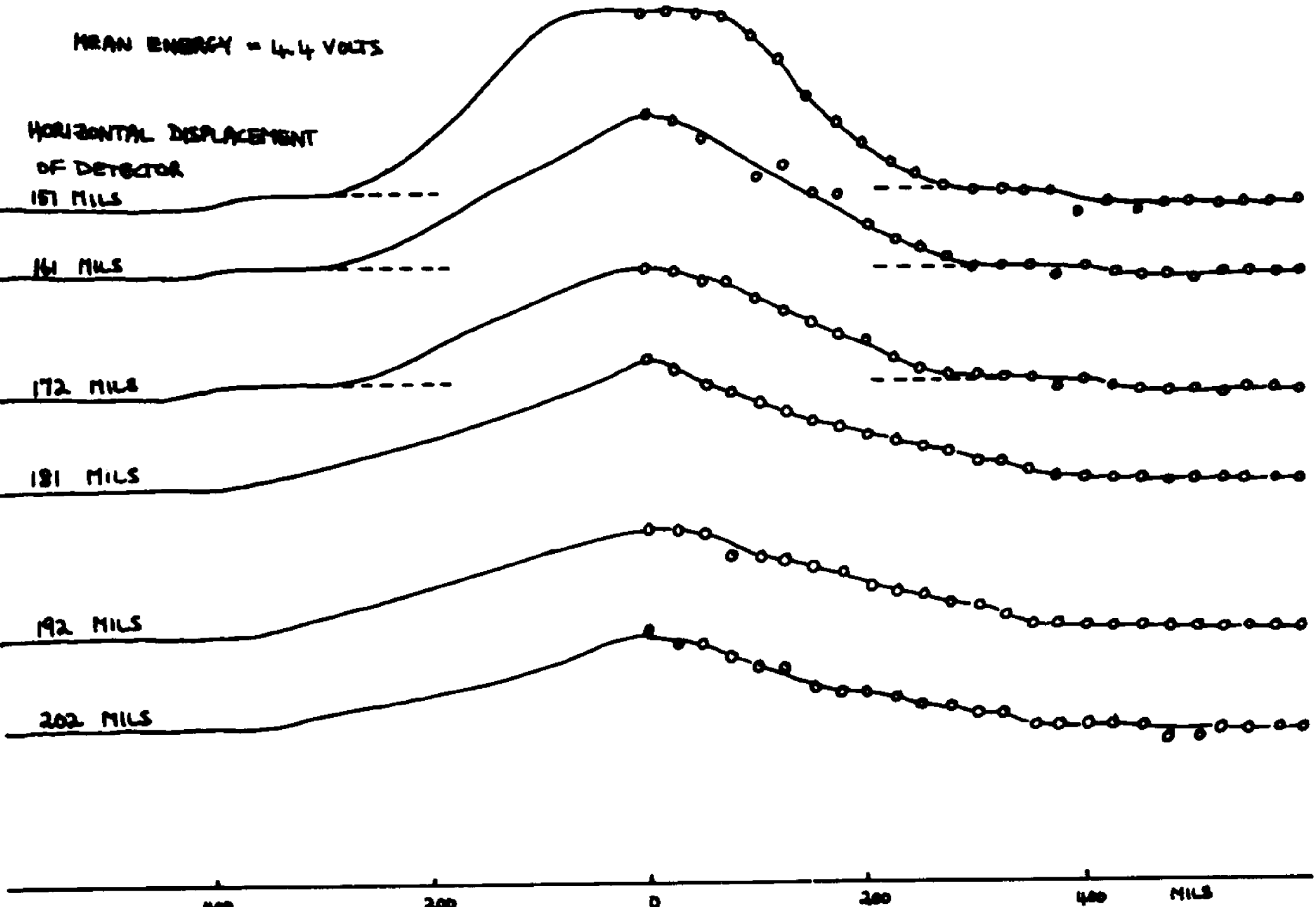
MEAN ENERGY = 4.4 VOLTS
HORIZONTAL DISPLACEMENT OF DETECTOR
151 MILS
161 MILS
172 MILS
181 MILS
192 MILS
202 MILS
400
200
0
200
400
MILS

FIGURE 29

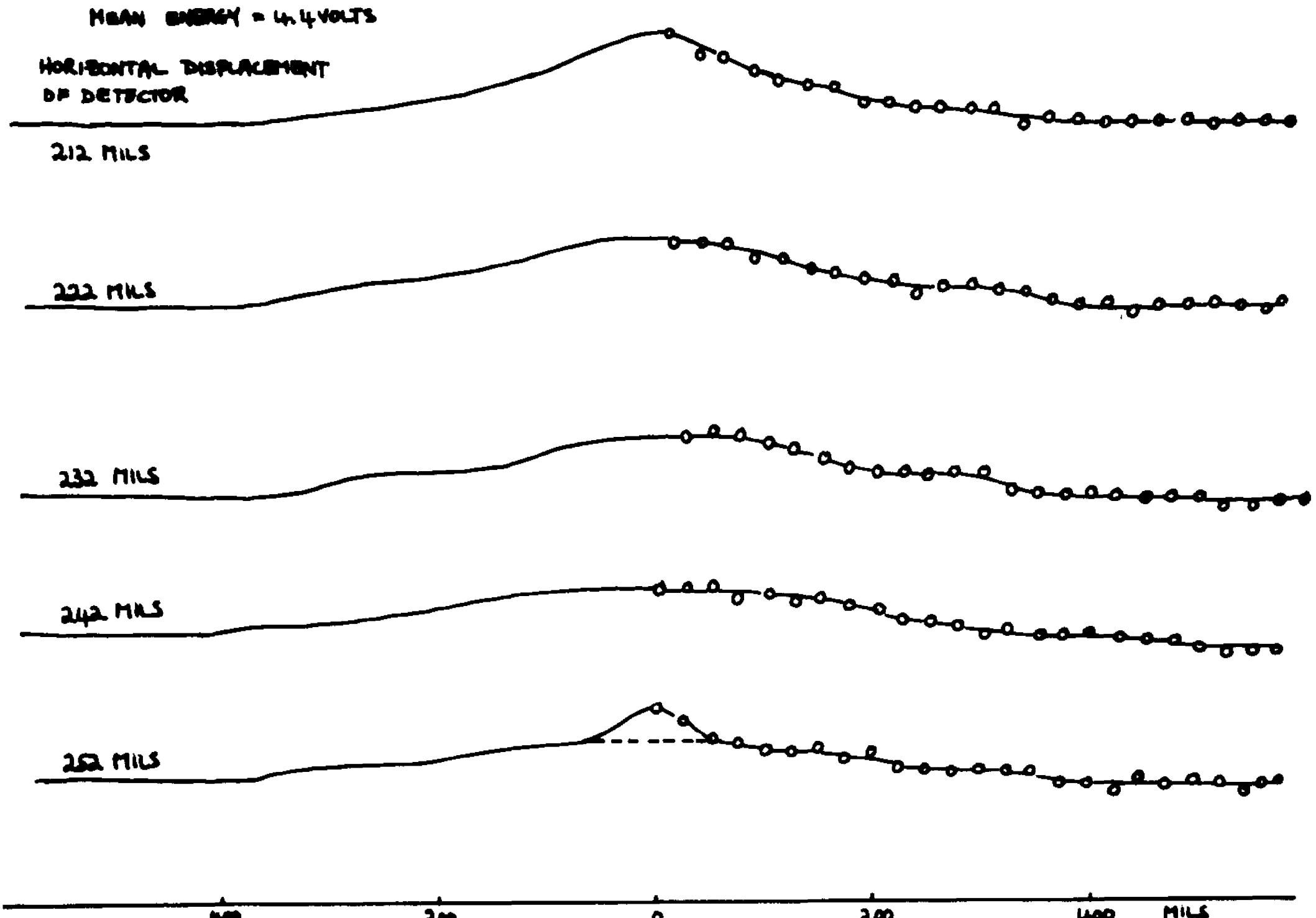
MEAN ENERGY = 4.4 VOLTS
HORIZONTAL DISPLACEMENT OF DETECTOR
212 MILS
222 MILS
232 MILS
242 MILS
252 MILS
400
200
0
200
400
MILS

FIGURE 30

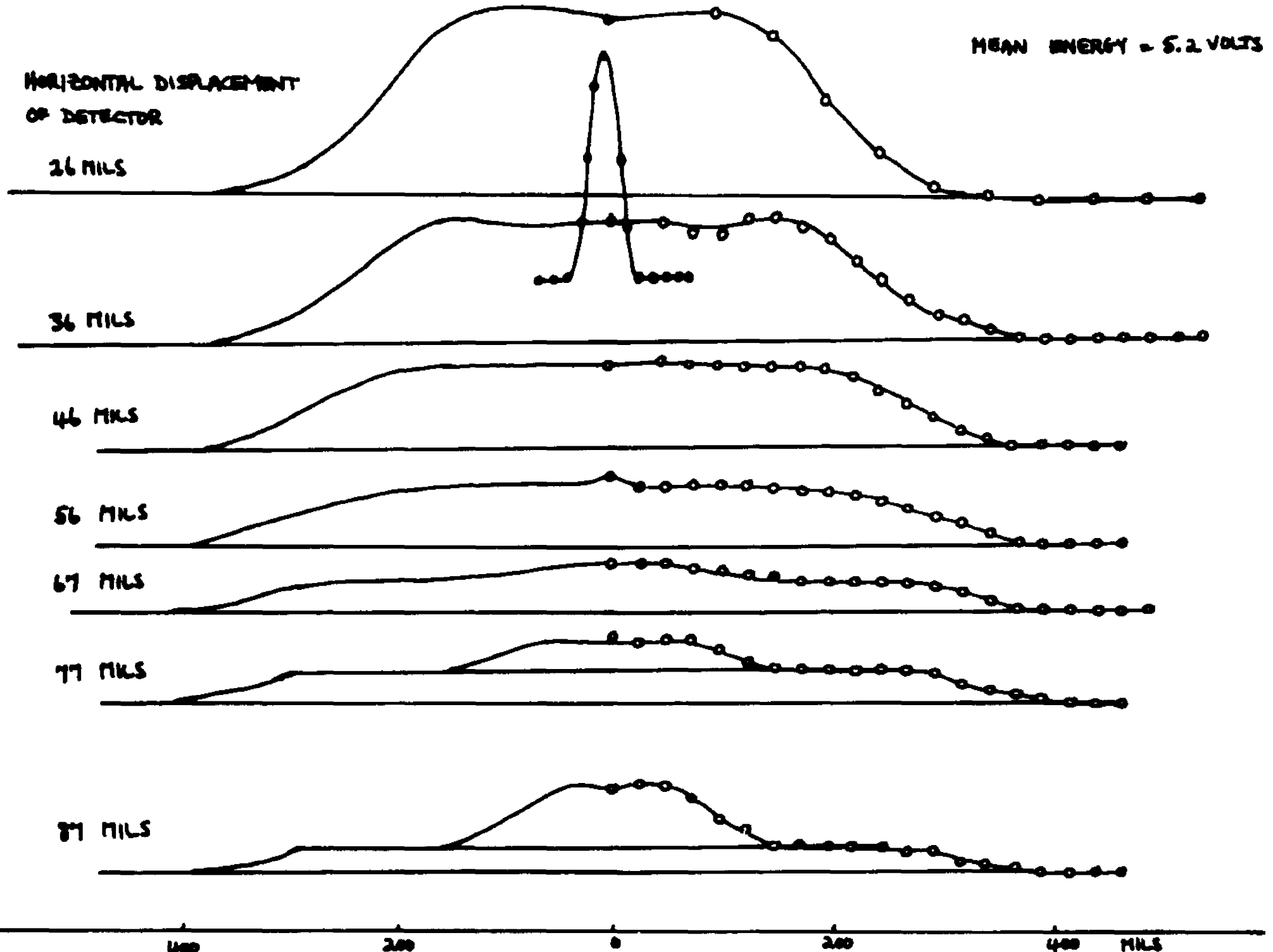
MEAN ENERGY = 5.2 VOLTS
HORIZONTAL DISPLACEMENT OF DETECTOR
26 MILS
36 MILS
46 MILS
56 MILS
67 MILS
77 MILS
87 MILS
400
200
0
200
400
MILS
VERTICAL POSITION OF DETECTOR

FIGURE 31

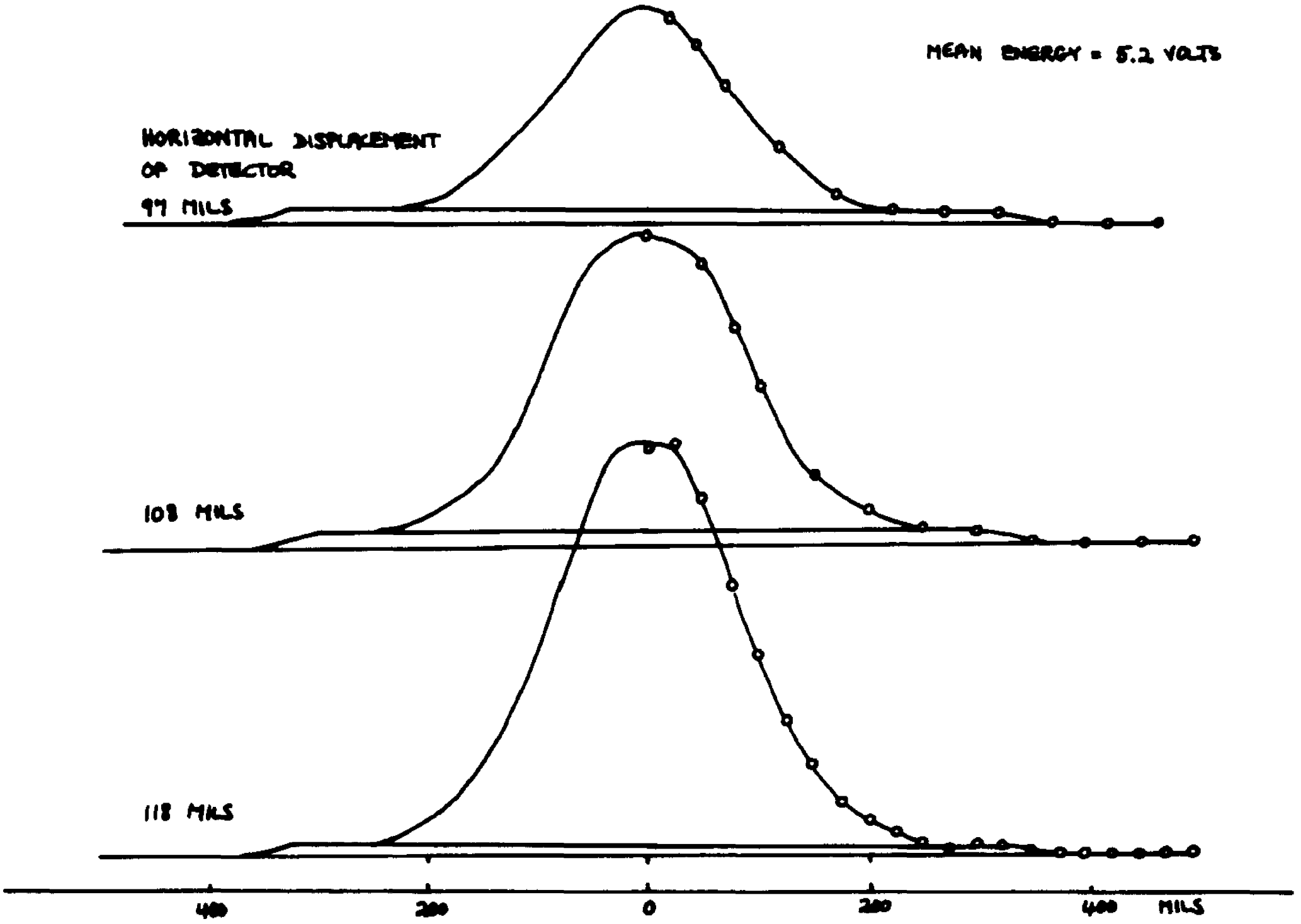

FIGURE 32 VERTICAL DISPLACEMENT OF DETECTOR ⟶

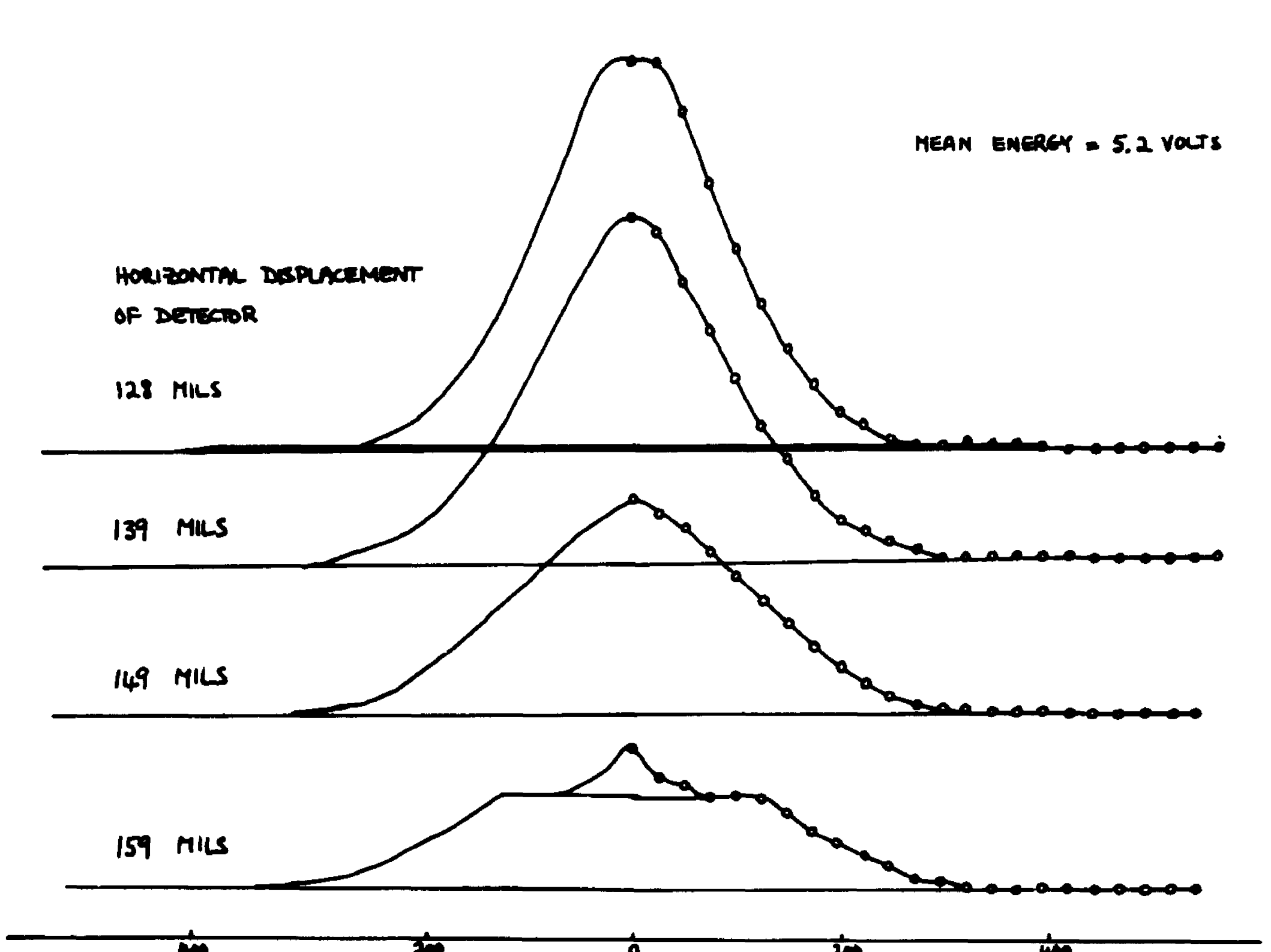

FIGURE 22 VERTICAL DISPLACEMENT OF DETECTOR

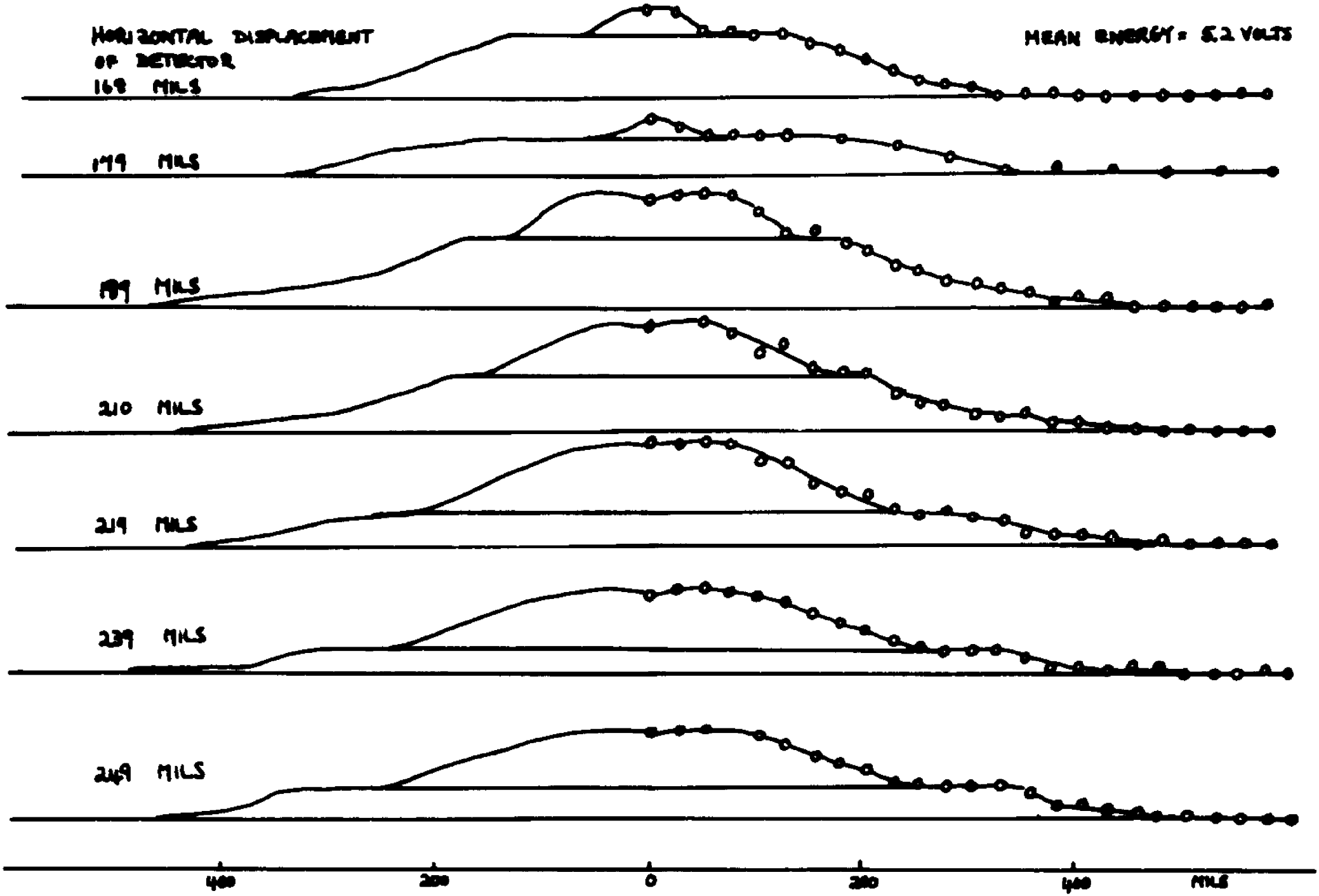

FIGURE 34 VERTICAL DISPLACEMENT OF DETECTOR ⟶

shown that at any horizontal detector position for which inelastically scattered atoms can reach the detector, the vertical profile is divided into two or more regions. The uppermost part of the curve represents elastic scattering only, and the rest of the curve corresponds to a combination of both elastic and inelastic scattering events. If the upper part of the profile can be properly extrapolated, it should be possible to separate elastic and inelastic events.

Figures 31 thru 34 demonstrate most clearly how the technique works. The detector was first scanned to a position close to the unscattered atom beam where only elastic events can be recorded. As the detector moves out from the unscattered atom beam in the horizontal direction, the profiles broaden and flatten out, the signal at any point decreasing. This is in agreement with the fact that the form factor AFF, which is a measure at any vertical position of the detector of the fraction of all atoms detected for a given scattering angle θ, decreases as θ increases i.e. as the detector displacement is increased. The maximum vertical displacement for a scattered atom is determined by

$$x = \beta_1 \sin \theta$$

and consequently increases as the detector is scanned from the beam axis. The most important feature of these profiles is the fact that they are flat over a wide range.

When the detector is scanned to positions greater than 57 mils, a new feature is clearly evident. A small peak appears at the center of the profile, and this grows as the detector displacement increases, until it reaches a maximum at a detector position of 118 mils. This peak represents scattered atoms that were excited from the ground to the first excited state. The fact that the peak does not occur at a single detector position, but rather builds up over a range, is a consequence of the atom and electron velocity ditributions and the finite widths of the atom beam and detector. However, because of the flatness of the curve representing elastic events, it is not difficult to separate the contributions to the total signal of elastic and inelastic events . One simply extrapolates the flat part of the curve in the region where only elastic scattering can occur to the region where both types of scattering can occur. The lines in Figures 31 thru 34 represent the division.

As the detector is moved beyond 118 mils, the inelastic peak broadens and is reduced in magnitude in the same way as the elastic peak. Beyond 148 mils, the contribution to the signal from elastic scattering is negligible. At a detector position of 159 mils, another peak is observed at the center; this corresponds to excitation from the ground state to the 3d state. This peak reaches a

maximum at about 219 mils, and as did the other peaks flatten out as the detector is displaced further. Again contributions to the total signal from each of the two inelastic processes can be evaluated by extrapolating the profile corresponding to the 1st excitation event into the region where both types of scattering occur.

Figure 31 through 34 also show areas computed for each type of scattering at each detector position. Although the experiment is not ideal in the sense that a given detector position corresponds to a given polar angle θ it can be assumed that only atoms scattered by electrons within a small range of θ are scattered into the detector. This average can be calculated using the relationships between atom and electron scattering angles and the known position of the detector. The computed areas can thus be plotted as a function of electron polar scattering angle and a differential cross section obtained. An absolute scale for the resulting curve was arrived at in the following manner.

If the electron and atom beams are assumed to be monochromatic, and the atom current density uniform over its cross-section area, equation (30) can be integrated to give

$$\Delta N_S(Z) = \frac{1}{HL\beta} \frac{I_e I_A}{V} \int_{z - D/2}^{z + D/2} dz' \sigma(\theta)(\varphi_2 - \varphi_1) \qquad (32)$$

where ΔN_S is now the number of atoms reading the detector for

excitation of one channel only and I_e and I_A are the total electron and atom currents respectively. If it is further assumed that the detector is sufficiently narrow so that θ does not vary across the detector width D, then the total number of atoms scattered between Z-D/2 and Z+D/2 is given by

$$\Delta N_S(Z) = \frac{2\pi D}{HL\beta V} I_e I_A \sigma(\theta) \qquad (33)$$

where θ is related to Z through the transformation equations.

Equation (31) can be integrated over all angles with the same assumptions as above to obtain an expression for the total cross-section. Thus we have

$$\sigma_{TOTAL} = \frac{VH}{I_e I_A} I_S^T = KI_S^T \qquad (34)$$

Where I_S^T is now the total scattering out current i.e. the total number of atoms scattered from their initial trajectories. The current I_S^T is obtained by scanning the detector into the unscattered atom beam, and integrating the measured scattering out signal over the beam cross-section. In practice the detector is placed on the beam axis and the total scattering signal at this position is obtained by scanning the detector over the beam height. The resulting current is increased by the ratio of total atom current to the current intersected by the detector at this position, and I_S^T is thus found.

This method minimizes the error in I_S^T due to atoms being scattered into the detector from that side of the atom beam profile on which the electron beam is incident. A vertical profile of the scattering out signal is shown at the top of figure 31.

In an independent experiment conducted in this laboratory measurements of σ_{total} have been made to a high degree of accuracy. With these values of σ total and the measured I_S^T, a value for K in (34) is determined. Equation (33) can now be rearranged to yield

$$\sigma(\theta) = \frac{L\beta}{2\pi D} \left(\frac{\Delta N_S}{I_S^T} \right) \sigma_{total} \qquad (35)$$

Thus $\sigma(\theta)$ is found in terms of the measured qualities ΔN_S and I_S^T and the accurately measured value of σ_{total}. The area corresponding to ΔN_S and I_S^T were computed using the same vertical scale. Since $\sigma(\theta)$ is proportioned to the ratio of these two numbers, factors converting areas to scattering signals cancel, and it is unnecessary to have a precise knowledge of the height of the detector. An important source of systematic error is thus eliminated.

Figures 35 through 40 show differential cross-sections computed

in this manner for all three energies.

A differential run at 1.0 e Volts was also obtained and compared with the theoretical work of Karule[6] and recent experimental work by Collins[13]. The results are shown in Figure 41. Since a 2-state close coupling approximation is expected to give accurate results at this energy, the excellent agreement between theory and experiment validates both Karule's calculations and the normalization procedure used in the present experiment. The rather pooreer agreement with Collins' work is probably caused by the assumptions he had to make to obtain the total scattering at each detector position. (In Collins' experiment, the detector could not be moved out of the plane of scattering, and his data had to be divided by the form factor $\gamma(\theta, V, E)$ integrated over the velocity distributions of both electron and atom beams. This factor depends critically on the details of the distributions at small angles).

The maximum error in the absolute values for the differential cross-sections is estimated to be ± 13%. This arises from the uncertainty in electron energy (5%), uncertainty in ΔN_S(10%), I_S^T (5%) and σ_{total}(5%). It should be pointed out here that although the values used for σ_{total} were obtained in a companion experiment designed specifically to measure this cross-section, these

values are in excellent agreement with total cross-section measurements made in the present experimental arrangement, with less refined calibration procedures.

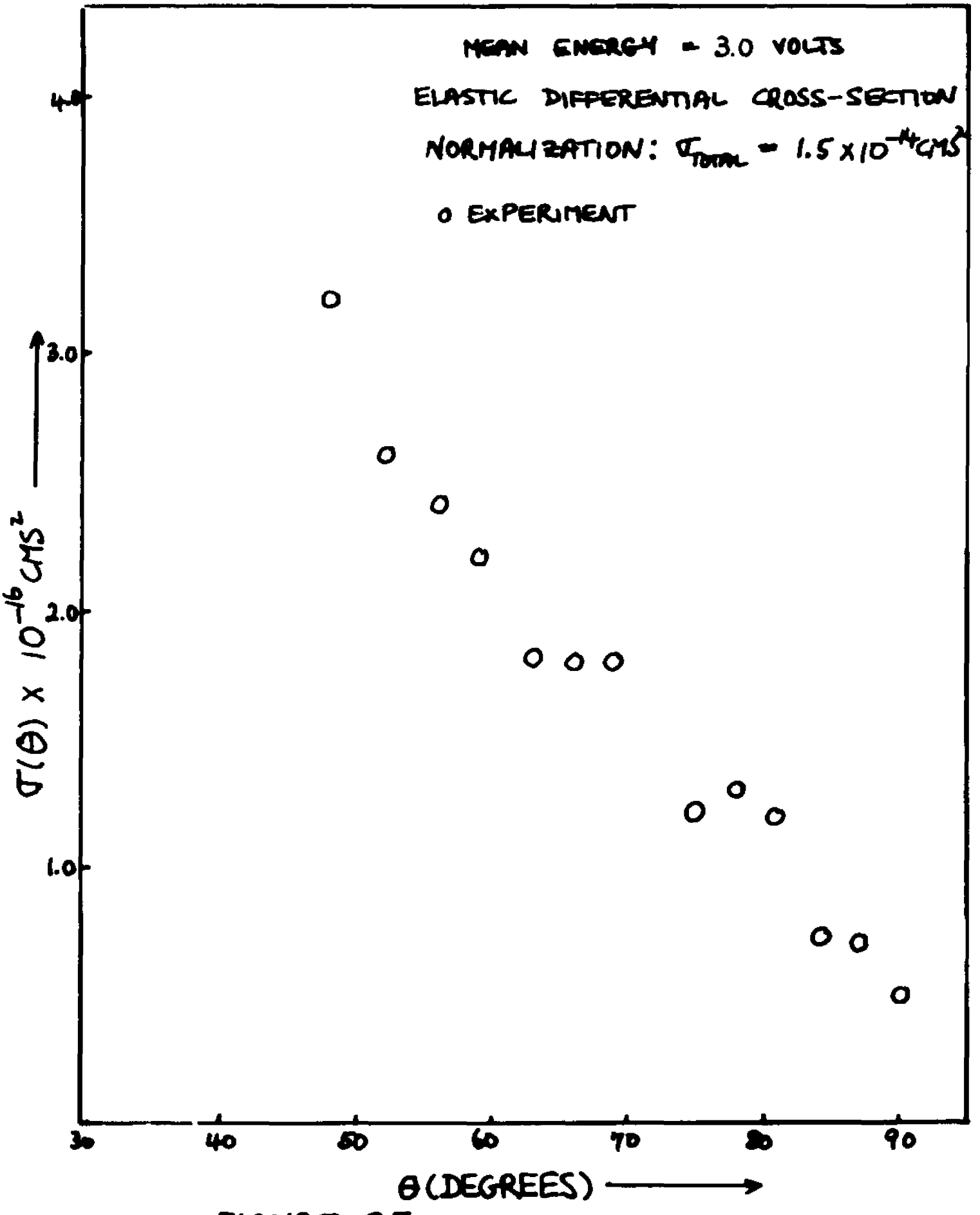
MEAN ENERGY = 3.0 VOLTS
ELASTIC DIFFERENTIAL CROSS-SECTION
NORMALIZATION: $\sigma_{TOTAL} = 1.5 \times 10^{-14} CMS^2$
o EXPERIMENT
4.0
3.0
2.0
1.0
$\sigma(\theta) \times 10^{-16} CMS^2$
30
40
50
60
70
80
90
θ (DEGREES)

FIGURE 35

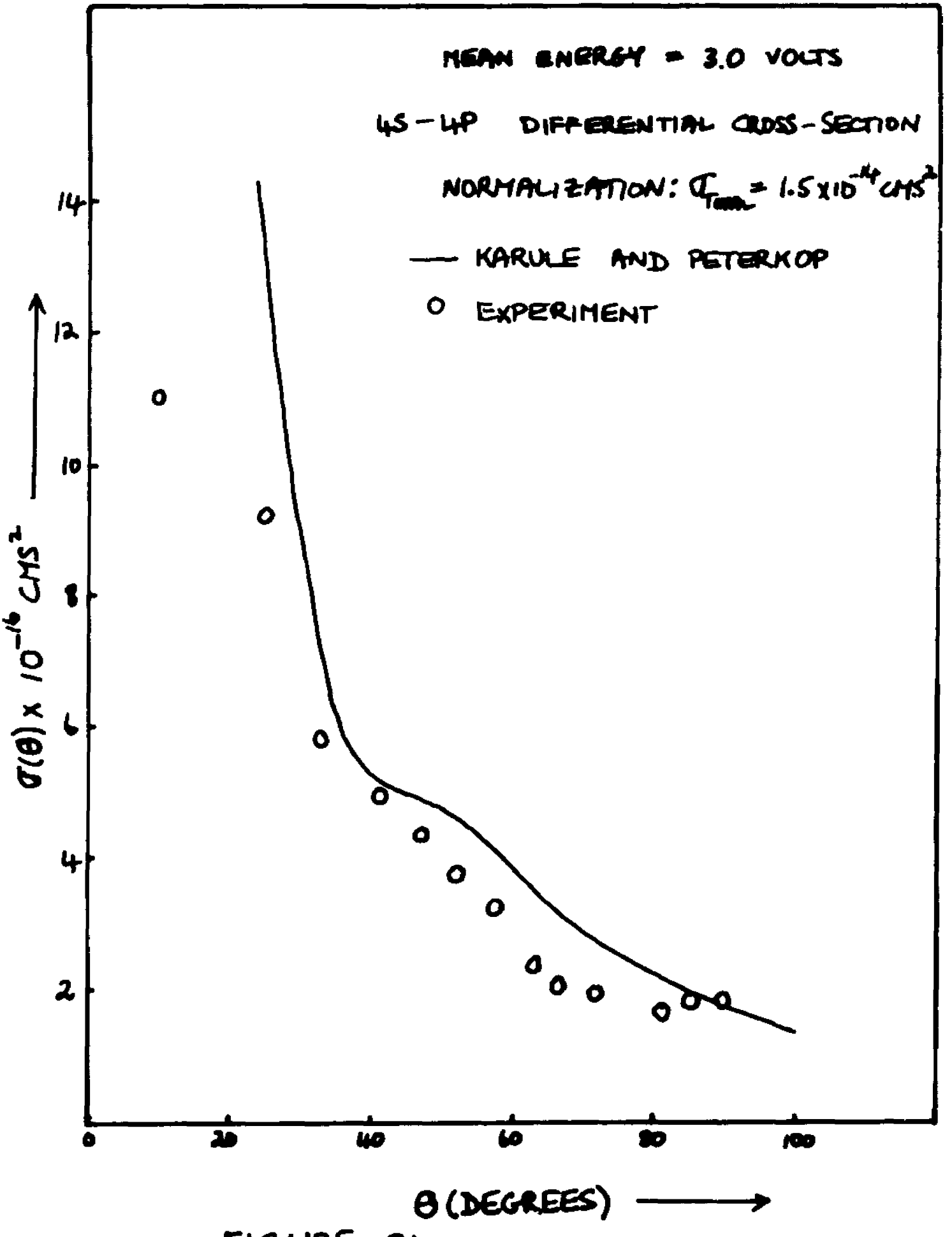
MEAN ENERGY = 3.0 VOLTS
4S – 4P DIFFERENTIAL CROSS-SECTION
NORMALIZATION: $\sigma_{Total} = 1.5 \times 10^{-16}$ CMS^2
— KARULE AND PETERKOP
O EXPERIMENT
$\sigma(\theta) \times 10^{-16}$ CMS^2
14
12
10
8
6
4
2
0
20
40
60
80
100
θ (DEGREES) ⟶

FIGURE 36

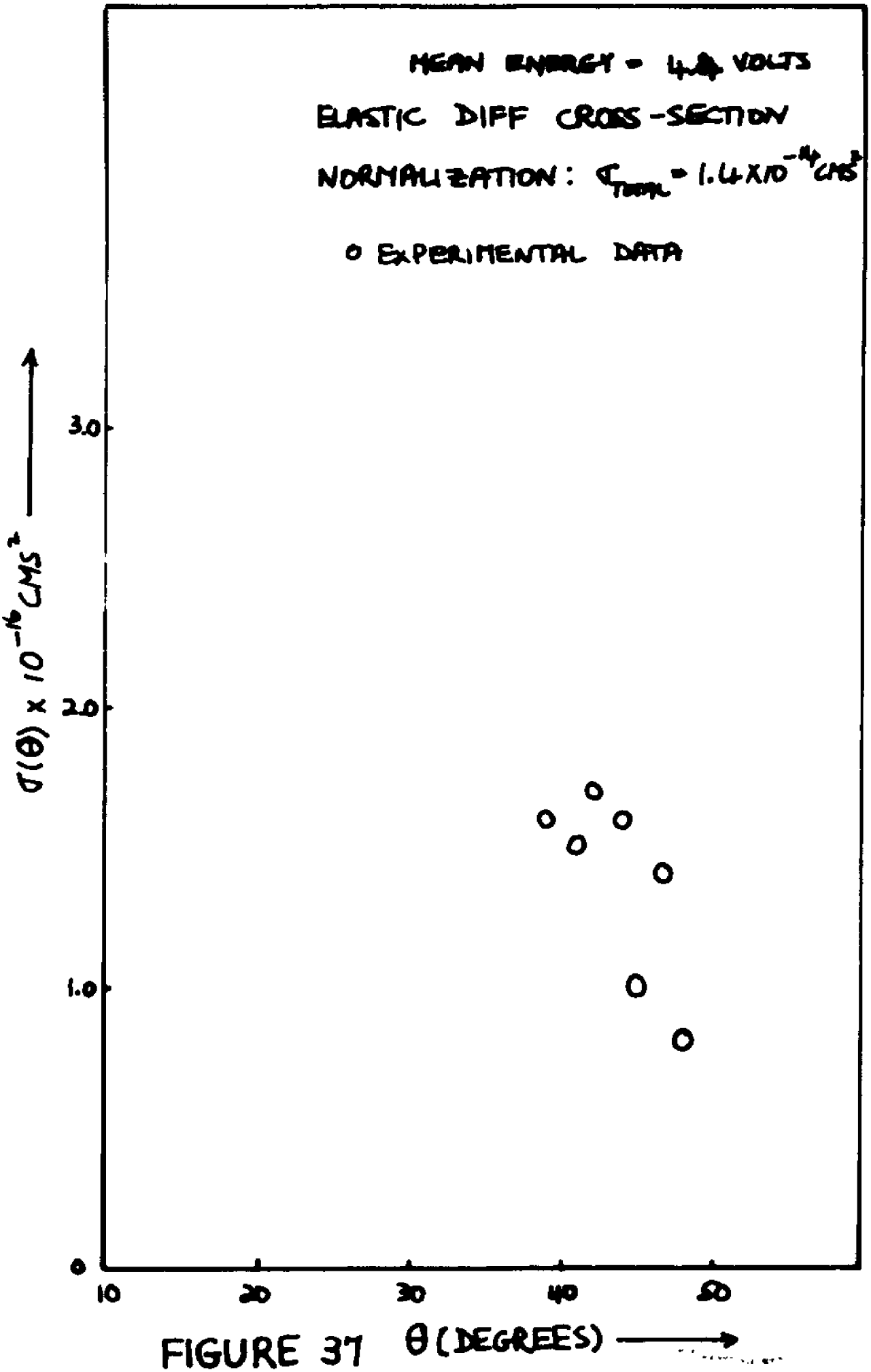
MEAN ENERGY = 4.8 VOLTS
ELASTIC DIFF CROSS-SECTION
NORMALIZATION: $\sigma_{TOTAL} = 1.4 \times 10^{-16}$ CMS^2
o EXPERIMENTAL DATA
$\sigma(\theta) \times 10^{-16}$ CMS^2
3.0
2.0
1.0
0
10
20
30
40
50
θ (DEGREES)

FIGURE 37

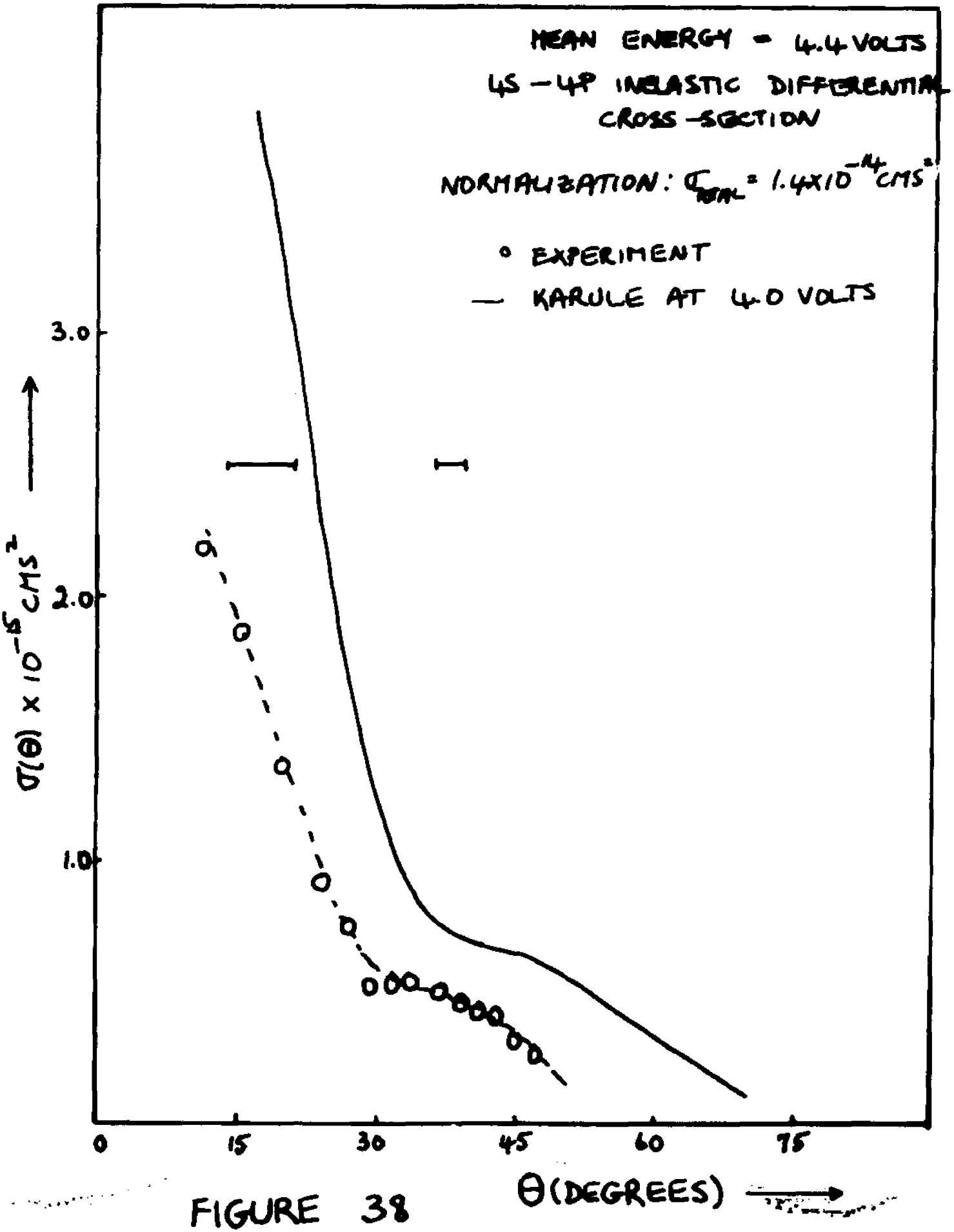
MEAN ENERGY = 4.4 VOLTS
4S – 4P INELASTIC DIFFERENTIAL CROSS-SECTION
NORMALIZATION: $\sigma_{TOTAL} = 1.4 \times 10^{-14}$ CMS^2
° EXPERIMENT
— KARULE AT 4.0 VOLTS
$\sigma(\theta) \times 10^{-15}$ CMS^2
3.0
2.0
1.0
0
15
30
45
60
75
θ(DEGREES)

FIGURE 38

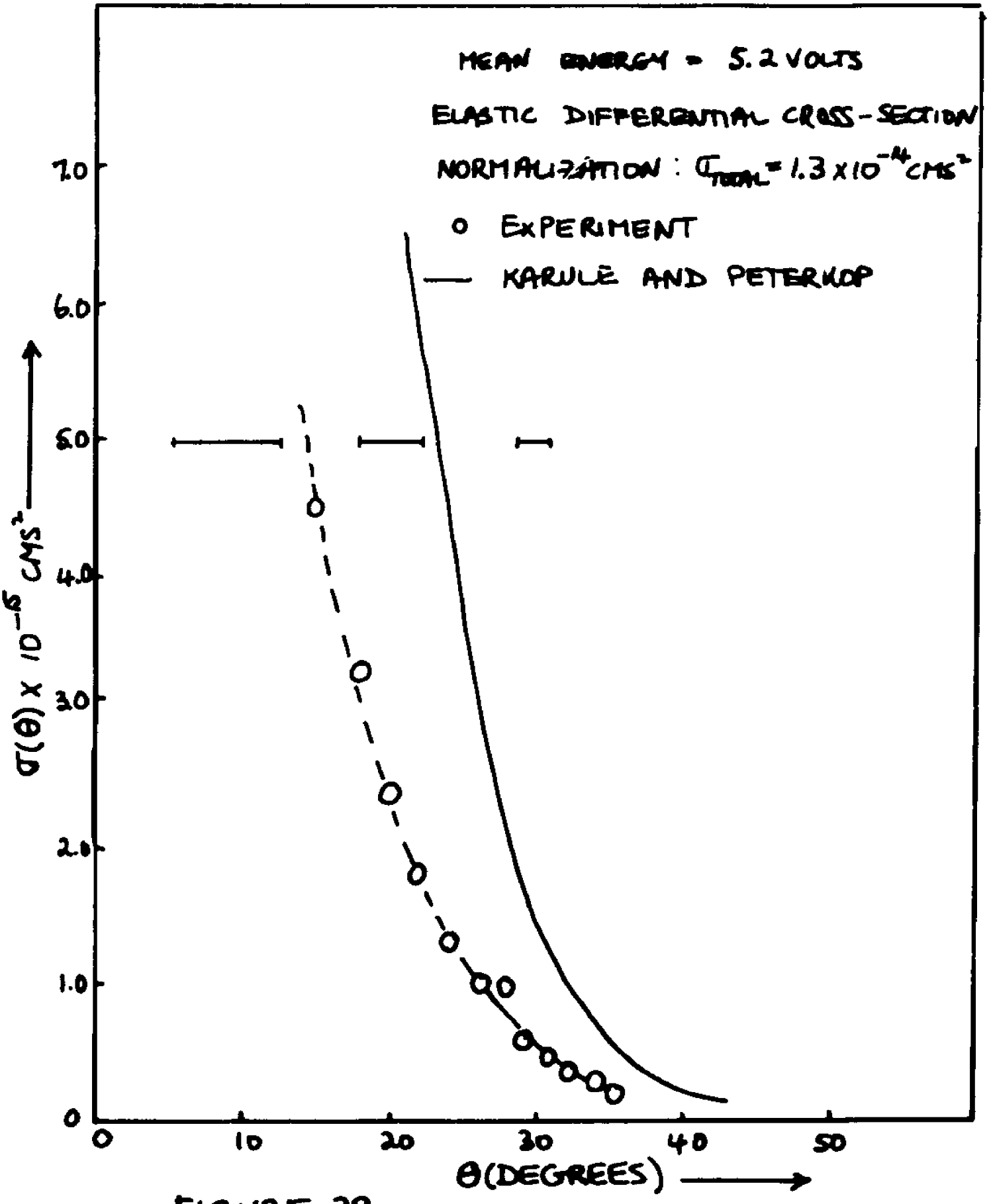
MEAN ENERGY = 5.2 VOLTS
ELASTIC DIFFERENTIAL CROSS-SECTION
NORMALIZATION : $\sigma_{TOTAL} = 1.3 \times 10^{-14}$ CMS^2
o EXPERIMENT
— KARULE AND PETERKOP
$\sigma(\theta) \times 10^{-15}$ CMS^2
0
1.0
2.0
3.0
4.0
5.0
6.0
7.0
0
10
20
30
40
50
θ(DEGREES)

FIGURE 39

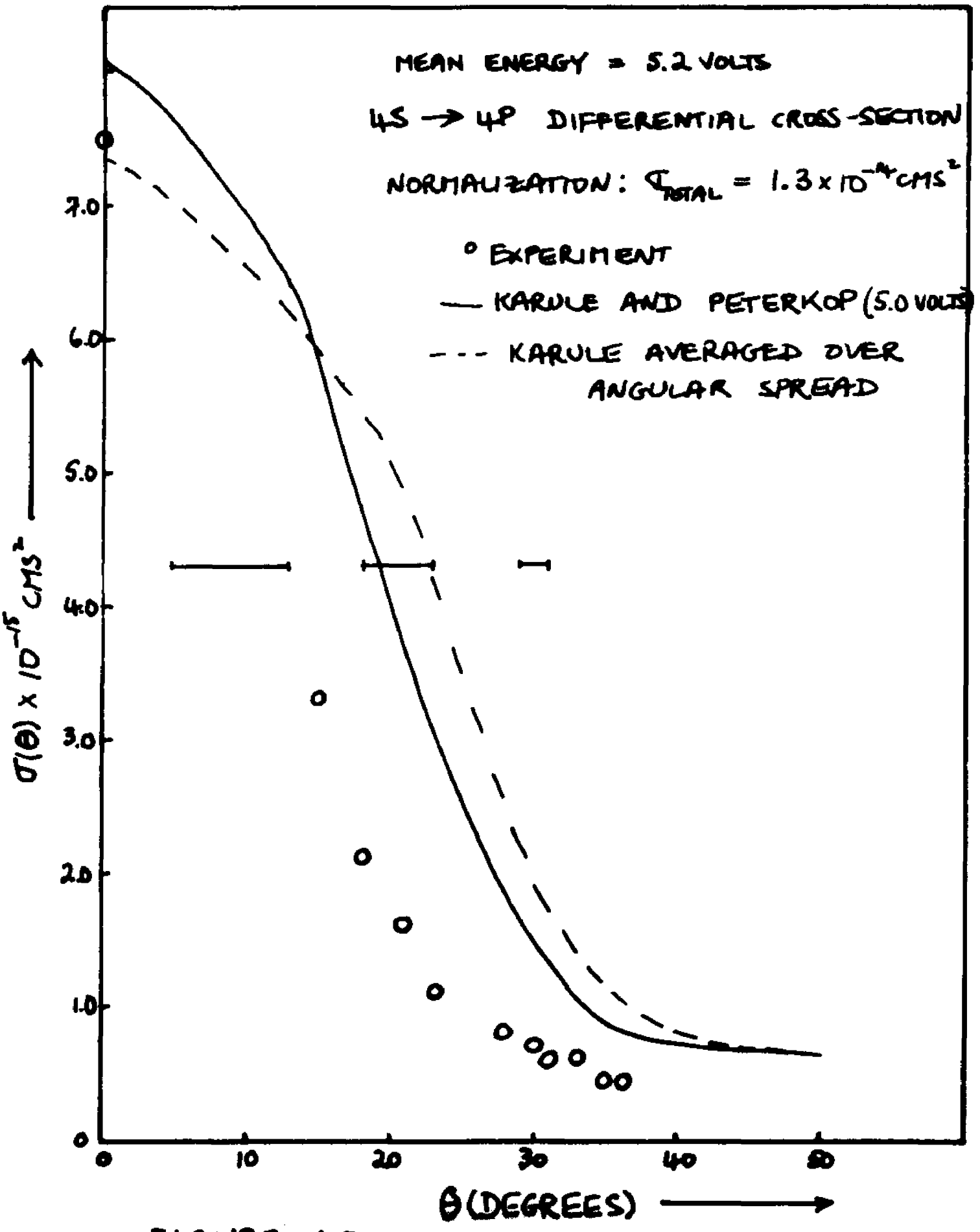
MEAN ENERGY = 5.2 VOLTS
4S → 4P DIFFERENTIAL CROSS-SECTION
NORMALIZATION: $\sigma_{TOTAL} = 1.3 \times 10^{-16} CMS^2$
° EXPERIMENT
— KARULE AND PETERKOP (5.0 VOLTS)
--- KARULE AVERAGED OVER ANGULAR SPREAD
$\sigma(\theta) \times 10^{-15} CMS^2$
0
1.0
2.0
3.0
4.0
5.0
6.0
7.0
0
10
20
30
40
50
θ (DEGREES)

FIGURE 40

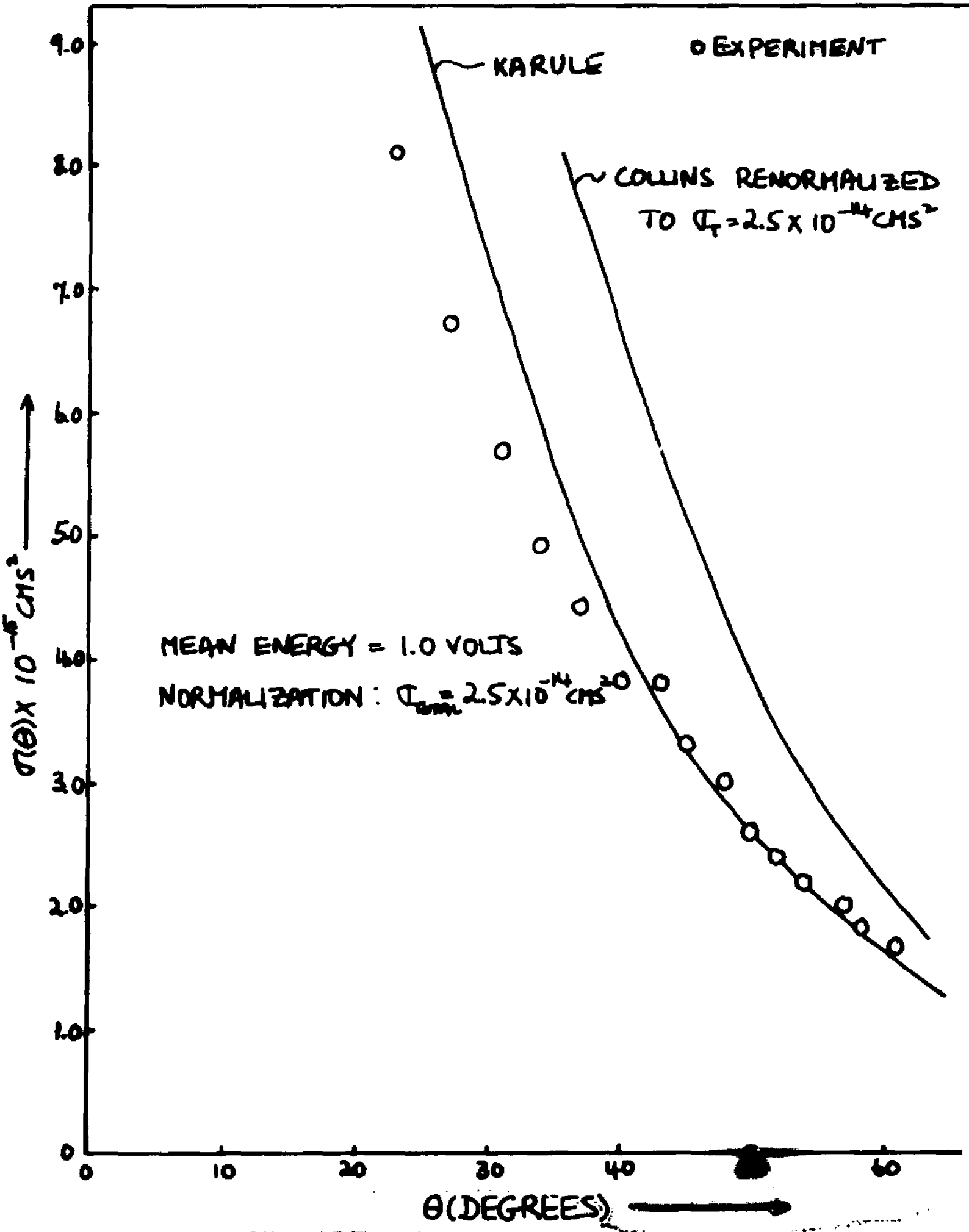
KARULE
EXPERIMENT
COLLINS RENORMALIZED
TO $\sigma_T = 2.5 \times 10^{-14}$ CMS^2
MEAN ENERGY = 1.0 VOLTS
NORMALIZATION: $\sigma_{norm} = 2.5 \times 10^{-14}$ CMS^2
$\sigma(\theta) \times 10^{-15}$ CMS^2
θ (DEGREES)
0
1.0
2.0
3.0
4.0
5.0
6.0
7.0
8.0
9.0
0
10
20
30
40
60

FIGURE 4

VII. Comparison of vertical profiles with theoretical predictions

The essential validity of the kinematics presented in the section on momentum transfer analysis has already been demonstrated by observation on the location of the excitation peaks. It is however important to compare the theoretical predictions of the variation of scattering signal with detector position with the raw scattering data. In the section on momentum transfer analysis it is shown that the scattered atom current reaching the detector is given by

$$\Delta N_S = \frac{2}{H}\iint I_e(E)\,dE\,\frac{dV}{V}\iint dx'_o\,dz'_o\,J_A(x'_o z'_o V)\int_{\theta_1}^{\theta_2}\sigma(\theta)\,\sin\theta\,\gamma_1(\theta,V,E)d\theta$$

where $\gamma_1(\theta, V, E)$ is the azimuthal form factor (AFF). The AFF is a function of X_o, the coordinate which describes the vertical position of the detector. We would like to examine the behavior of $\gamma_1(\theta, V, E)$ as a function of X_o for given θ, atom velocity V and electron energy E. Curve A of Figure 42 illustrates the dependence of AFF on the vertical coordinate X_o, for the 4S-4P inelastic channel. The values chosen for θ, V and E correspond to those calculated for the experimental curve D. Two features are

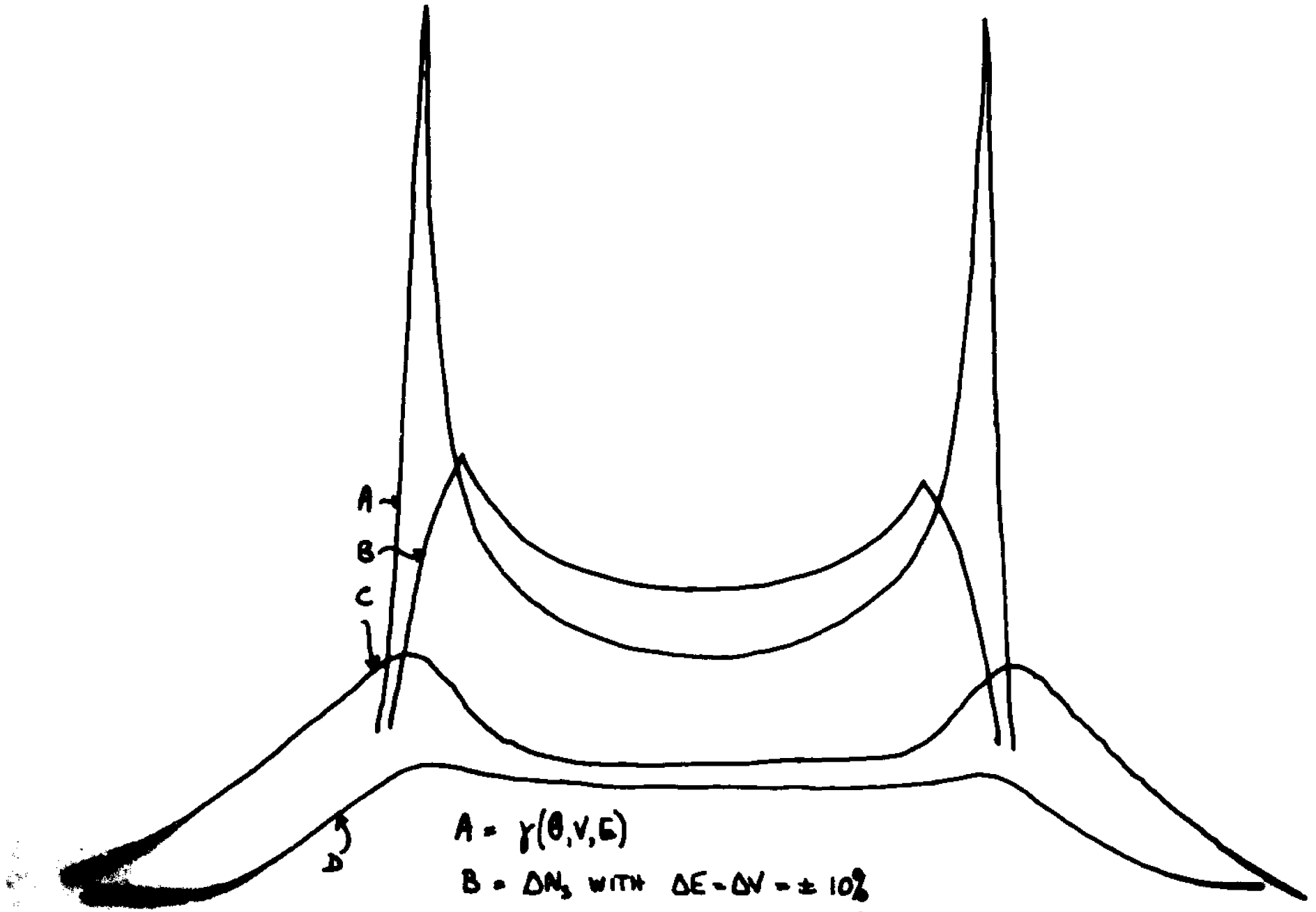
A
B
C
D
A = γ(θ,V,E)
B = ΔN₂ WITH ΔE = ΔV = ± 10%
C = ΔN₂ WITH ΔE = ΔV = ± 10%.
ENERGY = 3.0 VOLTS
D = EXPERIMENT

FIGURE 42

immediately evident: 1) The AFF is symmetrical about the plane of scattering, and 2) it is sharply peaked near the maximum value of X_o. Since it is to be expected that the shape of ΔN_s will be determined in large part by the AFF there is considerable disagreement between this simple theory and the raw data. Clearly factors such as the atom and electron velocity distributions, beam and detector widths and beam height have to be considered if predictions for ΔN_s are to agree with the observed profiles.

These factors are taken into account by integrating Equation 31 over all the variables. Rectangular distributions in $I_e(E)$ and $J_A(V)$ were assumed, the widths being taken as ±10% around the mean values. The atom beam current $J_A(X_o' Z_o')$ was assumed within a cross sectional area of 0.004" x 0.004", and the detector width assumed to be 0.010". Since the range of θ in the computation of ΔN_s is expected to be small ($\sim 10^o$), $\sigma(\theta)$ was assumed to be constant. This will only introduce an appreciable error in the calculations in the unusual case where the cross section is a very rapid function of angle. A computer program to compute ΔN_s as a function of X_o for the 4S-4P channel was written. Curve B of Figure 42 shows the

results of the calculations. The peaks have been considerably reduced in intensity, but the shape is still in poor agreement with the experimental data. In particular, the long tail in the data is not accounted for in any way by the above theory. Although detailed knowledge of the atom and electron velocity is not known here, ΔN_s was computed for a variety of distributions within reasonable bounds, and the shape of the curve did not change significantly.

Another factor to be taken into account is the finite component of the electron's momentum transverse to the collimating B-field. The equation for the number of atoms scattered into the detector modified to take this factor into account is given by

$$\Delta N_S = \frac{2}{H}\iiint I_e(E, \lambda)dE\frac{dV}{V}\, d\lambda \iint dx'_o\, dz'_o\, J_A(x'_o, z'_o, V)$$

$$x \int_{\theta_1(\lambda)}^{\theta_2(\lambda)} \sigma(\theta)\, \sin\theta\, [\varphi_2(\lambda) - \varphi_1(\lambda)]d\theta \qquad (36$$

The integration over λ in effect corresponds to a rotation of the coordinate system about the y-axis which is the direction of the atom beam. The detector coordinates this change with each value of λ and are related through the transformation equations:

$$x = x_o \cos \lambda - z_o \sin \lambda$$

$$z = x_o \sin \lambda + z_o \cos \lambda$$

where x_o, z_o are the detector coordinates in the initial $\lambda = 0$ frame. Thus θ_1, θ_2, φ_2 and φ_1 are functions of λ though their dependence on x, z and the integrations must be carried out in the order shown in Equation 36.

It is very difficult to estimate the shape of the transverse momentum distribution function, but a reasonable guess was made and is shown in Figure 43. The geometry of the interaction region is such that the smaller the component of transverse momentum, the greater the electron current passing through the atom beam. ΔN_s was calculated again with this new variable and the results are shown in curve C of Figure 42. This curve is now in better agreement with experimental results. In particular notice the flatness of the curve in the center region and that the long tail observed in the experimental data is now present in the theoretical curve. Because of the great amount of computer time required to carry out the last calculation, it wasn't possible to vary the parameters to see if better agreement could

TRANSVERSE MOMENTUM DISTRIBUTION OF ELECTRON BEAM

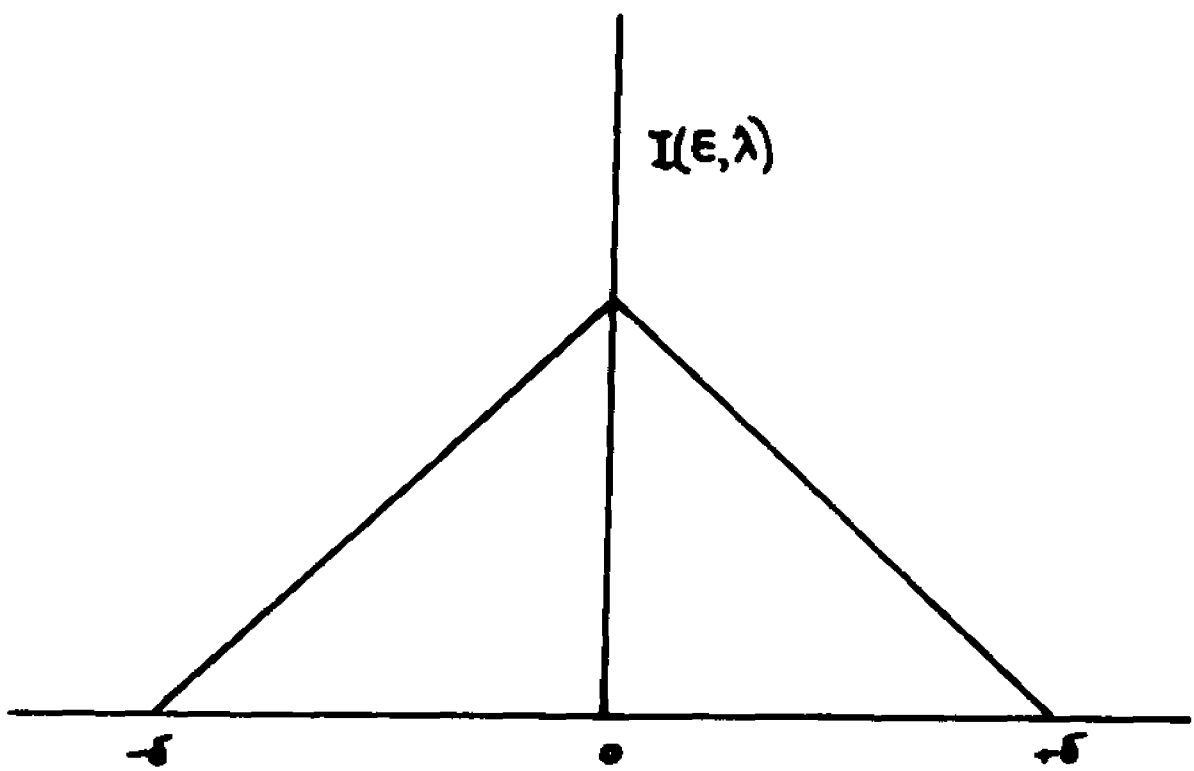

$$\delta = \tan^{-1}\left(\frac{p_\perp}{p_\parallel}\right) = \tan^{-1}(0.15)$$

$p_\perp$ = TRANSVERSE MOMENTUM OF ELECTRON

$p_\parallel$ = PARALLEL MOMENTUM OF ELECTRON

FIGURE 43

be obtained. However at this point the reasonably good agreement was thought sufficient to further justify the technique for separating elastic and inelastic events which was based upon empirical considerations.

VIII. Uncertainty in electron angle and angular resolution of the apparatus

In an experiment designed to measure the differential cross-section, it is important to examine the angular resolving power of the detection system in some detail. Collins has treated the problem, but neglected to take into account the finite widths of the unscattered atom beam and hot wire detector

The transformation equations relating atom and electron scattering angles yield the following expression for the uncertainty in the electron polar scattering angle, θ

$$\Delta\theta = \left\{\left(\frac{\partial\theta}{\partial V}\right)^2 (\Delta V)^2 + \left(\frac{\partial\theta}{\partial E}\right)^2 (\Delta E)^2 + \left(\frac{\partial\theta}{\partial\Psi}\right)^2 (\Delta\Psi)^2\right\}^{1/2}$$

$$= \left\{\left(\frac{\Delta V}{V}\right)^2 + \left(\frac{\Delta E}{2E}\right)^2\right\} \tan 1/2\,\theta + \left(\frac{MV}{mv}\right)^2 \left(\frac{L\,\Delta z}{\sin\theta}\right)^2\Bigg]^{1/2} \qquad (39)$$

where ΔV and ΔE are the uncertainties in atom velocity and electron energy, and ΔZ is the sum of atom beam and detector widths. (It is assumed here that the atom beam current profile is rectangular With this assumption, the uncertainty in θ due to the combined widths of the detector and atom beam is equivalent to that calculated by assuming that the detector width is the sum of both).

It is clear from the above expression that even in the case where the electron and atom beams are perfectly monochromatic, the angular resolution is poor at small and large angles because of the $1/\sin\theta$ term. Physically, this arises because the recoil angle Ψ is proportional to $(1-\cos\theta)$ so that small variations in Ψ at these angles give rise to large variations in θ. The factor $\tan(1/2\theta)$ in the term involving ΔV and ΔE results in a monotonically increasing contribution to the uncertainty in θ from 0 to π arising from the electron and atom velocity distributions. This contribution, almost negligible at small angles of recoil, results in a rapid deterioration of the system resolution at large angles and is an unavoidable consequence of this technique.

The angular resolution was evaluated for various values of ΔV and ΔE for elastic scattering at 1.0 eVolts and 4S-4P inelastic scattering at 5.0 eVolts. The results are shown in Figures 44 and 45 where $\Delta\theta$ is the difference between the maximum and minimum angle at any given detector position. Arrows indicate the positions of 0°, 90° and 180° scattering. The features mentioned above are clearly evident. The improvement in resolution at the largest average angles results from the fact that atoms from the high energy parts of the atom velocity are scattered by the slowest electrons in

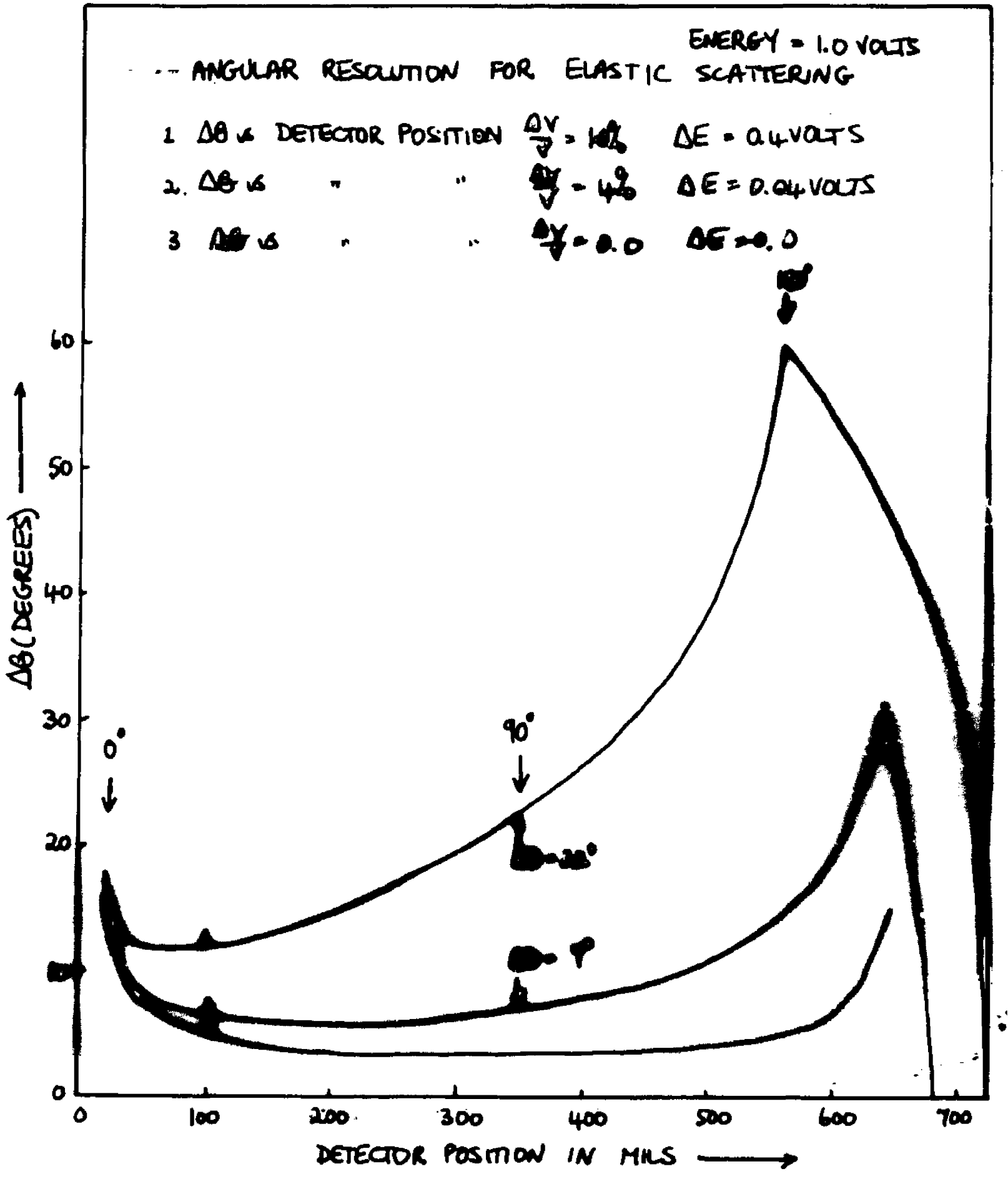
ENERGY = 1.0 VOLTS
-- ANGULAR RESOLUTION FOR ELASTIC SCATTERING
1 Δθ vs DETECTOR POSITION ΔV/V = 10% ΔE = 0.4 VOLTS
2. Δθ vs " " ΔV/V = 4% ΔE = 0.04 VOLTS
3 Δθ vs " " ΔV/V = 0.0 ΔE = 0.0
Δθ (DEGREES)
0
20
30
40
50
60
0°
90°
0
100
200
300
400
500
600
700
DETECTOR POSITION IN MILS

FIGURE 44

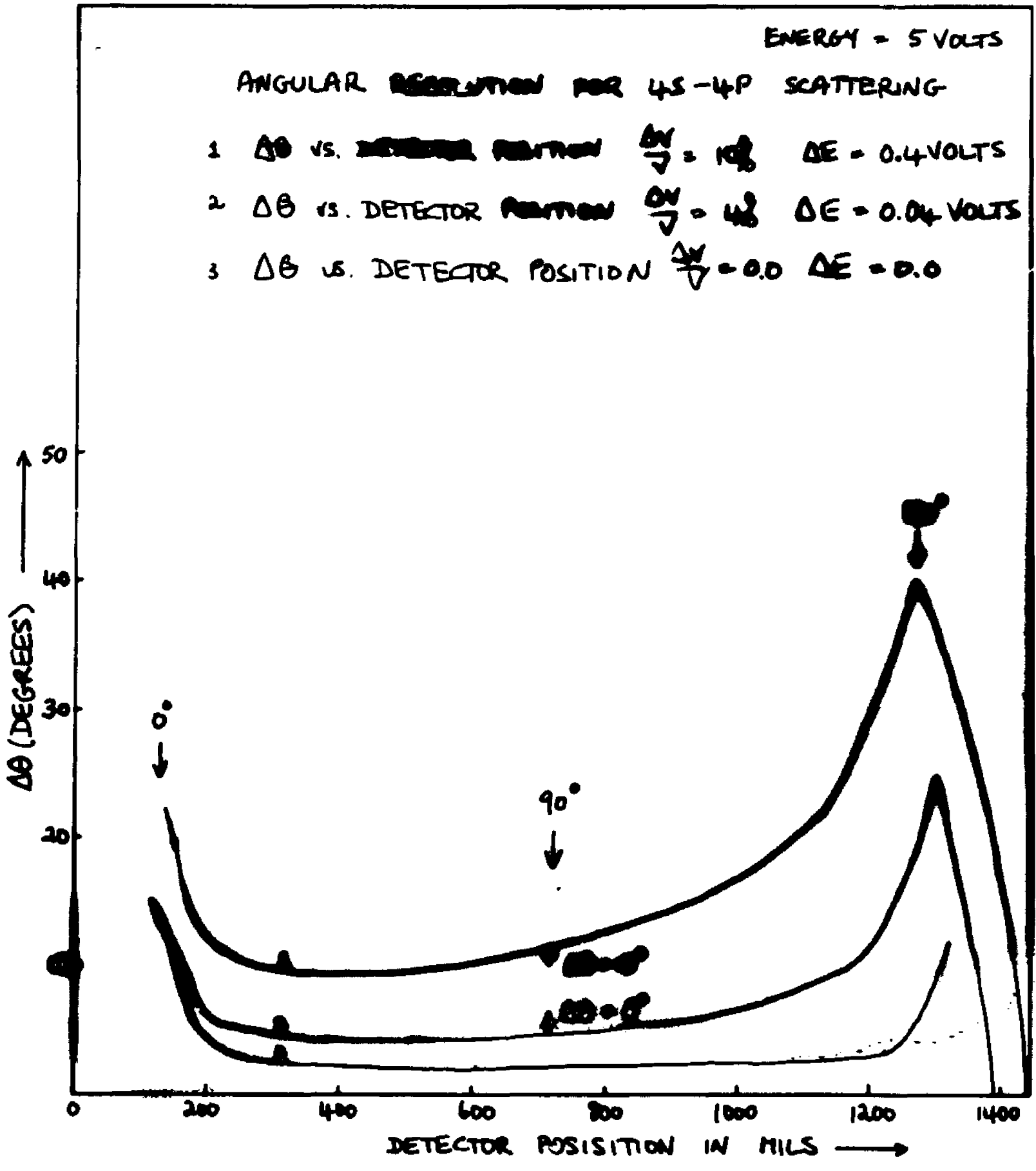
ENERGY = 5 VOLTS
ANGULAR [redacted] FOR 4S-4P SCATTERING
1 Δθ vs. [redacted] ΔE = 0.4 VOLTS
2 Δθ vs. DETECTOR [redacted] ΔE = 0.04 VOLTS
3 Δθ vs. DETECTOR POSITION ΔE = 0.0
Δθ (DEGREES)
50
40
30
20
0°
90°
0
200
400
600
800
1000
1200
1400
DETECTOR POSISITION IN MILS

FIGURE 45

the electron energy distribution at angles of recoil smaller than the angular displacement of the detector. This offers interesting possibilities for the observation of 180^{o} scattering at high resolution, though only scattering for angles less than 100^{o} was investigated here.

The curves representing $\Delta V/V = 10\%$ and $\Delta E = 0.40$ Volts are appropriate for the present experiment. For the angular range investigated at 5.0 volts, the resolution is typically 10^{o}. At lower electron energies, the angular spread increases as ΔE becomes an increasingly greater fraction of the electron energy. This is demonstrated in the curve for elastic scattering at 1.0 Volts, where the resolution varies from a minimum of 12^{o} at small angles to 60^{o} at large angles

Figures 44 and 45 also show plots for $\Delta V/V = 4\%$ and $\Delta E = 0.04$ Volts which is the best selectionpresently attainable from atom beam velocity selectors and electron monorchromators. The improvement in resolution is small compared to the price paid in signal tonoise ratio. Electron monochromators typically yield currents on the order of 10^{-7} amperes in comparison to the 200 μamperes used in this experiment while the atom beam current for a 4% velocity spread can be expected to fall by a factor of 5. The signal to noise ratio is thus reduced by a factor of 10^{4}.

Finally, since the differential cross sections are obtained by relating electron to atom recoil angles, the angular uncertainty of

the cross sections depends on the accuracy of the transformation equations. This accuracy is determined almost entirely by the uncertainty in absolute energy determination of the electron and atom beams. Horizontal error bars are included in the figures illustrating the differential cross-sections. These were computed assuming the atom velocity was known to ±4% and the electron energy to within ± 0.10 eVolts.

IX. Comparison of theory with experiment

The only theoretical results available for comparison with the present experimental data are those of Karule and Peterkop[6] using a 2-state close coupling approximation including exchange for partial waves L=0 through 8. They tabulate K-elements which are related to T-elements through equation 12. The differential cross section for matrix 4S - 4P scattering is related to the T-elements in the following way

$$\sigma(\theta) = \frac{1}{8k^2} \sum_S (2S+1)\left[\left|\sum_{\ell=1} \left\{-A_\ell T^S(\ell+1) + B_\ell T(\ell-1)\right\} P_\ell^1(\theta)\right|^2 + \left|\sum_{\ell=0} \left\{-C_\ell T^S(\ell+1) - D_\ell T^S(\ell-1)\right\} P_\ell^0(\theta)\right|^2\right] \quad (40)$$

where $A_\ell = \left(\frac{2\ell+3}{2\ell+2}\right)^{1/2}$ $\qquad B_\ell = \left(\frac{2\ell-1}{2\ell}\right)^{1/2}$

$$C_\ell = \left(\frac{(2\ell+3)(\ell+1)}{2}\right)^{1/2} \qquad D_\ell = \left(\frac{\ell(2\ell-1)}{2}\right)^{1/2}$$

$$P_\ell^0(\cos\theta) = P_\ell(\cos\theta)$$

$$P_\ell^1(\cos\theta) = -\sin\theta \quad \frac{d}{d(\cos\theta)} \quad P_\ell(\cos\theta)$$

$P_\ell(\cos\theta)$ = Legendre Polynomial

The notation $T^S(\ell \pm 1)$ refers to the cases where the electron is scattered with angular momentum $\ell = L \mp 1$, L being the total angular momentum. The total spin S can be either 1 or 0 corresponding to the symmetric and antisymmetric forms of the spin wave function. The theoretical cross sections are shown in Figures 36, 38, 39, 40. Since the cross sections are not rapid functions of energy, it is not unreasonable to compare Karule's results at 4.0 and 5.0 Volts with the present data at 4.4 and 5.2 Volts

Considering the experimental errors involved, experiment and theory agree very well, especially in the overall magnitude of the cross sections. The displacement of theoretical and experimental curves at 4.4 Volts and 5.2 Volts can be explained by the angular uncertainty in the experimental $\sigma(\theta)$.

In the run at 5.2 volts, the theoretical curve was averaged over the relevant angular spread in Figure 45, and the result shows that distortion of the differential curve is not great.

The total measured 4S - 4P cross section from 0^o to 36^o, which is independent of angular assignment and averaging, was compared with the theoretical cross section integrated over the same angular range. The results were as follows:

EXPERIMENT $\quad 2\pi \int_0^{36^o} \sigma(\theta) \sin(\theta)\, d\theta = 0.34 \times 10^{-14}\ cms^2$

Energy = 5.2 Volts

THEORY $2\pi \int_0^{36^\circ} \sigma(\theta) \sin\theta \, d\theta = 0.39 \times 10^{-14} \text{cms}^2$ Energy = 5.0 Volts

Finally, the total cross section in the angular range $0 - 17^\circ (\pm 3^\circ)$ for excitation to the 3d, 5S states* was computed to be

$4S \rightarrow \left.\begin{matrix} 5S \\ 3d \end{matrix}\right\}$ $2\pi \int_0^{17^\circ} \sigma(\theta) \sin\theta \, d\theta = 2.2 \times 10^{-16} \text{cm}^2$ Energy = 5.2 Volts

No theoretical estimates of this cross section are available

Since it was expected that the 2-state approximation would yield poor results above 2.6 volts, the generally good agreement between theory and experiment is somewhat surprising. However it should be pointed out that Karule extended the calculations up to L=8 partial waves. At 4 and 5 volts the T-elements corresponding to L=8 are quite large indicating that higher L states may be important These would cause an increase in the cross section. If, as Burke has shown in hydrogen, the inclusion of more states in the eigenfunction expansion reduces the cross section, the overall effect of a better calculation might not significantly alter the magnitude of the cross sections.

---

*The energy separation between 5S and 3d is 0.05 volts The levels are thus degenerate as far as the energy resolution of this experiment is concerned.

X. Conclusion

The success of the atom beam recoil technique in measuring absolute differential cross sections has been amply demonstrated in the preceding pages. Since almost all of the presently available techniques for monitoring excitation processes have had to rely on cross sections determined previously (and usually in the 1930's), the need for remeasurement of certain cross sections as standards is clearly evident.

In his review of experiments on electron impact excitation of atoms, Fite (2) writes that "the history of excitation processes is, in large part, a history of ingenuity in devising detectors for the products of the excitation process; but, unfortunately, very few of these detectors have been developed to the point of reliability and accuracy such that they can be used to determine absolute excitation cross sections ....." It is in this context that the recoil technique should be judged. Clearly the ability to measure absolute cross sections without resort to normalization by indirect methdds is an important new development in the study of excitation processes.

Finally, it should be emphasized that the recoil method affords the best opportunity for measuring 0° scattering. This scattering can in principle be obtained from observation of the scattered electrons. In practice the unscattered electron beam complicates this measurement, and usually prevents a reasonable determination of it. This problem does not enter into the present experiment since observations are made on the atoms. It should, however, be recognized that the 0° scattering reported here is averaged over a small range of angles (typically 0° - 15°). Further, the recoil method is the only technique which can be used to study 180° scattering. Although the angular resolution at large angles is very poor, with detailed knowledge of the electron and atom velocity distributions, a folding in technique can be used to compare theoretical and experimental large angle scattering.

Thus the importance of the technique described in this thesis lies in its ability to observe small and large angle scattering and measure absolute cross sections. In the light of Fite's remarks, it is possible that the cross section

at 1.0 eVolts where theory and experiment are in such good agreement can be used as a normalization standard for future scattering experiments.

Appendix A

Haeff[17] has investigated space charge effects in a long magnetically focused electron beam similar to the one used here, and has derived expressions relating space potential to electron current density for one dimensional beams. Since Celotta[15] has shown that the potential in the region of interest is determined solely by the walls, a solution of Poisson's equation in 1 dimension is sufficient. A cross section of the electron beam generally is shown in Figure 46. To find the potential at the center for a given applied potential at the walls $x = \pm b$, Poisson's equation is solved in the region $0 < |x| < a$ and Laplace's equation in the region $a < |x| < b$. Solutions are matched at $x=a$. The following two equations are then easily derived:

$$\frac{9}{64} \cdot \frac{Id}{1.313 V_B^{1.5}} = \frac{(d/t)(1-p)(1+2p)^2}{\{1+4/3(d/t-1)(1-p)(1+2p)\}^{3/2}} \qquad (A-1)$$

$$\frac{V_B}{V_A} = \{1+4/3\ (d/t-1)(1-p)(1+2p)\} \qquad (A-2)$$

where V_o = potential at $x=0$

V_B = potential at $x=\pm b$

V_A = potential at $x=\pm a$

$d = 2b = 0.062''$

$t = 2a = 0.032''$

I= total electron current

$p = (V_o/V_A)^{1/2}$

The Newton-Raphson method was used to find the roots of (A-1). Values of p for a given current I and applied potential V_B were thus found. These are substituted into (A-2) to yield values of V_A. V_o is then obtained from the definition of p. The computer program prints values of V_o versus I for a given potential V_B.

It is easily shown from Poisson's equation that the potential at any point within the electron beam is given by

$$4/3(V_x^{1/2}-V_o^{1/2})\ ^{1/2}(V^{1/2}+2V_o^{1/2}) = (kj)^{1/2}x \qquad (A-3)$$

where V_x = potential at x

$k=16\pi(2e/m)^{-1/2}$

j= electron current density in amperes/m^2

This equation can be solved numerically for V_x as a function of x using an iterative technique with the value V_o computed above. For the currents used in the present experiment, the potential V_x at x=±0.002" is different from V_o by no more than 0.01 Volt. Since the atom beam height is 0.004" and is centered at x=0, V_o can thus be taken as the average potential of the electrons traversing the atom beam.

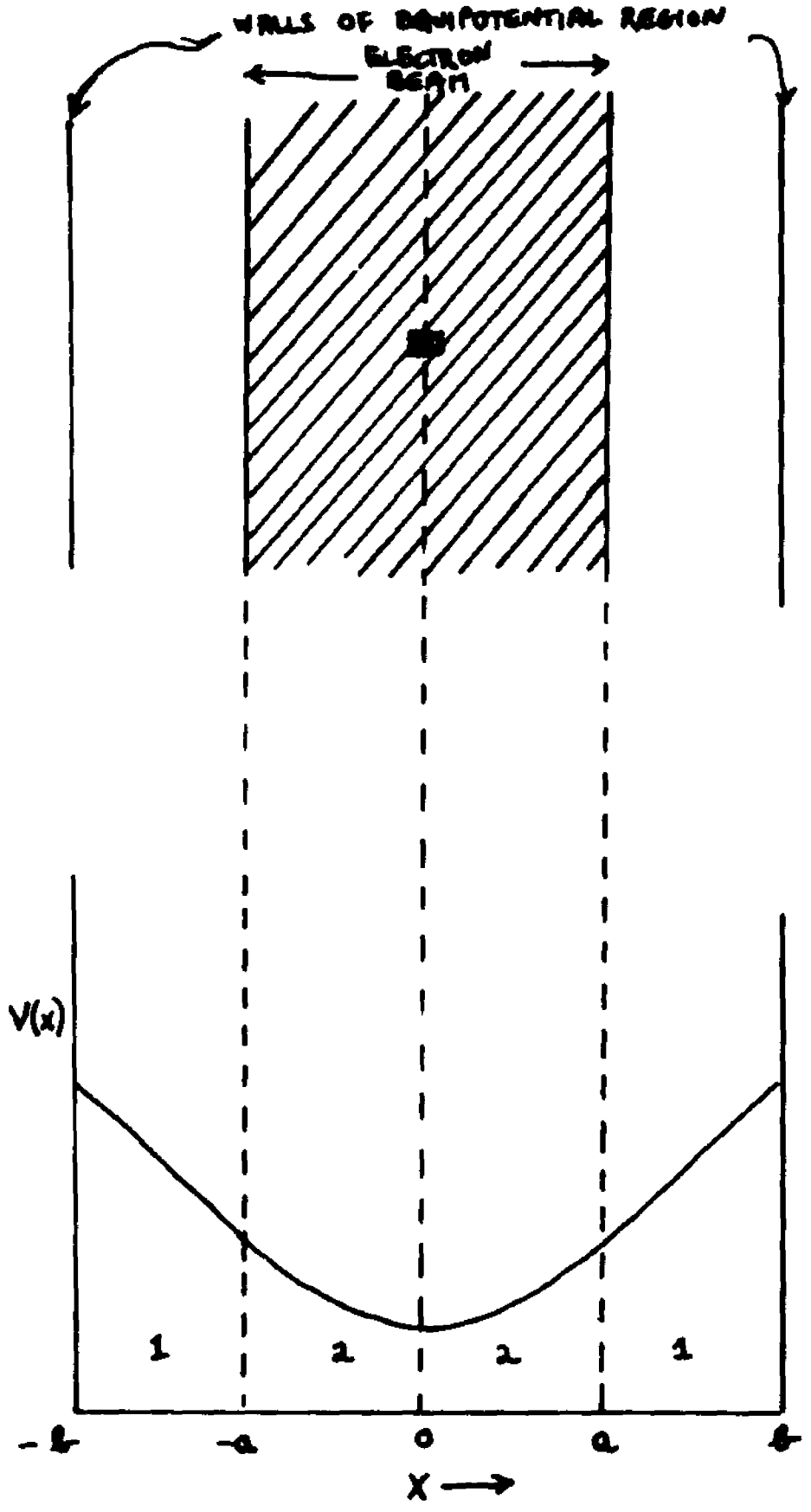

POTENTIAL IN REGIONS 1 SATISFIES LAPLACE'S EQN
POTENTIAL IN REGIONS 2 SATISFIES POISSON'S EQN

FIGURE 46

REFERENCES

1. B. L. Moiseiwitsch and S.J. Smith, Rev. Mod. Phys., Vol. 40, P. 238 (1968).

2. W. L. Fite in Atomic and Molecular Processes, (1962), Ed. by D. R. Bates.

3. K. Rubin in Proceedings of the IVth International Conference on the Physics of Electronic and Atomic Collisions, University of Laval, Quebec, Canada (1965).

4. P. G. Burke and K. Smith, Rev. Mod. Phys. Vol. 34, P. 458 (1962).

5. I. C. Percival and M. J. Seaton, Proc. Cam. Phil. Soc., 53, 654 (1957).

6. E. M. Karule and R.K. Peterkop, in Atomic Collisions III, edited by Y. Ia. Veldre (Latvian Academy of Sciences, Riga (1965)). [Translation: JILA Information Center Report No. 3, University of Colorado, Boulder, Colorado] .

7. P. G. Burke, S. Ormonde and W. Whitaker, Proc. Phys. Soc., Vol. 92, P. 319 (1967).

8. L. Castillejo, I.C. Percival and M.J. Seaton, Proc. Roy. Soc. (London), A254, 259 (1960).

9. R. M. Sternheimer, Phys. Rev , 127, 1220 (1962).

10. R. Gaspar, ACTA. Phys. Acad. Sci. (Hungary), 2 151 (1952).

11. N. F. Ramsey, Molecular Beams, Oxford (1956).

12. B. Bederson and K. Rubin, Atomic Energy Commission Tech. Report No. NYO-10, 11M (1962).

13. R.E. Collins, Ph. D. Thesis, New York University, 1968. (unpublished)

14. P. N. Eisner, Ph. D. Thesis, New York University, 1969. (unpublished)

15. R. Celotta, Ph. D. Thesis, New York University, 1969. (unpublished)

16. K. Rubin, B. Bederson, M. Goldstein and R.E. Collins, Phys. Rev. 182, 201 (1969).

17. A. V. Haeff, Proc. I.R.E., P. 586, (1939).